THE FLORIDA STATE UNIVERSITY

COLLEGE OF ARTS AND SCIENCES

APPLICATIONS OF EFFECTIVE FIELD THEORIES TO THE MANY-BODY NUCLEAR PROBLEM AND FRUSTRATED SPIN CHAINS

By

COSIMO FELLINE

A Dissertation submitted to the
Department of Physics
in partial fulfillment of the
requirements for the degree of
Doctor of Phylosophy

Degree Awarded:
Fall Semester, 2004

The members of the Committee approve the dissertation of Cosimo Felline defended on November 2, 2004.

Jorge Piekarewicz
Professor Directing Dissertation

Ruby Krishnamurti
Outside Committee Member

Simon Capstick
Committee Member

Samuel Tabor
Committee Member

Pedro Schlottmann
Committee Member

The Office of Graduate Studies has verified and approved the above named committee members.

ACKNOWLEDGEMENTS

I would like to thank for their help and support: my advisor, Prof. Jorge Piekarewicz; all members of the Defense Committee, Prof. Simon Capstick and Prof. Pedro Schlottmann for helpful discussions; Jan Burgy, Sergio Fagherazzi, Giulia Manca and Alessandro Stocchino; Prof. Alberto Devoto, my undergraduate advisor at the University of Cagliari; my family and my friends; Lisi.

TABLE OF CONTENTS

LIST OF TABLES

LIST OF FIGURES

ABSTRACT

Modern effective-theory techniques are applied to the nuclear many-body problem and frustrated quantum spin chains. A novel approach is proposed for the renormalization of nucleon-nucleon operators in a manner consistent with the construction of the effective potential. To test this approach a one-dimensional, yet realistic, nucleon-nucleon potential is introduced. An effective potential is then constructed by tuning its parameters to reproduce the exact effective-range expansion and a variety of bare operators are renormalized in a fashion compatible with this construction. Predictions for the expectation values of these effective operators in the ground state reproduce the results of the exact theory with remarkable accuracy (at the 0.5% level). We illustrate the main ideas of this work using the elastic form factor of the deuteron as an example. We also apply the COntractor REnormalizator technique to the study of frustrated anti-ferromagnetic zig-zag spin chains with arbitrary half-integer spin. A basis is employed in which three neighboring spins are coupled to a well-defined value of total angular momentum. The basis is then truncated to retain only the lowest lying energy states, and the Hamiltonian renormalized to reproduce the low-lying energy spectrum of the original system. We prove the necessity of retaining two, rather than one, lowest energy eigenstates as frustration is increased. A finite size scaling approach is used to extract ground state energy densities in good agreement with DMRG calculations and spin gaps in qualitative agreement with the disappearance of the Haldane phase around $\alpha = 0.3$. Moreover, we are able to develop a renormalization group equation that predicts accurately the ground state energy density of the chain in the thermodynamic limit.

CHAPTER 1

INTRODUCTION

The amateur physicist who stumbles across this work and glances upon its table of contents could perhaps be surprised in finding such different subjects bound into a single piece of research and could be hard-pressed to find a connection between them. Magnetic spin chains are constructed out of ions, which in turn have nuclei at their core; and, possibly, you can use quantum mechanics and Schrödinger equation to solve them. But, he might think, that's about it. After all, nucleon interactions dwell with the core of matter and their properties are not immediately connected to our everyday experience; on the other hand, spin chains are at the heart of matter's bulk properties, and magnetism is something we deal with on a regular basis. The respective energy scales are also strikingly different: the former are in the million electron volt (MeV) range and can be accessed only with the use of powerful particles accelerators, while the latter are about six orders of magnitude smaller. Of course, the connections are deeper than that, but I feel that at this point I'd take some time to explain to the reader the research process that brought us to test such different fields and join them in this unified and, we hope, coherent work.

This thesis is concerned with the subject of effective field theories (EFT), low energy approximations to arbitrarily high-energy physics. This field is hardly new, having been around for decades: nuclear physicists in particular have in the past researched it abundantly, in an effort to tackle the many-nucleon interaction problem and to find a way around the apparent impossibility to solve exactly the fundamental theory of nuclear interaction, Quantum Chromo Dynamics (QCD). These attempts have periodically been frustrated by the extreme difficulty of the problem, but the rewards that a final and comprehensive solution promised have made many physicists unwilling to give it up. This is not to say that great leaps forward were not made: the Shell Model (SM) is now a powerful tool at our disposal and the paradigm of great part of nuclear physics investigations. However, as we will see in

detail in the following sections, it is not exempt from defects. The effort to improve some of its shortcomings through the employment of EFT was the starting point of this research. On the other hand, EFT techniques have been proved to be extremely successful in fields other than nuclear physics, such has high-energy and condensed matter. It seemed therefore natural to explore some of these new avenues, and as we went along our goals became wider. We were motivated in the first place by the conviction that such a challenging subject required as large a testing ground as possible and secondly by the desire to show the variety of applications of our methods.

1.1 Effective theories for the Shell Model

The apparent impossibility to solve QCD exactly is largely due to the fact that it possesses characteristic mass scales, which implies that many of its aspects will surface in different proportions depending on how the momentum transfer Q of a given process compares to each one of these scales. QCD has an intrinsic mass scale $\Lambda_{\rm QCD} \sim 1$ GeV associated with the mass of most hadrons ($m_\rho, m_{\rm N}, \ldots$) and chiral symmetry breaking, but a large portion of traditional nuclear physics, including pion physics and the structure of lighter nuclei, involves momenta comparable to a much smaller scale, $\Lambda_{\rm nucl} \sim 100$ MeV. A third scale $Q^2/\Lambda_{\rm QCD} \sim 10$ MeV is connected to non-relativistic kinetic energies and binding energies per nucleon. As it happens, QCD is highly non-perturbative in the region characteristic of most low-energy nuclear physics phenomena. The lack of an exact nuclear force derived from first principles has led to the appearance of nucleon-nucleon (NN) potentials built phenomenologically from experimental data [1, 2, 3, 4, 5, 6]. These are commonly determined starting from underlying models (often based on symmetry properties) from which a parametrized mathematical *ansatz* is derived. The parameters are then tuned to reproduce low-energy NN scattering properties (below pion production threshold) and deuteron properties (binding energy, root-mean-square radius, etc.) Even in this simplified form, the problem still turns out to be of difficult solution. All present-day NN potentials incorporate meson physics into their long- and intermediate-range sections: a long-range one-pion exchange tail is a common established feature. However, while they agree on the presence of a highly repulsive hard-core, the details of the latter vary from

one potential to another, so that predictions for heavier nuclei are often model sensitive [7]. In addition, phenomenological potentials often provide incorrect descriptions of binding energies for light nuclei, even the simplest beyond the deuteron such as ^{3}He or ^{4}He [8], so that three-nucleon (NNN) interactions have to be introduced in order to "tune" the results [9, 10]. Moreover, the short-distance hard core translates into a very weak momentum dependence, which implies that low- and high-momentum states will contribute to a given process in roughly the same amounts. In order to be diagonalized exactly, this strongly pathological potential would require in theory a basis set too large to be tractable in most computational approaches. Despite these shortcomings, the development of NN phenomenological potentials has achieved a great level of sophistication (some of these potentials require the tuning of over 40 parameters!) Combinations of NN and NNN potentials solved with Green Function Monte Carlo (GFMC), correlated Hyper-spherical Harmonics or Faddeev-Yakubovsky methods can predict with great accuracy properties of light nuclei [10, 11]. Calculations of nuclei with $A = 10$ have been performed using the GFMC method, with the current limit lying probably at $A \sim 12$ [11, 12].

Given such limitations, exact solution of the generalized many-body problem in its purest form is far out of reach and the Shell Model (SM) is still the standard paradigm for its treatment [13]. In the SM, single particle harmonic oscillator wave-functions are used to form the basis set (the employment of HO states allows the separation of center-of-mass and relative coordinates.) While the exact Hamiltonian for an A-nucleon system operates in an (essentially) infinite Hilbert space with an upper momentum Λ_∞, the SM Hamiltonian operates on a reduced model space $|SM\rangle$ which is limited by a second, smaller, momentum scale Λ_{SM}. This essentially separates the full Hilbert space in a low-momentum retained subspace which can be extracted through the action of a projection operator P and an excluded high-momentum subspace defined by the complementary operator $Q = 1 - P$. To motivate this truncation the SM assumes, in analogy with Brueckner's theory of matter, that contributions to the wave-function coming from the high-momentum space can be integrated out in a rapidly convergent series in the number of nucleons that interact at the same time outside the truncated space. Moreover, the presence of the strongly repulsive short-range part in all realistic NN interactions will produce pathologically intractable results unless the bare Hamiltonian is renormalized to an effective Hamiltonian $H_{\rm eff}$. Once we are assured of

its existence, the problem is to find an effective $H_{\rm eff}$ which is simple enough to be useful. The basic tenet of the SM procedure is that the effective Hamiltonian will converge to the exact one as the size of the truncated basis increases and converges to the full Hilbert space, *provided no approximations are made.* However, this is in most practical cases unobtainable, since $H_{\rm eff}$ will in general be composed of A-body induced interactions which cannot be evaluated exactly. Shortly after the SM first appeared, attempts to develop a perturbative expansion for $H_{\rm eff}$ were frustrated by the finding that its convergence was extremely hard to come by. For example, third order corrections were shown to comparable in magnitude to second order terms (albeit of opposite sign [14]). These additional difficulties led to the birth of phenomenological effective interactions, which are often reduced to a two-body renormalized interaction determined for a two-nucleon sub-system or two-nucleon cluster. In many common applications, the unavoidable A-body corrections are swept under the carpet, so to speak, and assume the form of generalized many-body terms, often including all of the residual nucleons, and parametrized in order to obtain agreement with experimental data. The issue of many-body interactions is indeed very complex and difficult, encompassing the elusive difference between "real" and "effective" interactions. As mentioned above, model sensitivity of phenomenological NN potential has forced the inclusion of three-body, albeit small, "real" interactions. For decades nuclear physicists have debated whether these corrections have a physical counterpart or simply represent an *ad-hoc* fix to substitute for the inability to recover the real two-body interaction. The nature of effective interactions, on the other hand, is intrinsically induced by the truncation procedure. In other words, they are the price one pays for excluding important high-energy states from the process. One of the greatest strengths of the SM is that the technology developed for direct diagonalization is now quite remarkable, including powerful methods such as Lanczos and Monte Carlo sampling. However, the use of phenomenological interactions ultimately undermines the possibility of achieving a methodical derivation, starting from an underlying theory, of effective potentials and operators, which puts serious limitations on the employment of the the shell model as a predictive tool. Therefore it is perhaps not too surprising that many authors have recently pointed out a series of "uncontrolled approximations" embedded in SM implementation [15, 16, 17]. Among these are the following: 1) The symmetries of the original Hamiltonian (Hermiticity and translational invariance) are lost in the renormalization

process, even though Hermiticity is often enforced by hand. 2) The shell model truncated space wave-functions are always orthogonal and normalized to unity, independently of the size of the model space. 3) In order to improve agreement with experimental data, shell model interactions are often forced to depend on fictitious, non-physical parameters. For example, calculation of the Brueckner G-matrix which often substitutes an effective expansion of the potential, depends on a "starting energy" parameter in order to account for intermediate-state average energies. 4) Most importantly, effective operators are almost never treated in a consistent fashion. More plainly, there is no *systematic* way to derive effective potentials and operators from basic principles. Furthermore, even when an effective potential is derived from realistic NN potentials, it is common practice to retain bare, rather than renormalized, operators. The last point has been remarked by many authors and is worth being emphasized. We stress that the possibility to renormalize operators in a manner consistent to the modifications of the underlying Hamiltonian must be a fundamental feature of any reliable effective theory and has thus far been lacking in past approaches.

In recent years, a great deal of attention has been given to Effective Field Theories (EFT) as a possible key to the solution of some of these issues [18, 19, 20, 21, 22, 23, 24]. In fact, the very reason that causes NN potentials to be highly intractable is also the foundation of EFTs, since these were designed specifically to exploit the existence of mass scales in order to separate low- from high-energy physics [18]. EFTs could be defined as low-energy approximations to arbitrarily high-energy physics: their basic assumption is that the complicated, and likely unknown, short-distance details of a theory are hidden to a long-wavelength probe and it should then be possible to modify the corresponding portion of the real potential with a *simpler* one, leaving at the same time its low energy properties intact. In order to achieve this, the low-energy properties must be known in advance either from experiment or from solving the bare theory exactly at low energy. This procedure is also known as renormalization. As a simple analogy, consider loop calculations that occur in Quantum Electro Dynamics (QED), which include momenta $k \to \infty$. The first problem that one encounters is the appearance of divergent loop integrals. One way to solve it is to introduce an upper integration limit (cutoff) and solve the integrals as a function of this variable. Of course, such a quantity is entirely fictitious, and hopefully the final results will not exhibits any cutoff dependence. In addition, the physics as momenta approach

infinity is unknown: super-symmetry effects could be relevant, electrons could reveal an internal structure and so forth. Fortunately, renormalization theory affirms that, even though short-range physics may affect low-energies properties, its details are unimportant and there exist infinitely many short-range theories that replicate the same low-energy properties. EFTs are hence especially useful when the short-range theory is unknown but low-energy data are available. Regardless of the details associated with different implementations, such a theory is built according to the following procedure. 1) Separate the long- and short-distance parts of the interaction. The correct (and known) long-range part should be embedded into the theory unmodified. 2) Find a truncated basis set that includes only momentum states below a specific cutoff, so that high-energy, short-distance interactions are explicitly excluded. 3) Reintroduce the short-range part of the interaction via parametrized contact operators. In the context of low-energy nuclear physics, nucleons and pions are the EFT relevant degrees of freedom. At low interaction energies, the internal structure of hadrons remains hidden, and we could treat them as point-like particles for all practical purposes, which ultimately allows to substitute complicated interaction vertexes with simple contact terms. 4) Tune the parameters of the renormalized Hamiltonian to reproduce the low-energy part of the exact spectrum. The problem as defined here may still turn out to be of difficult solution when, even including only low-energy degrees of freedom, one still obtains an infinite collection of possible interactions. Therefore, a useful EFT must possess a power-counting scheme that establishes an ordering of all possible contributions to the process. The power expansion is in general carried as a function of the ratio Q/Λ, where Q is the physical quantity that defines the process, such as its energy or momentum, and Λ is a characteristic mass scale of the underlying physics and is much larger than Q. The challenge is then to identify the expansion variable, construct the ordering scheme and determine its radius of convergence. Many of these applications rely on Renormalization Group (RG) techniques [25, 26, 27] as a mathematical tool to tackle the power counting problem.

Parallel to the development of EFT-based perturbative expansion methods, recent computational advances have by the same token permitted the revival of 25-years old similarity transformation techniques, such as those proposed by Lee-Suzuki [28, 29, 30, 31]. In fact, a considerable amount of success has followed from their application to the many-body nuclear problem [32, 33, 34]. In theory, these method allows the determination of generalized

range-A renormalized interactions from the exact solution of A-nucleons sub-clusters. In practice, computational limitations restrict the number of solvable clusters. A finite expansion is then constructed out of the sum of all renormalized terms up to range-N. According to the procedure, an N-nucleon effective Hamiltonian contains N range-1 terms (corresponding non-interacting particles), $\frac{N(N-1)}{2}$ range-2 (pairwise interactions) and so forth. Once the effective potential is obtained to all orders for small systems, these terms can be embedded in calculations for larger ones, where the expansion can be carried out only partially. One hopes that the expansion converges fast enough that just a few low-range contributions may suffice to provide an accurate reproduction of the exact spectrum, leaving higher order terms in charge of fine tuning. Morningstar and Weinstein developed a similar technique known as COntractor REnormalization (CORE) [35, 36], which has recently been modified to treat the many-body nuclear problem [37]. In the last Reference it was shown how to combine the CORE approach with effective interactions methods, such as those discussed by Lepage [18]. In particular, accurate predictions for the ground-state energy of the three-body system were made with relatively little computational effort when both techniques were used in a complementary fashion. As discussed in recent publications [26], these similarity transformations methods may thus be included and understood in a more general context that merges their approach with EFT. It should be mentioned that, even in the framework of similarity transformation techniques, the employment of bare, rather than effective, operators remains a common practice.

In this work we exploit some of the concepts of low-energy EFT in the hope of improving some of these shortcomings. We adopt a version of the effective potential power expansion modified by Lepage, in which a Gaussian cutoff is introduced to exclude the high-momentum states. The parameters in the expansion can be tuned to reproduce low-energy scattering data modeled on a text book effective range expansion. Furthermore, we suggest an approach for the indispensable renormalization of operators that is consistent with the modification of the underlying Hamiltonian and wave-functions. In order to simplify the illustration of these concepts, we only work in a one-dimensional space. A model potential is introduced that mimics the same pathologies of a realistic NN interaction and will therefore provide a stringent test of our formalism [38].

1.2 Quantum spin compounds

In general, a magnetic system is a spatial arrangement of ions that interact only through their spins. The value of a single ion's spin is determined by the number of electrons in its outer shell, and can thus take on any half-integer or integer value. As we will see, many crucial properties of the system depend critically on whether the chain or ladder has an integer or half-integer spin. Interactions between spins are dominated by the exchange force, which is a consequence of the Coulomb repulsion between the electrons and of the antisymmetry of a many electron wave-function imposed by the Pauli principle. The exchange interaction between two spins $\vec{S}_1$ and $\vec{S}_2$ is given by the scalar product $J\vec{S}_1 \cdot \vec{S}_2$ where J is the strength of the interaction which in turn depends on the overlap between the atomic orbitals of the ions. Depending on the sign of J, the chain will display a ferromagnetic ($J < 0$) or an anti-ferromagnetic (AF) arrangement ($J > 0$). Other spin interactions are also possible between orbitals besides simple exchange: dipole-dipole interactions, anisotropic terms deriving from spin-orbit coupling and so on. Figure 1.1 illustrates some of the possible arrangements of spin lattices. A **spin chain** is a linear arrangements of magnetically interacting ions; in a chain with nearest-neighbor interactions, each ion is connected to the ones occupying adjacent sites. An assembly of decoupled spin chains forms a spin chain compound. A **spin ladder** is a union of two spin chains in which each ion also interacts with sites in the neighboring chain. These cross-interactions form the "rungs" of the ladder. A **"zigzag" chain** is a spin ladder arrangements in which each ion interacts with two neighboring sites in the other chain. AF zigzag chains display an important feature that we will consider extensively: they are "frustrated", in the sense that the magnetic interactions cannot be fully minimized by pairs of spins, because of a common interaction with a third site. The same effect appears in linear chains with competing nearest-neighbor (nn) and next-to-nearest-neighbor (nnn) interactions. Here, frustration effects can be described by a single parameter α defined as the ratio of the two interaction strengths J_{nnn} and J_{nn}. In the case where no nnn interactions are present $\alpha = \frac{J_{nnn}}{J_{nn}} = 0$. Interest in low-dimensional anti-ferromagnetic spin compounds has been stimulated by the wide variety of surprising properties particularly in the low-energy regime. This is especially true if frustration, both geometric and dynamic, is allowed to play a role. It is known that the cooperation of

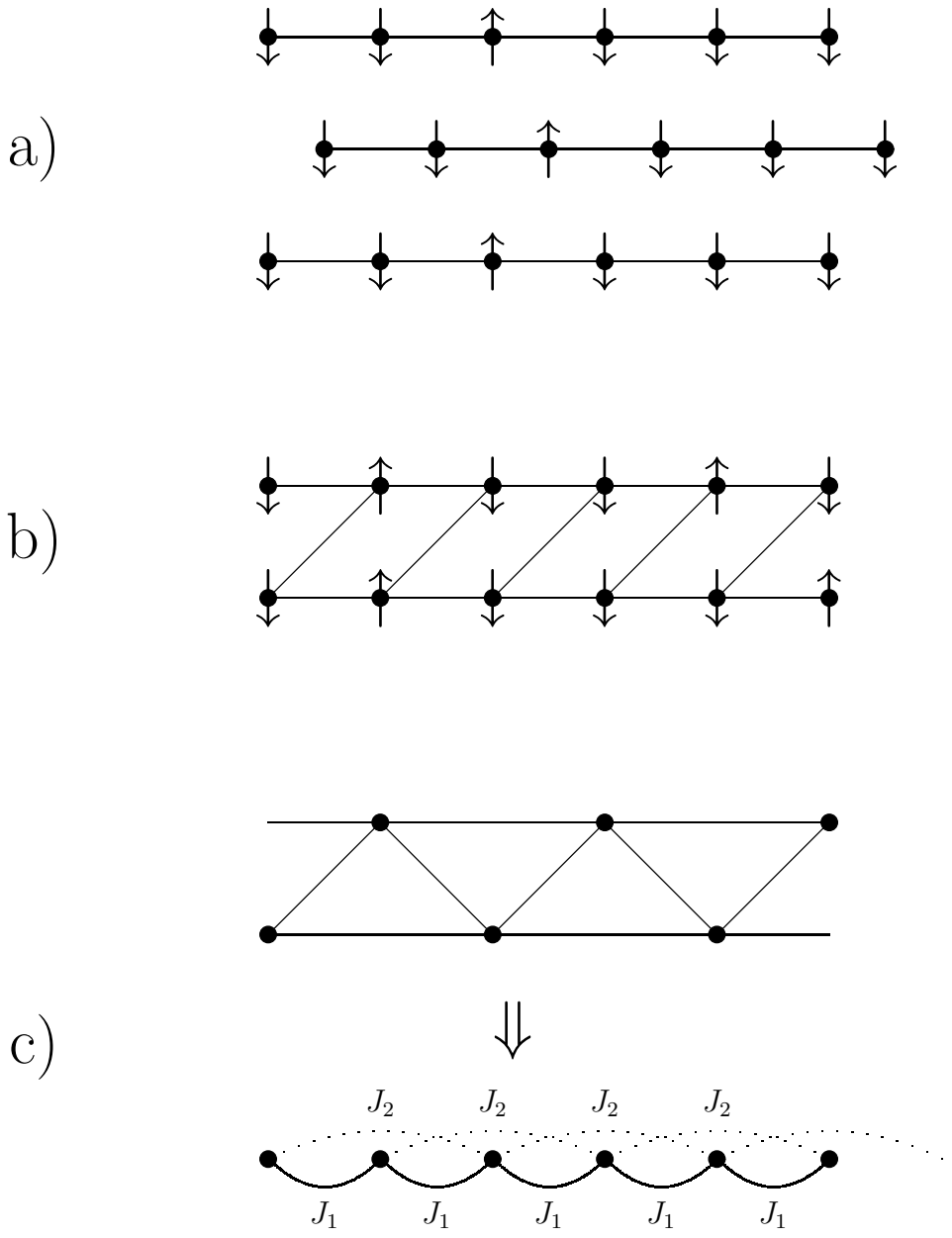

Figure 1.1. Different arrangements of spin composites. Spin chain with nearest-neighbor (nn) coupling (a), spin ladder (b) and spin "zigzag" chain mapped into a spin chain with next-to-nearest-neighbor (nnn) coupling.

frustration and quantum effects induces strong cooperative fluctuations and ultimately the creation of a large number of non-magnetic ground states and phase transitions. Indeed, the multiplicity of ground states is a staple characteristic of all frustrated systems, and accounts for many of their properties [39]. The study of the anti-ferromagnetic spin chain has also been stimulated by the fact that, for $\alpha = 0$ and $S = \frac{1}{2}$, Bethe found an exact solution that predicts the ground state energy density ($\varepsilon_{\text{exact}} = -\ln 2 + 1/4 = -0.443147$) and a vanishing singlet-triplet spin gap [40]. The excited states were found to be spin-$\frac{1}{2}$ excitations (spinons) created in pairs with energy $\epsilon(k) = \frac{1}{2}\pi \sin k$. The situation is radically different in the case of integer spin chains [41] where a spin-gap Δ has been conjectured by Haldane [42, 43] using a field theory approach based on a non-linear sigma model. Although the Haldane conjecture has not been proved analytically, there is strong evidence of its validity. Confirmation has come from Monte Carlo simulations and exact diagonalizations which yield a value for the spin gap $\Delta = 0.41049$. Moreover, half-integer chains exhibit no long-range order, which means that the average spin magnetization (or direction in space) is zero, that is $\langle \vec{S}_i \rangle = 0$. However, the correlation length (the probability of having any two spins aligned) has infinite range, scaling as the inverse of the distance between the two sites: $\langle S_n^z S_m^z \rangle \propto \frac{(-1)^{n-m}}{|n-m|}$. Predictions of ground state energy densities were also obtained for spin-$\frac{1}{2}$ chains using a variety of analytical [44] and computational [45, 46, 47] tools such as variational methods and Density Matrix Renormalization Group (DMRG) techniques [48, 49]. Also, an approximate spin-wave calculation by Anderson [50] was able to predict energy densities for arbitrary half-integer spins. Interestingly enough, this computation employs a $S \to \infty$ approximation, and consequently turns out to be more accurate for high values of the spin quantum number. However, it does surprisingly well in its worst-case-scenario ($S = \frac{1}{2}$), where it remains within 2.5% of Bethe's exact calculation. For low values of α, the system is in a spin liquid phase with gap-less excitations, but as α is increased, it undergoes a phase transition to a gapped dimerized phase. Intensive numerical studies [51, 52] predict the onset of the transition at $\alpha = 0.2411$, but it should be noted that the gap is predicted to be very small for $\alpha < 0.3$. The gap is expected to extend up to $\alpha \to \infty$, but it turns out to be exponentially small, scaling as $\Delta \sim \exp(-C\alpha)$, with C a constant. In this situation, the zig-zag chain is reduced to two decoupled Heisenberg linear chains. On the experimental side, compounds have been studied in both in the $\alpha \sim 0$ (single Heisenberg chain) and $\alpha \to \infty$

(two decoupled chains) regime. In the first category, the nearly gap-less phase has been observed in Cu[2-(2-amino-methyl)pyridine] and the coupling ratio estimated at $\alpha \approx 0.2$ [53]. Other compounds such as $(N_2H_5)CuCl_3$ belong to the second group and its magnetic properties have been determined to be surprisingly close to those in the single chain [54]. Hence, the distinction, both theoretical and experimental, between $\alpha \sim 0$ and $\alpha \to \infty$ is still an open question.

An effective theory approach can be attempted in the treatment of quantum spin compounds. Here, the determination of the relevant low-energy degrees of freedom can be quite complicated and is basically obtained by an appropriate grouping of the chain sites, often suggested by topological symmetries of the chain itself. CORE has already been tested on the study of Heisenberg spin ladders with AF coupling [55, 56, 57, 58, 59, 60]. Specifically, in Reference [55], a plaquette basis was defined from the coupling of four neighboring spins and it was shown that, so far as low-energy properties are concerned, the ladder can be mapped onto a spin-1 anisotropic ladder in which the coupling along the rungs is much stronger than the coupling between the rungs. One could argue, by an effective theory analogy with nuclear physics, that these new spin-1 "pseudo-particles" are to the original spins as hadrons in general are to the quarks that compose them. Moreover, the authors prove that low-energy properties of three-plaquette (and higher) ladders are very precisely reproduced through an effective Hamiltonian cluster expansion that only contains range-2 interactions. We are going to attempt a similar approach to the treatment of frustrated AF "zig-zag" spin chains. Here, symmetry suggests that the plaquette structure should be substituted by a "trimer" block composed of three neighboring spins. Spin-$\frac{1}{2}$ chains are initially considered but half-integer and integer chains are later included without effort. The study aims at reproducing in an effective theory context ground state energy densities and the gap-less spectrum of low-frustrated chains. Furthermore, we investigate the appearance of a gap as frustration is introduced in half-integer chains, as predicted in numerical computations. Our approach will be two-fold: on one hand we apply a finite size renormalization procedure to test the accuracy of CORE as compared to the exact solution and, secondly, we develop a renormalization group equation that allows us to predict properties of infinite chains.

1.3 Outline of thesis

This dissertation work could be ideally divided in two parts. The first one, which includes Chapter 2, 3 and 4, is dedicated to the treatment of nuclear potentials and operators. In Chapter 2, we will go through some of the main features of the implementation of our methods. Starting from an exact potential we will here be able to show in Chapter 3 how an effective potential can be developed that reproduces with great accuracy the deuteron's ground state properties. This method will then be extended to treat a variety of different operators. This Chapter is mainly composed of excerpts from our previous publications ([38]). In Chapter 4 I will extend some of the previous results to a three-nucleon system. Much of this Chapter illustrates multiple solution techniques of the three body problem and how the introduction of effective potentials can affect and simplify such calculations. The second part of the work consists of Chapter 5 and 6, where CORE will be applied to the renormalization of frustrated spin chains. The seventh and final chapter will contain our considerations and conclusions.

CHAPTER 2

EFFECTIVE FIELD THEORIES AND CORE

2.1 Renormalization of Schrödinger's equation

Proceeding along the lines suggested by Lepage [18], on whose approach we will rely heavily in this section, we apply an EFT to the solution of the non-relativistic Schrödinger equation. We will analyze the complications involved in the development of a perturbative expansion of a short-range potential and explore how EFT can help overcome these obstacles. The concepts put forward in this section will be a starting point for our applications in the next Chapter, when a similar effective potential expansion will be applied to a more concrete problem and the formalism of the method will be addressed more accurately. Here, however, I will worry less about working out mathematical details than about illustrating some of the general features of an EFT approach.

The problem at hand can be of two different natures. In one case, the potential may possess a short-range portion which is unknown. Alternatively, we might have to deal with a short-range potential of which we have complete knowledge, but which is too hard to solve, either analytically or computationally. Phenomenological NN potentials fall into the latter of the two categories. In both cases, however, EFT tells us that, so far as we only need to describe low-energy properties of the system, the details of the short-range interaction are irrelevant. The latter could then be somehow simplified and parametrized in order to reproduce low-energy data of the exact theory. I will here employ a toy potential from which low-energy data can be extracted computationally. My potential is constructed of the sum of a short-range part $V_s(\vec{r})$, which in a real application may possibly be unknown, and a known long-range part which for practical purposes I will take to be a Coulomb potential $-\frac{\alpha}{r}$. Here, the two sectors are explicitly separated for simplicity reasons but, of course,

this is not obtainable in most practical cases. Furthermore, in order to stress the concept that precise knowledge of the short-range section of the potential is not necessary, in the following derivation $V_s(\vec{r})$ will be left undefined. This is in accordance with basic ideas of EFT, which affirms that the specific form of the short-range part of the potential is irrelevant when working in the low-energy range, since it remains hidden to long-wavelength probes. Therefore, the Hamiltonian is defined as:

$$H = \frac{\vec{p}^2}{2m} + V(\vec{r}) \quad \text{with} \quad V(\vec{r}) = -\frac{\alpha}{r} + V_s(\vec{r}) \tag{2.1}$$

A first approximation can be made through the substitution $V_s(\vec{r}) \mapsto c\delta^3(\vec{r})$, so that:

$$H_{\text{approx}} = \frac{\vec{p}^2}{2m} - \frac{\alpha}{r} + c\delta^3(\vec{r}) \tag{2.2}$$

where c is a parameter to be fitted to the data. The first order perturbation energy shift is given by:

$$\Delta E_n^{(1)} = c\langle n|\delta^3(\vec{r})|n\rangle = c|\psi_n^{Coul}(0)|^2 = c\frac{\delta_{l,0}}{\sqrt{\pi}n^3} \tag{2.3}$$

The specific value of c could be determined by fitting this formula to the lowest bound state available (the lowest energy state can resolve the short-range potential to a lesser degree than any other, so the substitution $V_s(\vec{r}) \mapsto c\delta^3(\vec{r})$ is most accurate in this case). So far, we have used two approximations: first, we only used first order perturbation theory; second, we substituted the short-range interaction with a delta function, neglecting the fact that $V_s(\vec{r})$ possesses an internal structure of finite range. However, we quickly run into trouble if we try to improve any of these two approximations. For instance, we may wish to compute second order energy shifts, but the quantity:

$$\Delta E_n^{(2)} = \sum_{m\neq n} \frac{c^2\langle n|\delta^3(\vec{r})|m\rangle\langle m|\delta^3(\vec{r})|n\rangle}{E_n - E_m} \tag{2.4}$$

diverges as the momenta summed over approach infinity. Also, if we try to improve our $V_s(\vec{r})$ approximation and account for the fact that it has a finite range, the outcome is still disappointing. Since $V_s(\vec{r})$ is short-ranged, its Fourier transform is only weakly dependent

on the momentum transfer q. Therefore, we are justified in retaining only the first two terms in the expansion and then move back to position space:

$$V_s(\vec{r}) \xrightarrow{\text{F.T.}} v_s(q^2=0) + q^2 v_s'(q^2=0) + \ldots \xrightarrow{\text{F.T.}} c\delta^3(\vec{r}) + d\vec{\nabla}\delta^3(\vec{r}) + \ldots \tag{2.5}$$

However, the first order energy shift of the second term of the expansion ($\vec{\nabla}\delta^3(\vec{r})$) is, once again, divergent. These infinites are the same kind that appear in QED loop calculation. We may be tempted to conclude that any attempt to further improve this approximation is due to fail, since the delta function proved to be too singular for our purposes. We next illustrate how EFT manages to "soften" the potential thus overcoming these difficulties. We define a renormalized effective Hamiltonian as:

$$H_{\text{eff}} = \frac{\vec{p}^2}{2m} - \frac{\alpha}{r} + V_{\text{eff}}$$

where the effective potential V_{eff} must turn into the correct form of the exact potential as $r \to \infty$. In order to avoid the infinities that plagued the approach attempted previously, a cutoff Λ must be introduced. For example, the delta function can be smeared over a distance $a = 1/\Lambda$ comparable to the range of V_s, which has the effect of inhibiting momentum transfers of order Λ and larger. One way to accomplish this is to multiply the delta functions in Equation (2.5) by a Gaussian of half-width a:

$$\delta^3_\Lambda(\vec{r}) = \frac{\exp\left(-\frac{r^2}{2a^2}\right)}{(2\pi^{\frac{3}{2}})a^3} \tag{2.6}$$

By excluding high-momentum transfers, we have in effect mutilated the real potential, so that short-range interactions must be replaced by a series of contact terms obtained from the Taylor expansions of the Fourier transformed potential. The final result is:

$$V_{\text{eff}}(\vec{r}) = c\Lambda^2\delta^3_\Lambda(\vec{r}) + d_1\nabla^2\delta^3_\Lambda(\vec{r}) + d_2\nabla\cdot\delta^3_\Lambda(\vec{r})\nabla + ... \tag{2.7}$$

The form of the effective potential is now totally determined, and it is completely independent from the short-range theory: only the parameters are theory-specific and contain all the informations relative to the potential under study. One then proceeds to fit these parameters to the data. The exact parameterization procedure can vary wildly among different approaches and we will leave it to the next Chapter to define the details of our method.

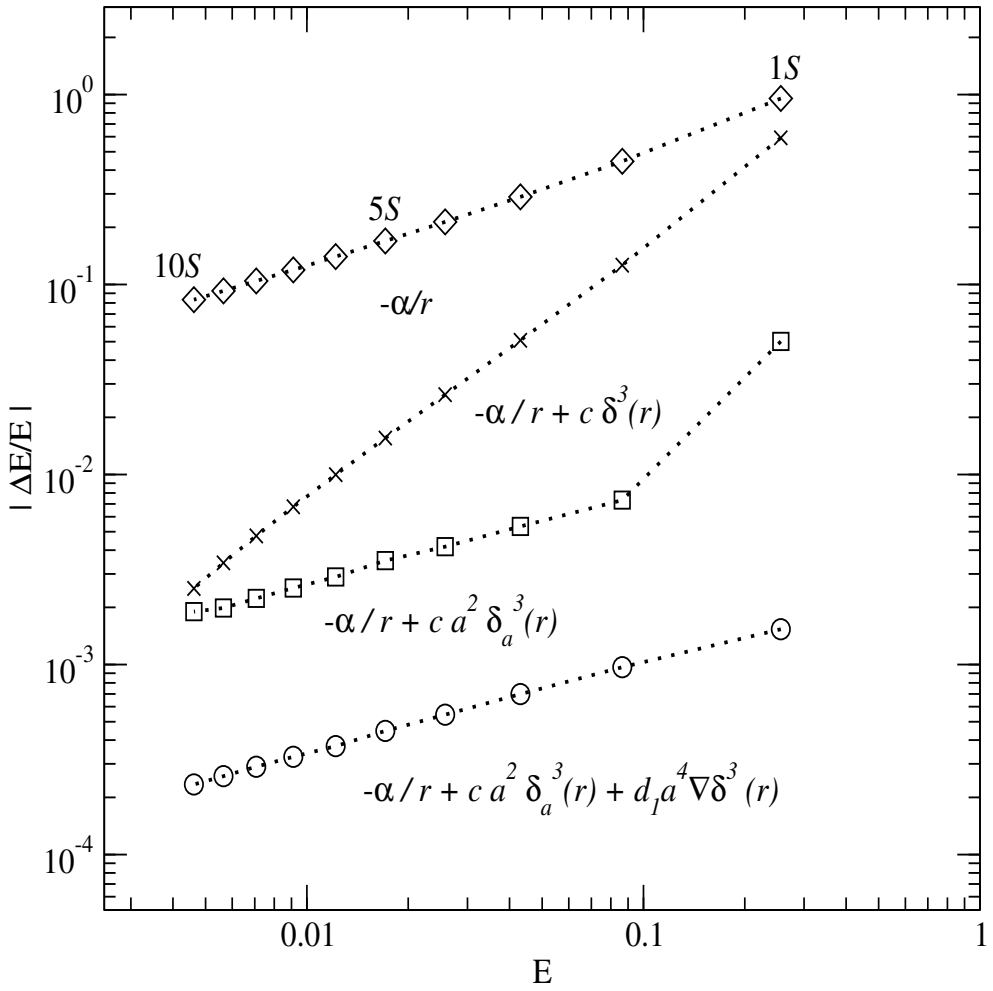

Figure 2.1. Relative errors of S states of the toy potential computed using different approximations. A second order effective potential can predict the exact ground state energy within 0.2%.

Here, we will simply state the results, which are shown in Figure 2.1. We computed energies of a variety of S-wave states of the exact Hamiltonian and of the corresponding renormalized operator. In the Figure we plotted the relative errors of each approximation with respect to the exact solution. The first approximation is obtained by excluding the short-range portion of the potential entirely and only retaining the Coulomb part of the interaction. In this case relative errors for high-energy states can be as high as 100% (for the 1S state.) This is indicative of the fact that, even though the perturbation is indeed short-ranged, it is not a

small one. Next, first order perturbation theory results are considered, with the perturbation replaced by a delta function. The approximation is successful enough but, as we have shown, cannot be improved any further. Finally, we included our EFT results, both first and second order, which show a decisive improvement of the predictions, even for low-S states, for which the approximation is supposedly less accurate. In fact, our second order effective potential predicts the ground-state energy within 0.2% of the exact value. These results are especially interesting given that they only required the tuning of two parameters.

2.2 CORE for the Shell Model

This approach to the many-body problem relies on the assumption (based on the Brueckner theory of matter) that the low-energy behavior of a large number of interacting nucleons can be approximated by retaining only few terms in a renormalized nucleon-cluster expansion. We now illustrate the fundamental points of a CORE implementation.

- In order to construct an effective operator for a range-N interaction in the cluster expansion we must be able to solve the corresponding N-body problem exactly. The effective operators obtained can then be embedded in the computations with range-$(N+1)$ or higher expansions. Choosing an adequate diagonalization basis is the first step in the procedure. It is usually a good idea to select a basis that reflects the symmetries of the bare Hamiltonian; for example, if the Hamiltonian is rotationally invariant, it could be useful to pick up states of definite total angular momentum.

- The basis set is reduced through a truncation scheme; that is, only states that contribute significantly to the low-energy spectrum are retained. Computations will be strongly simplified in this smaller Hilbert space.

- The effective Hamiltonian is renormalized by requiring that it should reproduce the low energy spectrum of the bare Hamiltonian exactly.

We adopt, as a starting point for the A-body system, the No-Core Shell Model approach [32, 33] which employs the one- plus two-body Hamiltonian:

$$H_A = \sum_{m=1}^{A} \frac{\vec{p}_m^{\,2}}{2m} + \sum_{m<n=1}^{A} V(|\vec{r}_m - \vec{r}_n|) \tag{2.8}$$

The kinetic part in Equation (2.8) can be split into a center-of-mass term and a term that only contains relative momenta. We modify H_A by inserting a center-of-mass Simple Harmonic Oscillator (SHO) potential: $\frac{1}{2}AM\Omega^2\vec{R}^2$ with $\vec{R} = \frac{1}{A}\sum_{i=1}^{A}\vec{r}_i$; this allows us to take into account the spurious center-of-mass contribution to the energy spectrum, which will be given by $E_A^\Omega = E_A + (\frac{3}{2} + n)\hbar\Omega$, where E_A is the actual intrinsic spectrum. The modified Hamiltonian, which now contains an artificial dependence on the oscillator frequency Ω can be cast into the form:

$$H_A^\Omega = \sum_{n=1}^{A}\left[\frac{\vec{p}_n^2}{2m} + \frac{1}{2}m\Omega^2 r_n^2\right] + \sum_{m<n=1}^{A}\left[V(\vec{r}_m - \vec{r}_n) - \frac{m\Omega^2}{2A}(\vec{r}_m - \vec{r}_n)^2\right]. \tag{2.9}$$

The lowest range contribution to the cluster expansion is the one-body (that is, no interactions) term:

$$H_{\text{eff}}^{(1)} = \sum_{n=1}^{A} h_n \equiv \sum_{n=1}^{A}\left[\frac{\vec{p}_n^2}{2m} + \frac{1}{2}m\Omega^2\vec{r}_n^2\right] \tag{2.10}$$

This one-body Hamiltonian is trivially diagonalized. The basis set is then truncated by retaining only the first N harmonic oscillator states. Once the effective range-1 term is constructed, one proceeds to find a renormalized Hamiltonian that contains range-2 (pairwise) interactions. To diagonalize the two-body Hamiltonian (we must be able to do it exactly) we retain a very large number of states $N_\infty \gg N$; we will then obtain eigenstates $|E_n\rangle$ with eigenvalues E_n for $n = 0, 1, \ldots N_\infty$. The truncated basis will be formed by the direct product of the retained one-body SHO states.

$$|\psi_n\rangle \equiv |n_1\rangle \otimes |n_2\rangle; \qquad (n = 1, 2, \ldots, N \times N) \tag{2.11}$$

This set of states will span a reduced Hilbert space that will be used to build the effective two-body Hamiltonian. We now introduce the imaginary time evolution operator e^{-tH} (usually referred to as the "contractor" operator [35, 36]). To observe its effect on the model states $|\psi_n\rangle$ we expand them in the $|E_n\rangle$ basis:

$$e^{-tH}|\psi_n\rangle = \sum_n e^{-tH}|E_n\rangle\langle E_n|\psi_n\rangle = \sum_n e^{-tE_n}|E_n\rangle\langle E_n|\psi_n\rangle. \tag{2.12}$$

One can then easily see that, in the limit of large t, the contribution from the lowest energy eigenstate will dominate. The overall effect of this operator on any model space state is

then to contract it onto the lowest eigenstate of the exact Hamiltonian with which it has a non-vanishing overlap. CORE, on the other hand, demands a one-to-one mapping of the model space onto the exact eigenstates space. We therefore must pay particular attention to the overlap of the truncated low-energy basis with the exact states. It will in general be necessary to perform a rotation of the truncated space $|\psi_n\rangle$ in order to construct a new basis set $|\xi_j\rangle$ which satisfies the following condition:

$$\lim_{t\to\infty} e^{-tH}|\xi_j\rangle \propto |E_j\rangle \tag{2.13}$$

The single-contraction condition of Equation (2.13), which in effect requires a systematic orthogonalization of the basis set, is the main feature that separates CORE from analogous similarity transformation techniques. The effective Hamiltonian for the two-body problem is now uniquely defined by the similarity matrix $S_{mn} \equiv \langle\phi_m|\xi_n\rangle$:

$$H_{\text{eff}}(1,2) \equiv S E_{\text{diag}} S^T. \tag{2.14}$$

where

$$E_{\text{diag}} \equiv \begin{pmatrix} E_0 & 0 & \cdots & 0 \\ 0 & E_1 & & \vdots \\ \vdots & & \ddots & 0 \\ 0 & \cdots & 0 & E_N \end{pmatrix} \tag{2.15}$$

The effective two-body interaction is obtained by subtracting the one-body terms from the total effective Hamiltonian. That is,

$$h_2(1,2) = H_{\text{eff}}(1,2) - h_1(1) - h_1(2). \tag{2.16}$$

The range-2 effective Hamiltonian for A nucleons contains a sum of one-body terms plus a series of pairwise interactions:

$$H_{\text{eff}}^{(2)} = \sum_{n=1}^{A} h_1(n) + \sum_{m<n=1}^{A} h_2(m,n). \tag{2.17}$$

In general, the complete renormalized Hamiltonian for an infinite lattice will be given by:

$$H_{\text{eff}} = \sum_{j=1}^{\infty}\sum_{r=1}^{\infty} h_r(j,\ldots,j+r-1) \tag{2.18}$$

CHAPTER 3

EFFECTIVE TWO-BODY POTENTIALS AND OPERATORS

3.1 Formalism

Part of the inspiration for the operator methods reported here arose from an especially simple derivation of effective-range theory which appears in the texts by Schiff and Taylor. The aim of this section is to adapt a textbook derivation of the effective-range formula in three spatial dimensions [61, 62], to the one-dimensional (1D) problem considered here. These ideas are then used for the construction of an effective interaction that reproduces the scattering length and effective range of the exact (*i.e.,* bare) theory. Finally, an approach is proposed for the renormalization of operators in a manner consistent with the construction of the effective interaction.

3.1.1 Effective-range formula

To arrive at the effective-range formula we proceed along the lines of Schiff and Taylor [61, 62], adapting their derivation to the one-dimensional case considered here. The even-parity solution of the scattering problem satisfies the time-independent Schrödinger equation

$$\left[\frac{d^2}{dx^2} + k^2 - U(x)\right]\psi_k(x) = 0 \quad \Big(k^2 \equiv 2\mu E \ \text{ and } \ U(x) \equiv 2\mu V(x)\Big)\,, \tag{3.1}$$

subject to the following boundary conditions:

$$\lim_{x\to 0}\psi_k(x) \;=\; 1 + \mathcal{O}(x^2)\,, \tag{3.2a}$$

$$\lim_{x\to\infty}\psi_k(x) \;=\; \phi_k(x) \equiv \cos(kx) - \tan\delta(k)\sin(kx) = \frac{\cos\big(kx+\delta(k)\big)}{\cos\delta(k)}\,. \tag{3.2b}$$

Note that $\phi_k(x)$ denotes the solution of the free Schrödinger ($U(x) \equiv 0$) equation that coincides with $\psi_k(x)$ at large x. It then follows immediately from Schrödinger's equation that

$$\frac{dW(\psi_k,\psi_0)}{dx} = k^2\psi_k(x)\psi_0(x) \;, \tag{3.3a}$$

$$\frac{dW(\phi_k,\phi_0)}{dx} = k^2\phi_k(x)\phi_0(x) \;, \tag{3.3b}$$

where the Wronskian of f and g is defined as

$$W(f,g)(x) \equiv \begin{vmatrix} f(x) & g(x) \\ f'(x) & g'(x) \end{vmatrix} = \Big[f(x)g'(x) - f'(x)g(x)\Big] \;. \tag{3.4}$$

Upon integrating the difference of Equations (3.3) one obtains

$$\Big[W(\phi_k,\phi_0)(x) - W(\psi_k,\psi_0)(x)\Big]_0^\infty = k^2\int_0^\infty dx\Big(\phi_k(x)\phi_0(x) - \psi_k(x)\psi_0(x)\Big) \;. \tag{3.5}$$

The contribution from the upper limit of the integral to the left-hand side of the equation vanishes, as $\psi_k(x)=\phi_k(x)$ at large distances. Further, as the derivative of the exact scattering solution vanishes at $x = 0$ [see Equation (3.2a)] the Wronskian $W(\psi_k,\psi_0)$ vanishes as well. This yields

$$W(\phi_k,\phi_0)(x=0) = \Big[\phi_k(0)\phi_0'(0) - \phi_k'(0)\phi_0(0)\Big] = k^2\int_0^\infty dx\Big(\phi_k(x)\phi_0(x) - \psi_k(x)\psi_0(x)\Big) \;, \tag{3.6}$$

which in turn generates the well known effective-range formula

$$k\tan\delta(k) = \frac{1}{a_0} - k^2\int_0^\infty dx\Big(\psi_k(x)\psi_0(x) - \phi_k(x)\phi_0(x)\Big) = \frac{1}{a_0} - \frac{r_0}{2}k^2 + \mathcal{O}(k^4) \;. \tag{3.7}$$

Note that the (even-parity) scattering length and effective range parameters have been defined as

$$a_0^{-1} = \lim_{k\to 0} k\tan\delta(k) \;, \quad r_0 = 2\int_0^\infty dx\Big(\psi_0^2(x) - \phi_0^2(x)\Big) \;. \tag{3.8}$$

3.2 Effective Potential

The purpose of this section is to summarize briefly the main points from Ref. [37] which will, in turn, motivate our proposed method for constructing effective operators. To start, a bare one-dimensional NN interaction with the same pathologies as a realistic interaction is

assumed. That is, the bare potential is given by the sum of a strong short-range repulsive and a medium-range attractive exponentials:

$$V(x) = V_{\rm s}\ e^{-m_{\rm s}|x|} + V_{\rm v}\ e^{-m_{\rm v}|x|}\ . \tag{3.9}$$

The two masses were chosen to be equal to $m_{\rm s}=400$ MeV and $m_{\rm v}=783$ MeV, respectively, while the strengths of the potentials ($V_{\rm s} = -506$ MeV and $V_{\rm v} = +1142.49$ MeV) were chosen to give a binding energy and point root-mean-square (rms) radius for the symmetric ("deuteron") state of $E_{\rm b}=-2.2245$ MeV and $r_{\rm rms}=1.875$ fm, respectively.

Employing an option originally suggested by Lepage[18], and later adapted by Steele and Furnstahl [63, 64] to treat the NN interaction, we propose a gaussian cutoff for the effective potential of the form

$$V_{\rm eff}(x) = \frac{1}{a}\left(c + d\frac{\partial^2}{\partial\xi^2} + e\frac{\partial^4}{\partial\xi^4} + \ldots\right)\exp(-\xi^2)\ ; \quad \xi \equiv x/a\ . \tag{3.10}$$

The parameters of the effective potential (c, d, $e, \ldots$) are fixed to reproduce the low-energy scattering phase shifts. That is, one adjusts the parameters until the following equation is satisfied:

$$\begin{aligned} k\tan\delta(k) &= \frac{1}{a_0} - k^2\int_0^\infty dx\Big(\psi_k(x)\psi_0(x) - \phi_k(x)\phi_0(x)\Big) &(3.11)\\ &= \frac{1}{a_0} - k^2\int_0^\infty dx\Big(\psi_k^{\rm eff}(x)\psi_0^{\rm eff}(x) - \phi_k(x)\phi_0(x)\Big)\ , &(3.12)\end{aligned}$$

where $\psi_k^{\rm eff}(x)$ is a scattering solution of Equation (3.1) with $V(x)$ replaced with $V_{\rm eff}(x)$. Note that as in Ref. [37], the gaussian cutoff parameter has been fixed at $a=1.16$ fm. The above condition may be rewritten in the following convenient form:

$$\delta\langle\mathcal{I}\rangle(k;c,d,\ldots) \equiv \int_0^\infty dx\Big(\psi_k(x)\psi_0(x) - \psi_k^{\rm eff}(x)\psi_0^{\rm eff}(x)\Big) \equiv 0\ . \tag{3.13}$$

Evidently, it is neither demanded nor expected that Equation (3.13) be satisfied for arbitrary large values of k. Rather, one follows a hierarchical scheme, based on power counting, that assures that observables in the bare and effective theory be indistinguishable at low energies. It should be emphasized that the specific form of the potential is somewhat arbitrary, as the short-range structure of the theory becomes encoded in the effective parameters.

As a simple illustration of this procedure we display in Figure 3.1 bare (solid line) and effective (dashed line) NN potentials. The bare potential, with its characteristic short-range

structure, yields a scattering length of $a_0 = 5.247$ fm and an effective range of $r_0 = 1.521$ fm, respectively. The calculation of low-energy phase shifts is repeated using the 2nd order effective potential [Equation (3.10)] with its two parameters (c and d) adjusted to reproduce the exact effective-range expansion to order k^2. The resulting parameters ($c = -0.039$ and $d = -0.160$) are natural and yield a smooth effective potential which as far as the low-energy properties of the theory are concern, is practically indistinguishable from the bare potential. Indeed, bulk properties of the ground-state (henceforth referred to as the "deuteron") are predicted to be identical to those obtained in the bare theory. This is in spite of the vastly different short-range structure of the wave-functions (see inset in Figure 3.1).

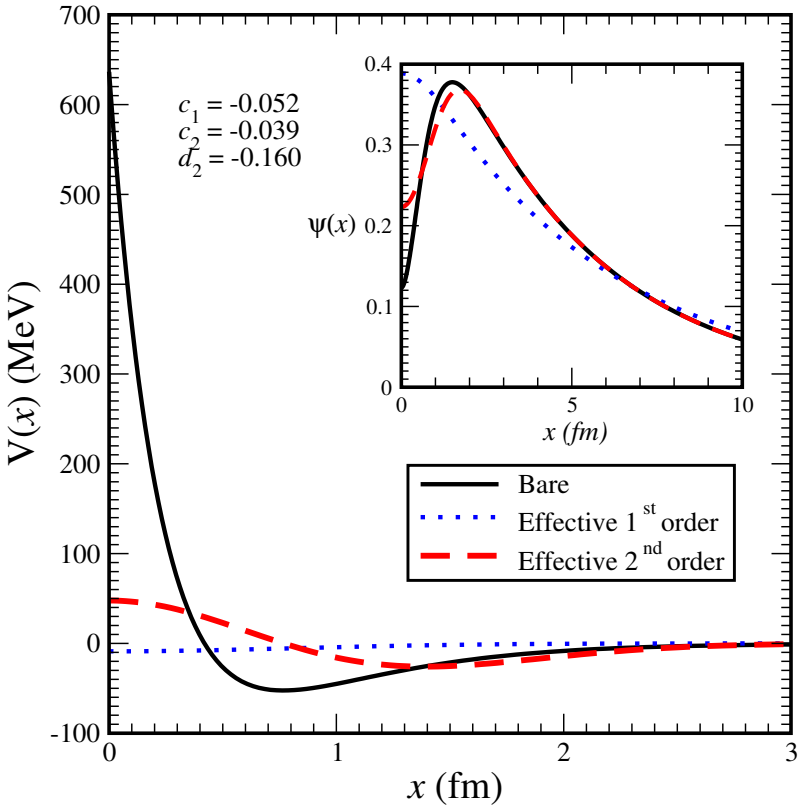

Figure 3.1. Bare (solid line), effective through 1st order (dotted line) and effective through 2nd order (dashed line) NN potentials in a realistic 1-dimensional model. The inset shows "deuteron" ground-state wave-functions. The sharp features of the bare potential are no longer present in the effective potentials. Although the short-distance structure of the wave-functions are different, the exponential falloff (binding energy) is unchanged.

3.3 Effective Operators

One of the main criticisms levied on traditional shell-model approaches is the lack of consistency between the construction of the effective potential and the renormalization (if any) of the bare operators [15, 16]. While important steps have been taken to correct this inconsistency, both in the area of low-dimensional quantum magnets [57] and nuclear structure [33], these are in the very early stages. Further, it is unknown how to construct effective operators that are consistent with both the effective theory and similarity-transformation based approaches.

In this contribution we propose an approach for the modification of operators that is consistent, indeed mimics, the construction of the effective potential. We assume that the momentum dependence of matrix elements of (simple) single-particle operators may be accounted for by an expansion in powers of k^2 having the same form as the effective-range formula [Equation (3.7)]. To do so one demands that matrix elements of effective operators ($\mathcal{O}_{\text{eff}}$) with scattering-wave solutions of the effective potential (ψ_k^{eff}) possess the same momentum dependence as those using the bare operators with the exact wave-functions. In analogy with the definition of the effective potential [Equation (3.10)], we parametrize the effective operators via

$$\mathcal{O}_{\text{eff}}(x; c, d, \ldots) = \mathcal{O}(x) \left[1 + \left(c + d \frac{\partial^2}{\partial \xi^2} + \ldots \right) \exp(-\xi^2) \right] . \tag{3.14}$$

This parameterization affects only the short-range behavior of the operator just as using the effective potential modifies only the short-range structure of the wave-function. The parameters c, d, ... (as before) are tuned to the low-k^2 behavior of the exact matrix elements. To be more specific about our procedure, we fit—in complete analogy to Equation (3.13)—the parameters of the effective operator by requiring that

$$\delta\langle\mathcal{O}\rangle(k; c, d, \ldots) \equiv \int_0^\infty dx \Big(\psi_k(x) \mathcal{O}(x) \psi_{k=0}(x) - \psi_k^{\text{eff}}(x) \mathcal{O}_{\text{eff}}(x; c, d, \ldots) \psi_{k=0}^{\text{eff}}(x) \Big) = 0 . \tag{3.15}$$

The integral in this expression is convergent as the effective theory demands that

$$\lim_{x\to\infty} \psi_k^{\text{eff}}(x) = \psi_k(x) , \tag{3.16a}$$

$$\lim_{x\to\infty} \mathcal{O}_{\text{eff}}(x; c, d, \ldots) = \mathcal{O}(x) . \tag{3.16b}$$

However, to insure that each term separately is convergent, we add and subtract the following term:

$$\int_0^\infty dx \Big(\phi_k(x) \mathcal{O}(x) \phi_{k=0}(x) \Big) \,, \tag{3.17}$$

where we recall that $\phi_k(x)$ is the free solution of the 1D scattering problem [see Equation (3.2b)].

To extract the parameters of the effective operator we now fit—in the spirit of the effective-range expansion—the low-energy matrix elements of the bare operator between bare scattering wave-functions according to

$$\langle \mathcal{O} \rangle_{\rm BB}(k) = \int_0^\infty dx \Big(\psi_k(x) \mathcal{O}(x) \psi_{k=0}(x) - \phi_k(x) \mathcal{O}(x) \phi_{k=0}(x) \Big) = \alpha + \beta k^2 + \dots \tag{3.18}$$

The parameters fixing the effective operators are then adjusted so that the above expansion be recovered. That is,

$$\langle \mathcal{O} \rangle_{\rm EE}(k) = \int_0^\infty dx \Big(\psi_k^{\rm eff}(x) \mathcal{O}_{\rm eff}(x; b, c, \dots) \psi_{k=0}^{\rm eff}(x) - \phi_k(x) \mathcal{O}(x) \phi_{k=0}(x) \Big) = \alpha + \beta k^2 + \dots \tag{3.19}$$

Note that when $\mathcal{O}(x) = \mathcal{O}_{\rm eff} = 1$ one recovers the effective-range expansion.

3.4 Results

In this section we compute matrix elements of various operators using three different schemes. The first scheme uses bare operators with bare wave-functions (we label these calculations as "B+B"); these should be regarded as "exact" answers. Second, we compute matrix elements in an approximation (labeled as "B+E") that uses effective wave-functions but retains bare operators. As we show below, for operators insensitive to short-range physics this inconsistency introduces small discrepancies. Yet, the more important the short-range physics, the greater the lack of accord. Finally, we perform calculations in a consistent low-energy approximation ("E+E") that employs both effective wave-functions and effective operators. Showing that these calculations are in excellent agreement with the exact (B+B) answers represents the central result of the present work.

Because of its simplicity, a natural place to start testing the proposed approach is the calculation of the root-mean-square radius of the deuteron, which is given by

$$\langle x^2 \rangle_{BB} \equiv \Big\langle \frac{1}{2} \sum_{n=1}^{2} \Big(x_n - x_{\rm cm} \Big)^2 \Big\rangle = \int_{-\infty}^{\infty} dx \frac{x^2}{4} \psi_{\rm gs}^2(x) = (1.87977)^2 \text{ fm}^2 \,. \tag{3.20}$$

The corresponding calculation in the effective theory requires a renormalization of the bare operator. To do so we follow the prescription outlined in the preceding section [see Equations (3.18) and (3.19)] to obtain

$$x^2_{\rm eff} = x^2 \left[1 + \left(c + d \frac{\partial^2}{\partial \xi^2} \right) \exp(-\xi^2) \right] \quad (c = 1.520, d = -0.305) \ . \tag{3.21}$$

In this manner the root-mean-square radius predicted by the effective theory becomes

$$\langle x^2 \rangle_{\rm EE} = \int_{-\infty}^{\infty} dx \frac{x^2_{\rm eff}}{4} \Big(\psi^{\rm eff}_{\rm gs}(x) \Big)^2 = (1.87988)^2 \ {\rm fm}^2 \ . \tag{3.22}$$

This represents a discrepancy of about 1 part in 10^4. While this result is gratifying and lends some validity to the approach, it hardly qualifies as a stringent test of the formalism. Although both the effective operator and the ground-state wave-function are modified at short distances (see Figure 3.1 and 3.2) the operator itself has so little support at short distances, that the two integrands [Equations (3.20) and (3.22)] become practically indistinguishable from each other (see Figure 3.3 and inset). Indeed, an acceptable result is obtained even when the operator is not properly renormalized:

$$\langle x^2 \rangle_{\rm BE} = \int_{-\infty}^{\infty} dx \frac{x^2}{4} \Big(\psi^{\rm eff}_{\rm gs}(x) \Big)^2 = (1.87834)^2 \ {\rm fm}^2 \ . \tag{3.23}$$

A more sensitive test of the approach is provided by the elastic form factor of the deuteron, which in one spatial dimension reduces to the following simple expression:

$$F_{\rm el}(q) = |\rho(q)|^2 \ , \quad \rho(q) = \int_{-\infty}^{\infty} dx \cos\left(\frac{qx}{2} \right) \psi^2_{\rm gs}(x) = 1 - \frac{q^2}{2} \langle x^2 \rangle + \mathcal{O}(q^4) \ . \tag{3.24}$$

The corresponding expressions in the B+E and E+E approximations are given by

$$\rho(q)_{\rm BE} = \int_{-\infty}^{\infty} dx \cos\left(\frac{qx}{2} \right) \Big(\psi^{\rm eff}_{\rm gs}(x) \Big)^2 \ , \tag{3.25a}$$

$$\rho(q)_{\rm EE} = \int_{-\infty}^{\infty} dx \left[\cos\left(\frac{qx}{2} \right) \right]_{\rm eff} \Big(\psi^{\rm eff}_{\rm gs}(x) \Big)^2 \ , \tag{3.25b}$$

with the effective operator renormalized at short-distances as detailed above. That is,

$$\left[\cos\left(\frac{qx}{2} \right) \right]_{\rm eff} = \cos\left(\frac{qx}{2} \right) \left[1 + \left(c(q) + d(q) \frac{\partial^2}{\partial \xi^2} \right) \exp(-\xi^2) \right] \ , \tag{3.26}$$

The renormalization procedure is illustrated in Figure 3.4 at the single momentum-transfer value of $q = 2$ fm^{-1}. Note, however, that the renormalization coefficients (c and d) must

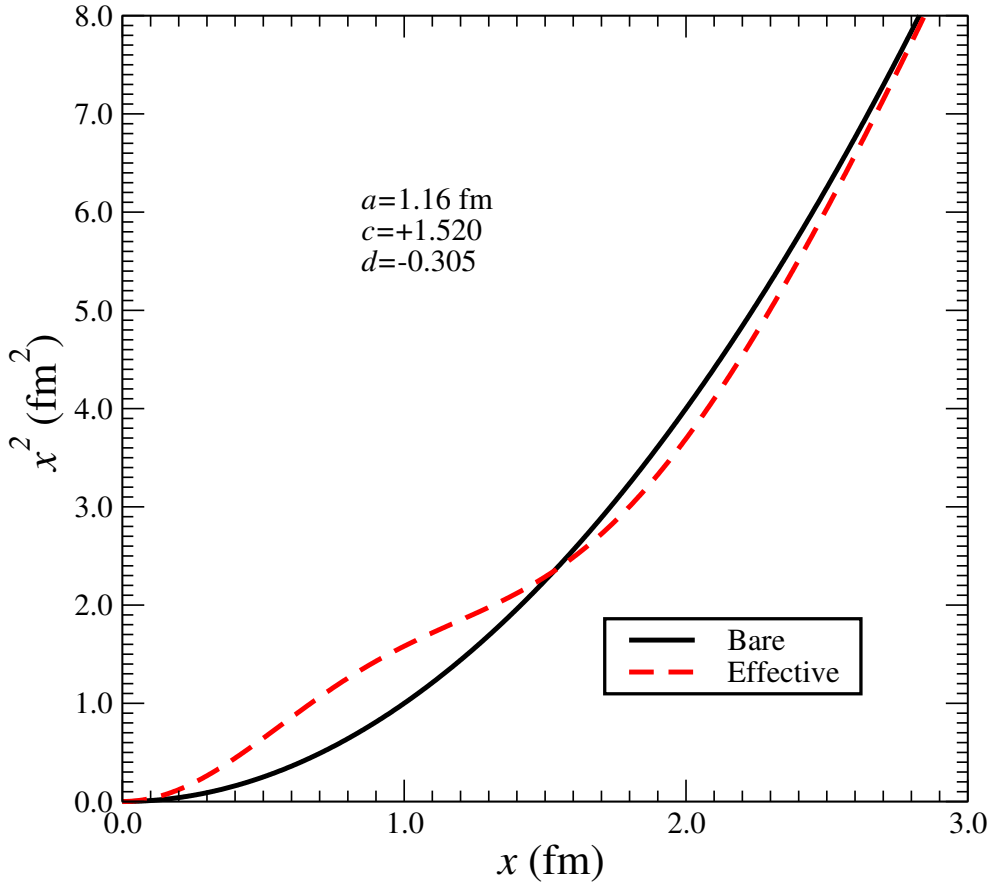

Figure 3.2. Bare (solid line) and effective (dashed line) x^2 operator

be tuned at each value of the momentum transfer q. The solid line in the figure displays an effective-range-like expansion for the bare operator $\mathcal{O}(x) = \cos(qx/2)$ [as described in Equation (3.18), with the slope and intercept clearly indicated in the figure (note that for clarity the plots are normalized to one at $k^2 = 0$). It becomes immediately evident that the predicted low-energy behavior of the exact theory can not be reproduced without a proper renormalization of the operator. Indeed, the B+E calculation predicts the wrong momentum dependence; the sign of the slope is wrong! In contrast, it becomes a simple matter to tune the parameters of the effective operator to reproduce exactly the low-energy behavior of the exact theory (dashed line). Having corrected the short-distance structure of the operator one proceeds to compute the elastic form factor of the deuteron, which now becomes a prediction

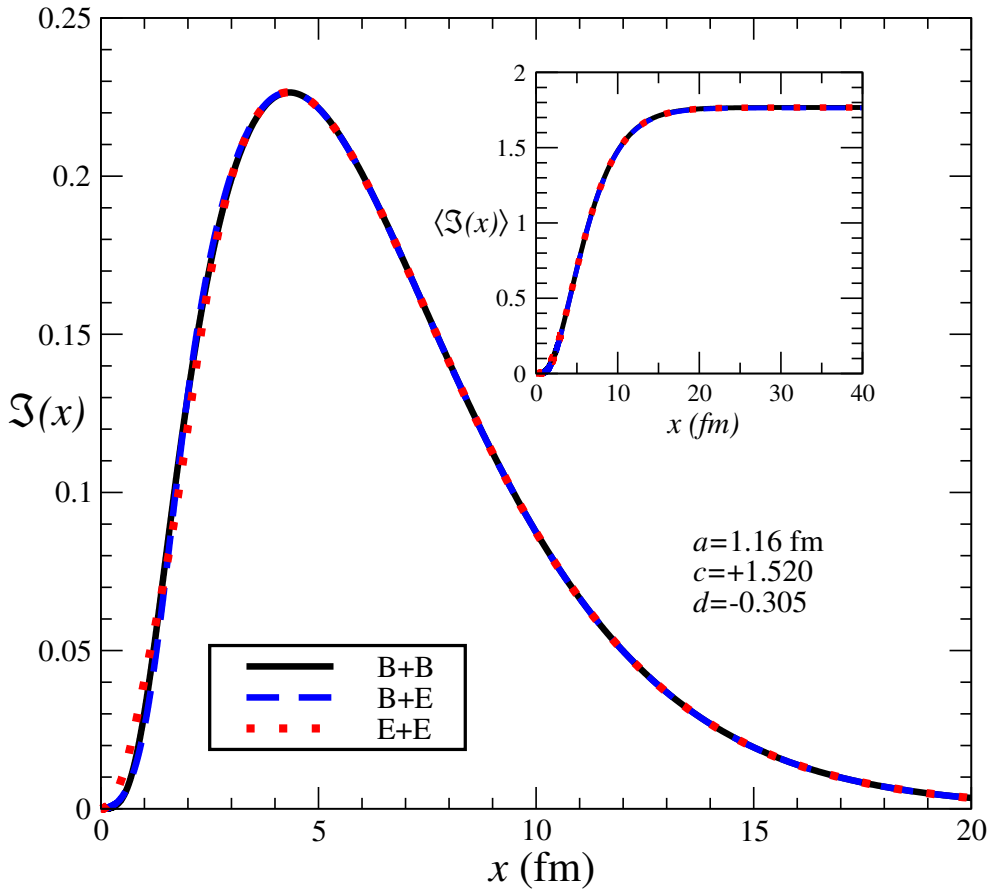

Figure 3.3. Integrands Equations (3.20) and (3.22). The dashed line represent a mixed integrand with a renormalized wave-function and a bare operator. The inset shows the cumulative integrand as a function of x.

of the effective theory. The structure of the form factor (again at $q = 2$ fm^{-1}) is shown in Figure 3.5, where bare (*i.e.*, $\cos(x)$) and effective operators are displayed as solid and dashed lines respectively. Both the effective deuteron wave-function (inset on Figure 3.1) and the effective operator differ considerably from their bare counterparts at short distances—and so is the product of the (square of the) wave-function with the operator (Figure 3.6). Yet the area under the curve (inset in Figure 3.6)—whose square is proportional to the elastic form factor—is essentially unchanged. For comparison, the exact (B+B) and effective (E+E) theories yield values of $F_{\rm el} = 0.02019$ and $F_{\rm el} = 0.02012$, respectively. In contrast, a (B+E)

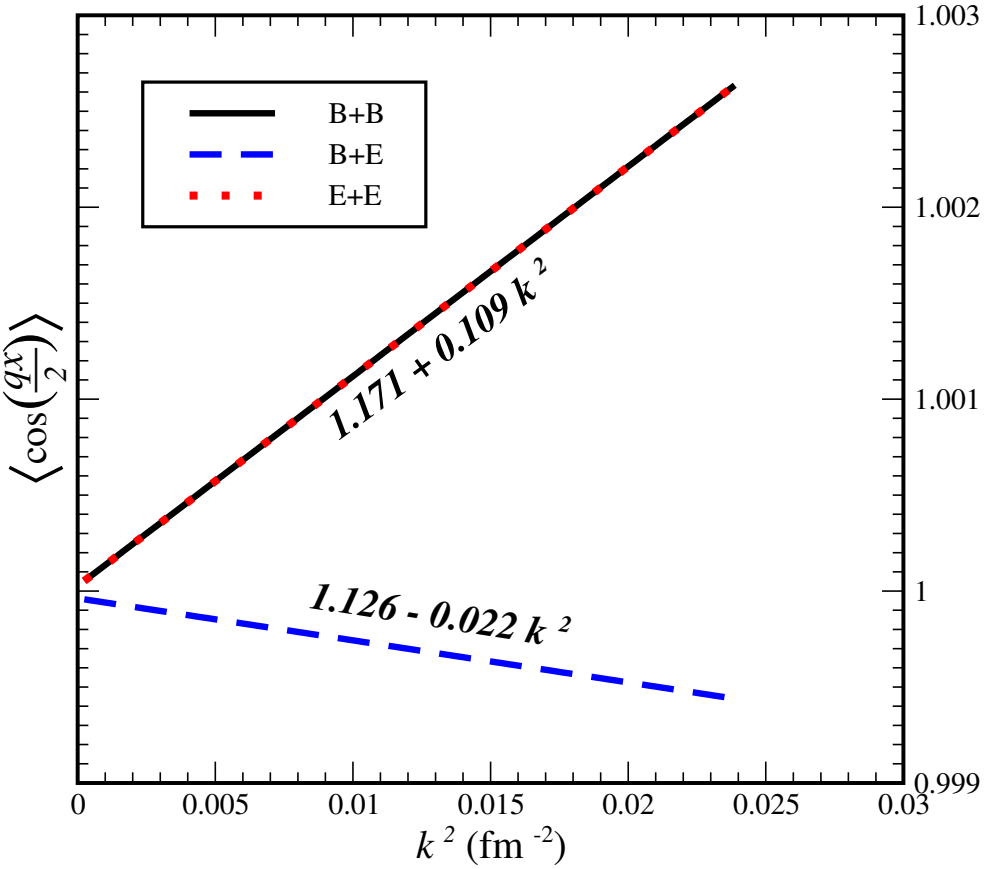

Figure 3.4. An effective-range-like expansion for the elastic form factor of the deuteron at $q = 2$ fm^{-1}. Calculations are displayed for the bare theory ("B+B"), the effective theory ("E+E"), and for a "hybrid" approximation that uses bare operators with effective wave-functions ("B+E"). The solid (B+B) and dotted lines (E+E) are identical (by construction) since the effective parameters (c and d) are tuned to reproduce the expansion for the bare theory.

calculation with an effective wave-function—but still with a bare operator—results in almost a 20% discrepancy ($F_{\rm el} = 0.017062$).

We conclude the discussion of the elastic form factor of the deuteron by displaying in Figure 3.7 its momentum-transfer dependence up to $q = 5$ fm^{-1}. Recall that effective parameters must be tuned for every value of q. It is evident from the figure that the renormalization of the operator at high-momentum transfers is essential, as it is at high q that the short-distance structure of the wave-function (and of the potential) is being probed.

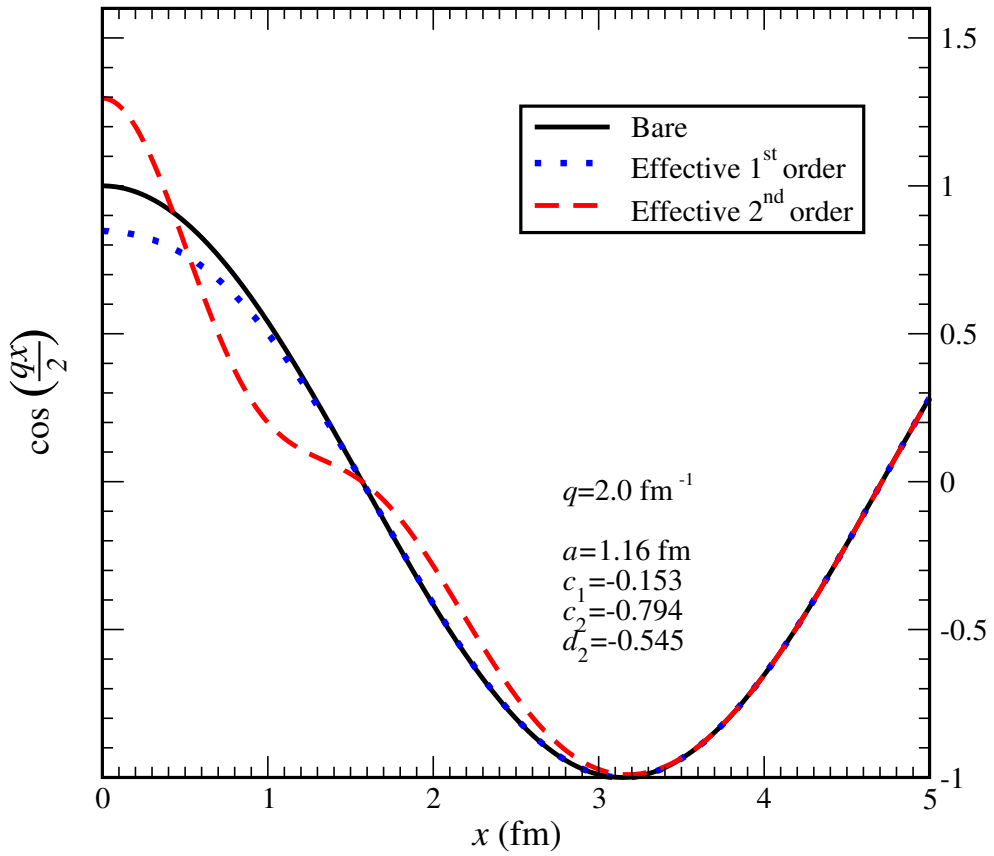

Figure 3.5. Bare (solid line), effective through 1st order (dotted line) and effective through 2nd order (dashed line) for the $\cos(x)$ operators.

Failing to correct the operator results in a rather poor representation of the elastic form factor (squares in the figure).

For completeness, and as a further stringent test of the formalism, we compute ground-state observables for an operator with an anomalous short-range structure: the Dirac delta function. In the bare theory the ground-state expectation value is simply given by the square of the deuteron wave-function at the origin. That is,

$$\langle \delta(x) \rangle = \int_{-\infty}^{\infty} dx \delta(x) \psi_{\rm gs}^2(x) = \psi_{\rm gs}^2(0) = 0.01521 {\rm fm}^{-1} \ . \tag{3.27}$$

As the sharp features of the bare potential are no longer present in the effective potential, the effective deuteron wave-function at short distances is considerably larger than the bare wave-

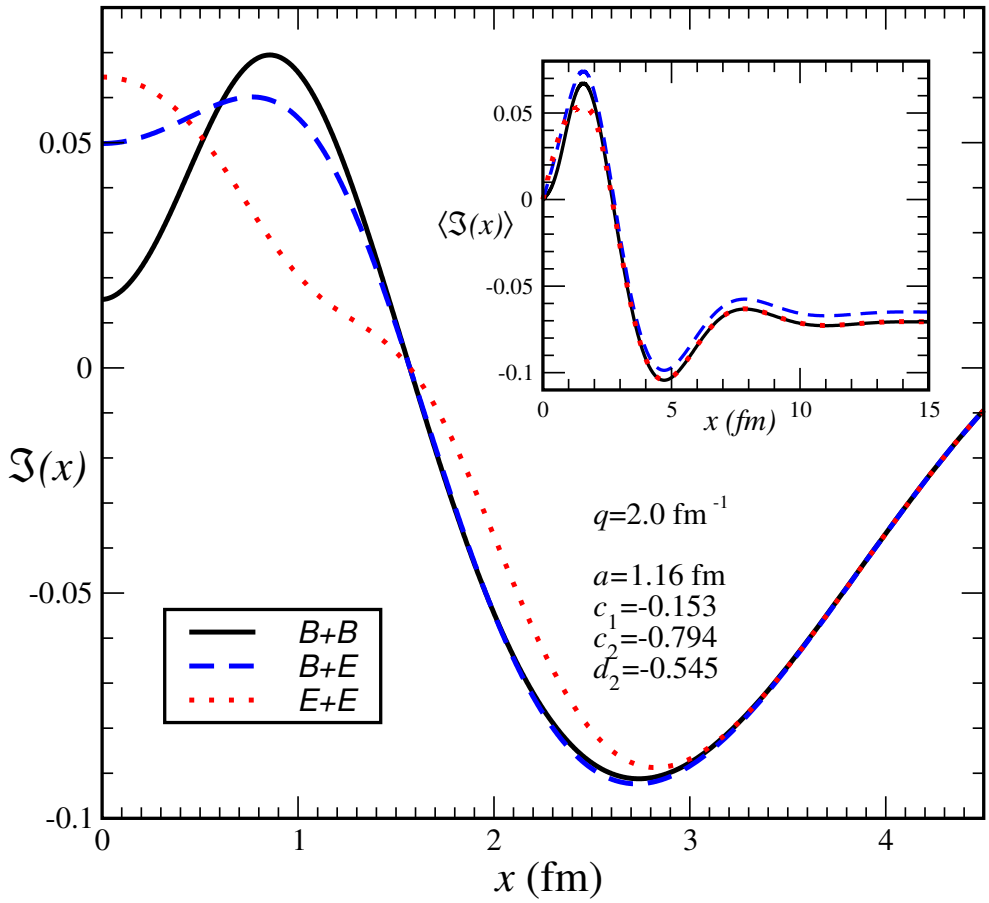

Figure 3.6. Product of the square of the wave-function with the operator $\cos(x)$ for the three calculations discussed in the text. The elastic form factor of the deuteron (at $q=2$ fm^{-1}) is proportional to the square of the area under the curve, shown in the inset as a function of x

function (see Figure 3.1). As a result, a (B+E) calculation using an effective wave-function but a bare delta-function operator grossly overestimates the result: $\langle\delta(x)\rangle_{BE}=0.04981\text{fm}^{-1}$. Instead, by following the renormalization procedure outlined above, one obtains an effective Dirac delta-function operator,

$$\delta_{\text{eff}}(x)=\frac{1}{a}\left(c+d\frac{\partial^2}{\partial\xi^2}\right)\exp(-\xi^2)\quad(c=0.250,d=-0.035)\ , \tag{3.28}$$

that yields a ground-state expectation value of $\langle\delta(x)\rangle_{EE}=0.01523$ fm^{-1}. This result deviates from the exact value by one part in a thousand.

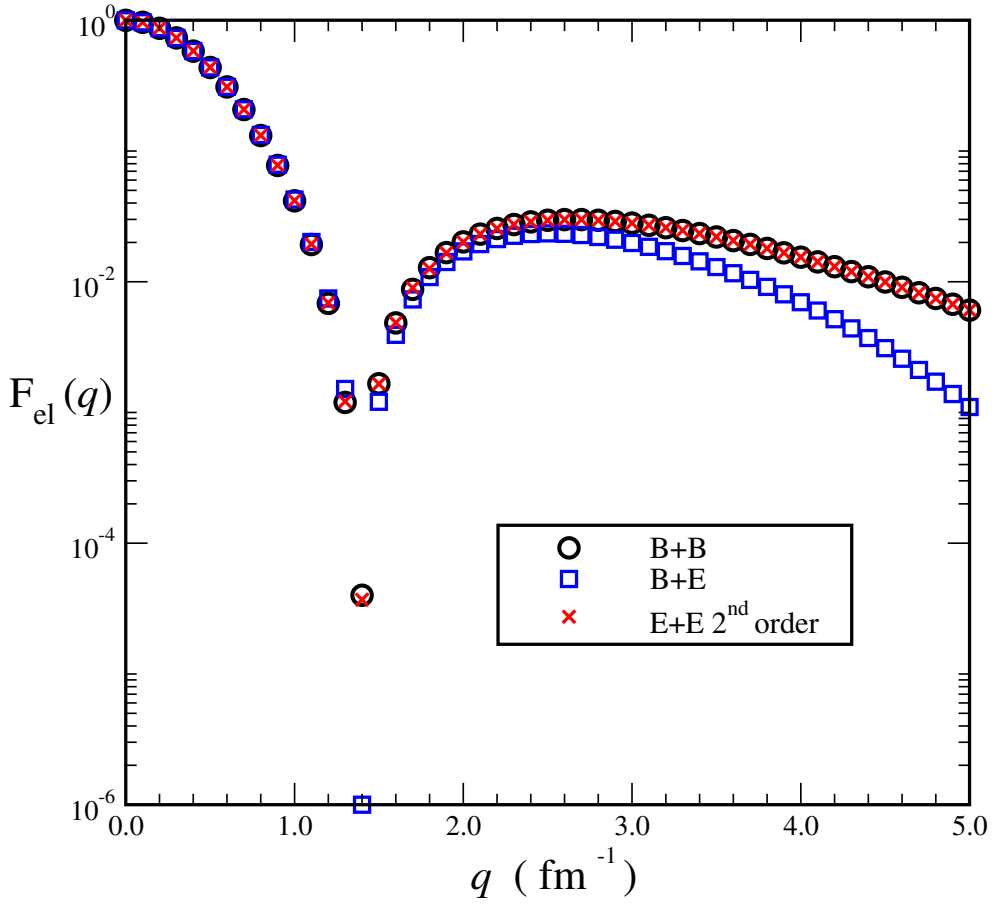

Figure 3.7. The elastic form factor of the deuteron in the three calculations discussed in the text. Note that the predictions from the effective theory (E+E) agrees with the exact theory at all values of the momentum transfer q.

In Table 3.1 we have compiled (for completeness) some of the results presented in graphical form. The operators appearing in this table are listed in order of the importance of their short-range components. For example, the root-mean-square radius of the deuteron depends little on the short-range structure of the wave-function while the Dirac δ-function operator depends exclusively on it. For each operator, we show the two effective coefficients c and d determined by the fitting procedure outlined above. All these are dimensionless quantities and it is gratifying that they are all of order one in keeping with the notion of "naturalness". We note that in some cases failing to renormalize the operator (B+E) leads

to discrepancies that are as large as 50% or even 100%. In contrast, calculations using effective wave-functions and effective operators (E+E) show excellent agreement with B+B calculations regardless of the short-range structure of the operator. We stress that all these are predictions of the effective theory, as the tuning of parameters is done in the scattering sector. In particular it is satisfying that, while there is no guarantee, the elastic form factor of the deuteron at $q=0$ deviates from unity by less than 2 parts in a thousand.

Table 3.1. Ground-state expectation values for various operators in the different approximation schemes described in the text. B+B indicates bare operators with bare wave-functions, B+E bare operators with effective wave-functions, and E+E effective operators with effective wave-functions. Note that the root-mean-square radii are given in fm and $\langle\delta(x)\rangle$ in fm^{-1}. Finally, the c and d coefficients are dimensionless parameters of the effective theory.

$\langle\mathcal{O}(x)\rangle$	c	d	B+B	B+E	E+E
$\sqrt{< x^2 >}$	$+1.51979$	-0.30545	1.87997	1.87834 (0.09%)	1.87988 (0.01%)
$\lvert\langle\cos(0)\rangle\rvert^2$	-0.02016	$+0.02985$	1.00000	1.00000 (0.00%)	1.00155 (0.16%)
$\lvert\langle\cos(x/2)\rangle\rvert^2$	-0.06440	$+0.13429$	0.04159	0.04261 (2.45%)	0.04181 (0.53%)
$\lvert\langle\cos(x)\rangle\rvert^2$	-0.79386	-0.54503	0.02019	0.01706 (18.4%)	0.02012 (0.35%)
$\lvert\langle\cos(2x)\rangle\rvert^2$	-0.52925	$+0.14806$	0.01541	0.00698 (220%)	0.01544 (0.19%)
$\langle\delta(x)\rangle$	$+0.24964$	-0.03501	0.01521	0.04981 (327%)	0.01523 (0.13%)

CHAPTER 4

CALCULATIONS FOR A ONE-DIMENSIONAL THREE-NUCLEON SYSTEM

4.1 Introduction

In Chapter 3 we illustrated how effective two-body potentials and operators can be constructed in the framework of Effective Field Theories. The calculations in this Chapter are meant to be a further stringent test of the reliability of such approach when applied to its natural extension, many-body systems. We will consider the simplest of these, the three-nucleon system in one dimension and propose a variety of different methods for the computation of its ground state energy. Our goal is to study how calculations employing bare potentials compare to identical calculations using two-body effective potentials. The Hamiltonian of such a system is given by:

$$H = \sum_{i<j}^{3} \frac{p_i^2}{2m} + V\left(|x_i - x_j|\right)$$

where $V(x)$ is a bare or effective two body potential. Recall that the bare potential is given by:

$$V_{\text{bare}}(x) = V_s e^{-m_s|x|} + V_v e^{-m_v|x|}$$

with $V_s = -506$ MeV, $V_v = 1142.49$ MeV, $m_s = 400$ MeV and $m_v = 783$ MeV, where the parameters have been tuned to reproduce exactly the ground state and binding energy of the real deuteron. We stress once more that this simple potential possesses those properties of realistic NN interactions which are most important to our purposes, namely a pathologically repulsive short-range "hard-core" and an exponentially falling long-range tail, and thus

constitutes a highly nontrivial test of our methods. Moreover, the effective potential is given by:

$$V_{\text{eff}}(x) = \frac{1}{a}\left(c + d\frac{\partial^2}{\partial\xi^2}\right)\exp(-\xi^2), \qquad \xi \equiv x/a$$

The parameters c and d were fixed to reproduce the low-energy scattering data of the bare potential. In the following, the Hamiltonian will be diagonalized, with both bare and effective potential, using a variety of different techniques. This will serve a three-fold purpose: first, we can verify the reliability of the range-two effective approximation by comparing the exact and effective spectra and therefore establishing the necessity, or lack-thereof, of higher-order (three-body) corrections. Secondly, we will be able to compare the rate of convergence of the exact and effective calculations as a function of the model space size, which represents a fundamental feature in computational applications. Third, we will be able to test and compare a variety of many-body algorithms.

4.2 Methods

4.2.1 No-Core Shell Model

The *ab-initio* No-Core Shell-Model (NCSM) approach [13, 33, 34, 65] begins with the one- and two-body non-relativistic Hamiltonian for the A-nucleons system

$$H = \sum_{n=1}^{A}\frac{\vec{p}_n^{\,2}}{2m} + \sum_{m<n}^{A} V\left(|\vec{x}_m - \vec{x}_n|\right) \tag{4.1}$$

Again, $V\left(|\vec{x}_m - \vec{x}_n|\right)$ represents a realistic NN interaction. One then modifies the Hamiltonian by adding a Simple Harmonic Oscillator (SHO) potential that depends exclusively on the center of mass coordinate $\vec{R} = (1/A)\sum_{i=1}^{A}\vec{x}_i$:

$$V^{\Omega}(\vec{R}) = \frac{1}{2}M\Omega^2\vec{R}^2 \tag{4.2}$$

This essential step is introduced in order to explicitly account for spurious center-of-mass kinetic contributions to the spectrum. The center-of-mass Hamiltonian $H^{\Omega}_{\text{c.m.}} = \vec{P}^2_{\text{c.m.}}/2Am +$

$\frac{1}{2}Am\Omega^2\vec{R}^2$, $\vec{P}_{\text{c.m.}} = \sum_{i=1}^{A}\vec{p}_i$ is later subtracted to obtain a purely intrinsic spectrum. The modified Hamiltonian has acquired a dependence on the SHO frequency Ω. That is,

$$\begin{aligned} H^{\Omega} &= H + V^{\Omega}(\vec{R}) \\ &= \sum_{n=1}^{A}\left(\frac{\vec{p}_n^{\,2}}{2m} + \frac{1}{2}m\Omega^2\vec{x}_n^{\,2}\right) + \sum_{m<n}^{A}\left[V\left(|\vec{x}_m - \vec{x}_n|\right) - \frac{1}{2A}m\Omega^2(|\vec{x}_m - \vec{x}_n|)^2\right] \\ &= H_0^{\Omega} + \tilde{V}^{\Omega} \end{aligned} \tag{4.3}$$

Now the Hamiltonian is composed of one-body SHO terms, easily accounted for, and a sum of two-body potentials depending only on relative distances. In the case of a one-dimensional three-body system, Equation (4.3) reduces to:

$$\begin{aligned} H^{\Omega}_{3-\text{body}} &= H_0^{\Omega} + \tilde{V}^{\Omega} \\ &= \sum_{n=1}^{3}\left(\frac{p_n^2}{2m} + \frac{1}{2}m\Omega^2 x_n^2\right) + \sum_{m<n}^{3}\left[V\left(|x_m - x_n|\right) - \frac{1}{6}m\Omega^2(|x_m - x_n|)^2\right] \end{aligned} \tag{4.4}$$

Explicitly, the intrinsic energy spectrum is obtained by simply subtracting the SHO spectrum with frequency Ω:

$$E_n = E_n^{\Omega} - \left(n_{\text{c.m.}} + \frac{1}{2}\right)\hbar\Omega \tag{4.5}$$

where $n_{\text{c.m.}}$ is the center-of-mass spectrum quantum number. Obviously, the final energy spectrum should be independent of the oscillation parameter Ω. Also, if we are only interested in the ground-state of the "internal" spectrum, $n = n_{\text{c.m.}} = 0$. In the case of a three body system we obtain $E_n = E_n^{\Omega} - \frac{1}{2}\hbar\Omega$. The Hamiltonian is diagonalized in a model SHO basis space built out of the direct product of three simple harmonic oscillators with the same oscillation parameter Ω:

$$|n_1 n_2 n_3\rangle \equiv |n_1\rangle \otimes |n_2\rangle \otimes |n_3\rangle \tag{4.6}$$

with $n_1 + n_2 + n_3 = N \leq N_{\text{basis}}$, so that all states are grouped into "shells" of total quantum number N. Recall that SHO wave-functions in position space are defined as [71]:

$$\langle x_i|n_i\rangle \equiv \phi_{n_i}(x_i) = \left(\frac{1}{\sqrt{\pi}2^{n_i}n_i!}\right)^{\frac{1}{2}} H_{n_i}(x_i)\exp\left(-\frac{x_i^2}{2}\right) \tag{4.7}$$

where $H_n(x)$ are Hermite polynomials of n^{th} degree. The first term of the modified Hamiltonian (4.4) can be trivially diagonalized in this basis:

$$H_0^{\Omega}\,|n_1 n_2 n_3\rangle = \left(n_1 + n_2 + n_3 + \frac{3}{2}\right)|n_1 n_2 n_3\rangle \tag{4.8}$$

while the second must be evaluated computationally. Since we only have to deal with two-body operators, one of the three space coordinates is simply a spectator, and evaluation of a matrix element yields a delta function factor in the corresponding quantum number. That is: $\langle n_1' n_2' n_3' | V(|x_1 - x_2|) | n_1 n_2 n_3 \rangle = \delta_{n_3, n_3'} \langle n_1' n_2' | V(|x_1 - x_2|) | n_1 n_2 \rangle$. Evaluation of the matrix elements involves computation of two-dimensional integrals of the form:

$$\langle n_1' n_2' | V(|x_1 - x_2|) | n_1 n_2 \rangle \;=\; \int_{-\infty}^{\infty} \int_{-\infty}^{\infty} \phi_{n_1'}(x_1) \phi_{n_2'}(x_2) V(|x_1 - x_2|) \phi_{n_1}(x_1) \phi_{n_2}(x_2) \, \mathrm{d}x_1 \mathrm{d}x_2 \tag{4.9}$$

which can be reduced to one-dimensional integrals through the coordinates transformation $R = (x_1 + x_2)/\sqrt{2}$, $X = (x_1 - x_2)/\sqrt{2}$ and employment of Moshinsky brackets $M_{mnp}(a, b)$ [66, 67, 68]:

$$\langle n_1' n_2' | V(|x_1 - x_2|) | n_1 n_2 \rangle = \sum_{N=0}^{n_1+n_2} M_{n_1 n_2 N}(1,1) M_{n_1' n_2' N}(1,1) \int_{-\infty}^{\infty} \phi_{n_1'+n_2'-N}(X) V(\sqrt{2}\,|X|) \phi_{n_1+n_2-N}(X) \, \mathrm{d}X \tag{4.10}$$

The transformation brackets $M_{mnp}(a, b)$ depend on the coefficients (a, b) of the orthogonal transformation parametrized as: $R = (ax_1 + bx_2)/\sqrt{2}$, $X = (bx_1 - ax_2)/\sqrt{2}$. In the case shown above $a = b = 1$. Also, $p = N$ is the SHO quantum number of the transformed "center-of-mass" coordinate R. For a derivation of Equation (4.10) and of the Moshinsky brackets for a generalized orthogonal transformation of coordinates, see Appendix A. The resulting matrix can be diagonalized by brute force using traditional algorithms such as QR decomposition, which will return the complete set of eigenvalues and eigenfunctions. However, it is easy to realize that we would quickly run into trouble as we attempt to solve the problem when the size of the matrix grows substantially. The number of arithmetic operators needed for this method scales as $\mathcal{O}(s^3)$, where s is the size of the matrix. In turn, this grows as N^3, due to degeneracies of the wave-functions. Therefore, the time required for diagonalization with QR is of order $\mathcal{O}(N^6)$. Clearly, we should be looking for more efficient and time saving methods to tackle the problem.

4.2.2 Lanczos method for the symmetric eigenvalue problem

As we have seen above, traditional methods of diagonalizing large matrices can be ineffective and time-consuming. However, the situation becomes more approachable if we

are not interested in the whole spectrum of eigenvalues. This is precisely our case, since in effective theory approaches one is usually interested in the low-lying eigenvalues and eigenvectors of the Hamiltonian. The Lanczos method [72, 73, 69] was specifically designed to solve large symmetric matrices, but has later been expanded to treat non-symmetric structures. It is a fast and effective method to compute *extreme* (lowest and highest) eigenvalues. The next section is devoted to describe the basics of this technique. A convenient point to start is the standard eigenvalue problem for a symmetric (real) matrix:

$$H\boldsymbol{x}_i = \lambda_i \boldsymbol{x}_i \tag{4.11}$$

This equation can be inverted to give

$$\lambda_i = \frac{\boldsymbol{x}_i^T H \boldsymbol{x}_i}{\boldsymbol{x}_i^T \boldsymbol{x}_i} \tag{4.12}$$

Equation (4.12) is called a Rayleigh quotient. For any specific value of i, if a trial starting vector q can be somehow guessed, these relationship can be used to obtain a new vector which is a better approximation to the exact ith eigenvector of H. If this procedure is iterated one obtains the so called power-method, which yields a convergent series to the exact eigenvector. It can be shown that the rate of convergence is higher for extreme eigenvectors. Also, the method can be improved if, instead of a single vector, we used a larger subspace $\mathcal{K}$ over which to perform the iteration. The Rayleigh-Ritz approximation to the kth eigenvalue of H is defined as:

$$y_k = \frac{\boldsymbol{q}_k^T H \boldsymbol{q}_k}{\boldsymbol{q}_k^T \boldsymbol{q}_k} \tag{4.13}$$

where $\boldsymbol{q}_k$ belongs now to $\mathcal{K}$. It can be shown that the eigenpair $(\boldsymbol{q}_k, y_k)$ is the best possible approximation to the eigenvalue pair of H, if $\boldsymbol{q}_k$ is obtained by a linear superposition of vectors lying *within the subspace* $\mathcal{K}$. Solving for $(\boldsymbol{q}_k, y_k)$ is equivalent to diagonalizing H in the subspace $\mathcal{K}$. All that is needed now is a suitable subspace over which to perform the approximation. The Lanczos algorithm employs a Krylov subspace, defined as:

$$\mathcal{K}(H, \boldsymbol{x}, k) = \text{span}\{\boldsymbol{x}, H\boldsymbol{x}, H^2\boldsymbol{x}, \ldots, H^{k-1}\boldsymbol{x}\} \tag{4.14}$$

In the Lanczos procedure, a set of orthogonal vectors that span a Krylov subspace are created through a recursion relationship. The first great advantage is that a newly created vector

must be orthogonalized only against the two previous ones, with significant gain in memory requirements and computation speed. Furthermore, it can be shown that, in the subspace spanned by these orthogonal vectors, the matrix has a tridiagonal form, which makes it extremely fast to diagonalize.

4.2.2.1 Practical Lanczos procedure

In this section we will translate the mathematical concepts of the previous section in a formalism more apt to our purposes, and illustrate the steps of a practical implementation of the method. One starts with a random vector $|\phi_0\rangle$. We then can define a new vector by applying the Hamiltonian to the initial state. Subtracting the projection over $|\phi_0\rangle$ one obtains:

$$|\phi_1\rangle = \hat{H}\,|\phi_0\rangle - \frac{\langle\phi_0|\,\hat{H}\,|\phi_0\rangle}{\langle\phi_0|\phi_0\rangle}\,|\phi_0\rangle \tag{4.15}$$

$$|\phi_2\rangle = \hat{H}\,|\phi_1\rangle - \frac{\langle\phi_1|\,\hat{H}\,|\phi_1\rangle}{\langle\phi_1|\phi_1\rangle}\,|\phi_1\rangle - \frac{\langle\phi_1|\phi_1\rangle}{\langle\phi_0|\phi_0\rangle}\,|\phi_0\rangle \tag{4.16}$$

We can therefore derive a recursive relationship:

$$|\phi_{n+1}\rangle = \hat{H}\,|\phi_n\rangle - a_n\,|\phi_n\rangle - b_n^2\,|\phi_{n-1}\rangle \tag{4.17}$$

where $n = 0, 1, 2, \ldots$ and

$$a_n = \frac{\langle\phi_n|\,\hat{H}\,|\phi_n\rangle}{\langle\phi_n|\phi_n\rangle}, \quad b_n^2 = \frac{\langle\phi_n|\phi_n\rangle}{\langle\phi_{n-1}|\phi_{n-1}\rangle} \tag{4.18}$$

It can be shown that in this basis the Hamiltonian has a tridiagonal form:

$$H = \begin{pmatrix} a_0 & b_1 & 0 & 0 & \cdots \\ b_1 & a_1 & b_2 & 0 & \cdots \\ 0 & b_2 & a_2 & b_3 & \cdots \\ 0 & 0 & b_3 & a_3 & \cdots \\ \vdots & \vdots & \vdots & \vdots & \ddots \end{pmatrix} \tag{4.19}$$

In essence then, the Lanczos procedure is implemented as follows:

1. Create a random vector x_0
2. At each step of the iteration compute a new orthogonal vector in Krylov subspace according to Equation (4.17).

3. At each step, compute new a_n and b_n that form a new triangular matrix of range n. Each step of the iteration creates a larger matrix.

4. Diagonalize the matrix and compute a new ground state energy λ_0. At every successive iteration a better approximation to the exact ground state is reached.

5. When $\left|\lambda_0^{n+1} - \lambda_0^n\right| < \epsilon$, convergence is obtained and the iteration is truncated. This usually happens for $n < 100$.

6. Iteration is interrupted regardless when $n = k$, where k is the range of the original matrix. In theory, at this point the Krylov subspace is equivalent to the original space, and H has simply undergone a similarity transformation into a tridiagonal form, so that the whole spectrum could be extracted. This ideal situation does not occur in practice since orthogonality of the vectors is lost due to floating point arithmetics.

It is easy to see that the essence (and most computationally demanding part) of the algorithm consists of a matrix multiplication as opposed to the actual diagonalization (remember that, since convergence is usually obtained by $n < 100$, one only has to diagonalize tridiagonal matrices of smaller range than 100.) This is a great advantage by itself, since matrix multiplication routines only scale as $\mathcal{O}(n^2)$. Furthermore, this makes it possible to avoid to store the matrix explicitly and take advantage of the structure of the problem. For example, in the case of sparse matrices, only the nonzero elements could be stored, with great memory storage advantages, and by simply modifying the matrix multiplication routine the performance of the program can be greatly improved.

4.2.3 Jacobi transformation method.

This method takes advantage of an orthogonal transformation of the Cartesian coordinates into Jacobi coordinates in order to construct a translationally invariant SHO basis set in which the center-of-mass coordinates are explicitly separated and can therefore be omitted [32]. This allows to significantly reduce the degrees of freedom of the theory and carry out the diagonalization in a much larger model space as compared to the standard shell model procedure illustrated in the previous section. One further advantage of this method is the flexibility of the transformation between SHO basis sets which allows to compute with ease

multi-dimensional integrals: this can come in extremely handy if many-nucleons effective range terms need to be included. We start from the Hamiltonian:

$$\hat{H} = \left(\frac{p_1^2}{2m} + \frac{p_2^2}{2m} + \frac{p_3^2}{2m}\right) + V\left(|x_1 - x_2|\right) + V\left(|x_3 - x_1|\right) + V\left(|x_3 - x_2|\right) \tag{4.20}$$

where $\{p_i\}$ are the canonical momenta associated with the coordinates $\{x_i\}$. The Jacobi coordinates are in general proportional to center-of-mass and relative coordinates of all nucleons or nucleons sub-clusters. In the case under consideration we define:

$$X \equiv \frac{1}{\sqrt{3}}\left(x_1 + x_2 + x_3\right); \quad \xi_1 \equiv \frac{1}{\sqrt{2}}\left(x_1 - x_2\right); \quad \xi_2 \equiv \frac{1}{\sqrt{6}}\left(x_1 + x_2 - 2x_3\right) \tag{4.21}$$

The above equations can be inverted to obtain:

$$x_1 - x_2 \equiv \sqrt{2}\xi_1; \quad x_3 - x_2 \equiv \sqrt{\frac{1}{2}}\xi_1 - \sqrt{\frac{3}{2}}\xi_2; \quad x_3 - x_1 \equiv \sqrt{\frac{1}{2}}\xi_1 + \sqrt{\frac{3}{2}}\xi_2 \tag{4.22}$$

which can be shown to compose a canonical set of transformations [70]. Hence the Hamiltonian in this new basis becomes:

$$H = \frac{p_X^2}{2m} + \left[\frac{p_{\xi_1}^2}{2m} + \frac{p_{\xi_2}^2}{2m} + V\left(\sqrt{2}\,|\xi_1|\right) + V\left(\left|\sqrt{\frac{1}{2}}\xi_1 - \sqrt{\frac{3}{2}}\xi_2\right|\right) + V\left(\left|\sqrt{\frac{1}{2}}\xi_1 + \sqrt{\frac{3}{2}}\xi_2\right|\right)\right] \tag{4.23}$$

where now $p_{\xi_1}$and p_{ξ_2} are the canonical momenta associated with the new variables ξ_1 and ξ_2. The first term of Equation (4.23) is the center-of-mass kinetic term, and can thus be dropped, since we are only interested in the intrinsic spectrum. The resulting differential equation is reminiscent of Equation (4.3) and can be treated in a similar fashion. The kinetic terms can be taken care of by adding and subtracting SHO potential terms of the form $V_{\mathrm{SHO}}(\xi_i) = \frac{1}{2}m\Omega\xi_i^2$. By doing this, the kinetic plus harmonic terms will give a contribution to the spectrum equal to $\left(n_i + \frac{1}{2}\right)\hbar\Omega$. A generic matrix element can therefore be written as:

$$\begin{aligned}\langle n_1 n_2|H|n_1' n_2'\rangle = {} & \delta_{n_1 n_1'}\left(n_2 + \frac{1}{2}\right)\hbar\Omega + \delta_{n_2 n_2'}\left(n_1 + \frac{1}{2}\right)\hbar\Omega + \\ & \delta_{n_2 n_2'}\langle n_1|[V(\sqrt{2}\,|\xi_1|) - V_{\mathrm{SHO}}(\xi_1)]|n_1'\rangle - \delta_{n_1 n_1'}\langle n_2|V_{\mathrm{SHO}}(\xi_2)|n_2'\rangle + \\ & \langle n_1 n_2|V\left(\left|\sqrt{\frac{1}{2}}\xi_1 - \sqrt{\frac{3}{2}}\xi_2\right|\right)|n_1' n_2'\rangle + \langle n_1 n_2|V\left(\left|\sqrt{\frac{1}{2}}\xi_1 + \sqrt{\frac{3}{2}}\xi_2\right|\right)|n_1' n_2'\rangle\end{aligned} \tag{4.24}$$

The integrals in the second line of Equation (4.24) are one-dimensional and can be evaluated trivially. The remaining two-dimensional integrals can be treated using the same Moshinsky

brackets technique used in the previous section: upon performing the rotation $\xi_1' = \sqrt{3}\xi_1/2 + \xi/2$, $\xi_2' = \xi_1/2 - \sqrt{3}\xi_2/2$ the potential in the first integral becomes a function of the variable ξ_2' only:

$$\langle n_1 n_2 | V\left(\sqrt{2}\left|\frac{1}{2}\xi_1 - \frac{\sqrt{3}}{2}\xi_2\right|\right)|n_1' n_2'\rangle = \sum_{N=0}^{n_1+n_2}\sum_{N'=0}^{n_1'+n_2'} \delta_{N,N'} M_{n_1 n_2 N}\left(\sqrt{\frac{3}{2}},\sqrt{\frac{1}{2}}\right) M_{n_1' n_2' N'}\left(\sqrt{\frac{3}{2}},\sqrt{\frac{1}{2}}\right) \times \int_{-\infty}^{\infty} \phi_{n_1'+n_2'-N'}(\xi_2') V(\sqrt{2}\,|\xi_2'|)\phi_{n_1+n_2-N}(\xi_2')\,\mathrm{d}\xi_2' \quad (4.25)$$

whereas the rotation $\xi_1' = \xi_1/2 + \sqrt{3}\xi_2/2$, $\xi_2' = \sqrt{3}\xi_1/2 - \xi_2/2$ makes the potential in the second one depend solely on ξ_1'.

$$\langle n_1 n_2 | V\left(\sqrt{2}\left|\frac{1}{2}\xi_1 + \frac{\sqrt{3}}{2}\xi_2\right|\right)|n_1' n_2'\rangle = \sum_{N=0}^{n_1+n_2}\sum_{N'=0}^{n_1'+n_2'} \delta_{n_1+n_2-N,n_1'+n_2'-N'} M_{n_1 n_2 N}\left(\sqrt{\frac{1}{2}},\sqrt{\frac{3}{2}}\right) M_{n_1' n_2' N'}\left(\sqrt{\frac{1}{2}},\sqrt{\frac{3}{2}}\right) \times \int_{-\infty}^{\infty} \phi_N(\xi_1') V(\sqrt{2}\,|\xi_1'|)\phi_{N'}(\xi_1')\,\mathrm{d}\xi_1' \quad (4.26)$$

See Appendix A for the derivation of these formulas.

4.2.4 Hyper-spherical harmonics (HH) method

Introducing the one-dimensional hyper-spherical coordinates r and θ defined by $\xi_1 \equiv r\cos\theta$ and $\xi_2 \equiv r\sin\theta$ into Schrödinger's Equation (4.23) one obtains:

$$\left\{\frac{\partial^2}{\partial r^2} + \frac{1}{r^2}\frac{\partial^2}{\partial\theta^2} + \frac{1}{4r^2} - k^2 - U(r,\theta)\right\}\psi(r,\theta) = 0 \quad (4.27)$$

where $U(r,\theta)$ is defined as:

$$U(r,\theta) \equiv \frac{1}{2m}\times \left\{V\left(\sqrt{2}\,|r\cos\theta|\right) + V\left(\frac{r}{\sqrt{2}}\left|\cos\theta - \sqrt{3}\sin\theta\right|\right) + V\left(\frac{r}{\sqrt{2}}\left|\cos\theta + \sqrt{3}\sin\theta\right|\right)\right\} \quad (4.28)$$

with $k^2 \equiv -2mE$ and $\psi(r,\theta) \equiv \frac{1}{\sqrt{r}}\phi(r,\theta)$. A solution to this differential equation can be attempted in the form of a Fourier expansion, in which the r and θ dependence is explicitly separated:

$$\phi = \sum_{m=0}^{\infty} \{g_m(r)\cos(\theta) + f_m(r)\sin(\theta)\} \tag{4.29}$$

It can be shown that Equation (4.27) can be reduced to a system of differential equations which couple the different modes (or channels) of the wave-function:

$$\hat{D}_{km}(r)g_n(r) - \sum_{m=0}^{\infty} \left\{U_{|n+m|}(r) + U_{|n-m|}(r)\right\} g_m(r) = 0 \tag{4.30}$$

For the derivation of Equation (4.30), see Appendix B.

4.3 Results

Using the NCSM method, we calculated ground states energies for basis sizes given by $N_{\text{basis}} = 10, 20, 30, 40, 50, 60$. The number of matrix elements in the three body matrix is given by $d = N_{\text{basis}}(N_{\text{basis}} - 1)(N_{\text{basis}} - 2)/2$. Hence, the largest matrix we diagonalized contained 102,600 elements. This is obviously not a large matrix by today standards, but it should be noted that it is *not* a sparse matrix, meaning that a non negligible portion of its elements are different than zero. Obviously, this slows down the diagonalization procedure, especially in the Lanczos method where only non-zero elements are accounted for. In the practical procedure, basic two body matrix elements in Equation (4.10) were calculated and filed. During the diagonalization procedure, only non zero three-body matrix elements were computed (once) and stored in memory.

In the JT method it is possible to span a much larger model space, since the center-of-mass degrees of freedom have been eliminated for the outset. In fact, the number of states is given by $d = N_{\text{basis}}(N_{\text{basis}} - 1)/2$, scaling simply as $\mathcal{O}(N_{\text{basis}}^2)$. We computed the ground states for model spaces of size up to $N_{\text{basis}} = 70$, which proved sufficient to achieve convergence.

Equation (4.30) for the HH method can be solved for example through Runge-Kutta integration, which, however, turns out to be numerically unstable as the number of channels is increased. A finite differences approach, together with Numerov's approximation for second derivatives, proves to be highly stable and efficient. The only drawback of this approach

is that the resulting matrix is not symmetric, and therefore cannot be diagonalized with a Lanczos algorithm as we applied it. We solved Equation (4.30) for a number of channels up to 12.

The convergence of the ground state to its true value E_{exact} as $N_{\text{basis}} \to \infty$ is represented by an unknown, complicated function, which we assume can be approximated by a polynomial in the neighborhood of $x = 1/N_{\text{basis}} \approx 0$. For each set of calculations, the ground state energy was extracted by fitting the points closer to $x = 0$ (we chose $N_{\text{basis}} \geq 30$ and $N_{\text{channels}} \geq 8$) to the linear formula:

$$y = a_0 + a_2 x^2 + a_3 x^3$$

where the constraint $a_1 = 0$ was imposed in order to obtain a minimum of the function at $x = 0$. The value of a_0 provides then the limiting value of E_{exact}. Results are shown in Figure 4.1, 4.2 and 4.3. Also, Table 4.1 contains the summary of the extrapolated results for all the different methods. The results show a very good agreement of the binding energy

Table 4.1. Compared results of three-nucleon ground state energies E_{exact} in MeV.

	Hyper-spherical Harmonics	Jacobi	No-core Shell Model
Bare	-6.278	-6.313	-6.313
Effective	-6.796	-6.918	-6.918

among the different methods. They also show, however, a discrepancy between bare and effective potential calculations, independent of the particular method employed, which is due in all likelihood to the effect of the neglected three- and possibly many-body induced effective interactions. Even taking this difference into account, it appears evident that each one of the effective potential calculations converges to the "exact" result much faster than the corresponding bare potential calculations, as shown in the respective Figures insets.

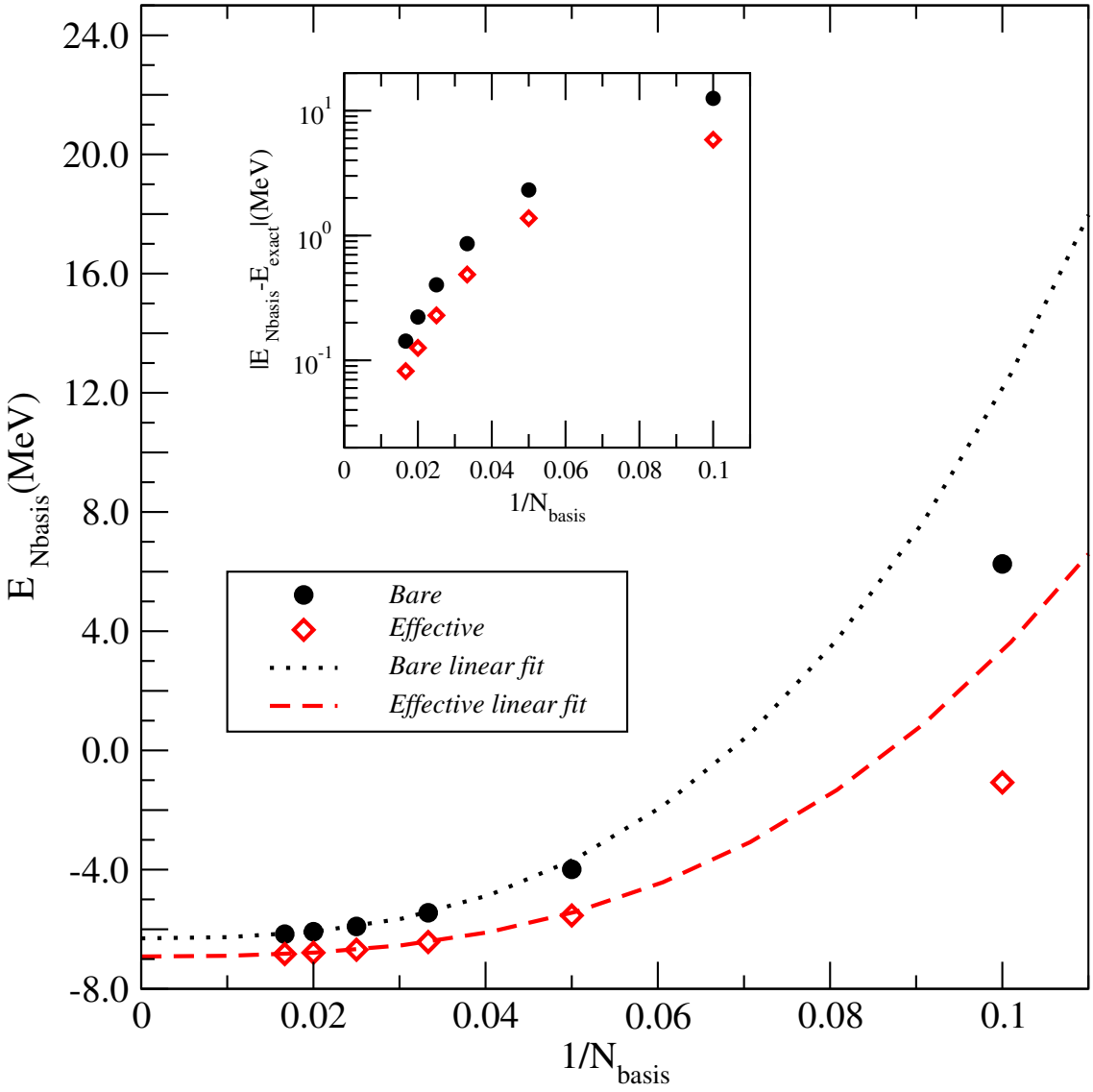

Figure 4.1. NCSM calculations of ground state energies for the three-body system in one dimension, obtained with a bare (circle) and an effective (diamond) interaction. The inset shows the corresponding rates of convergence. The linear fits for $N_{basis} \to \infty$ converge to the values $E_{\rm exact} = -6.313\,{\rm MeV}$ for the bare potential and $E_{\rm exact} = -6.918\,{\rm MeV}$ for the effective potential.

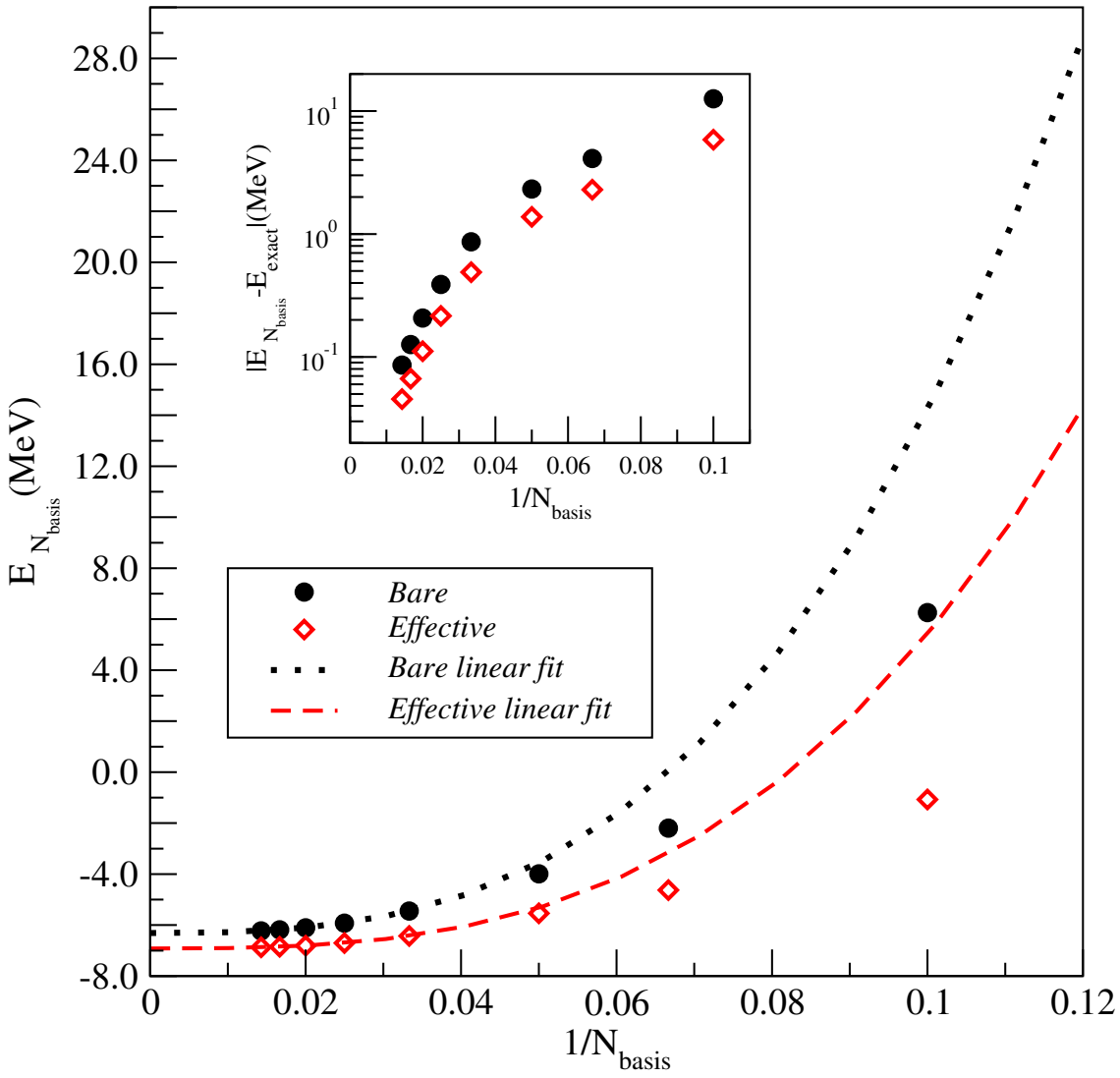

Figure 4.2. Jacobi transformation calculations of ground state energies for the three-body system in one dimension, obtained with a bare (circle) and an effective (diamond) interaction. The inset shows the corresponding rates of convergence. The linear fits for $N_{basis} \to \infty$ converge to the values $E_{\rm exact} = -6.313\,{\rm MeV}$ for the bare potential and $E_{\rm exact} = -6.918\,{\rm MeV}$ for the effective potential.

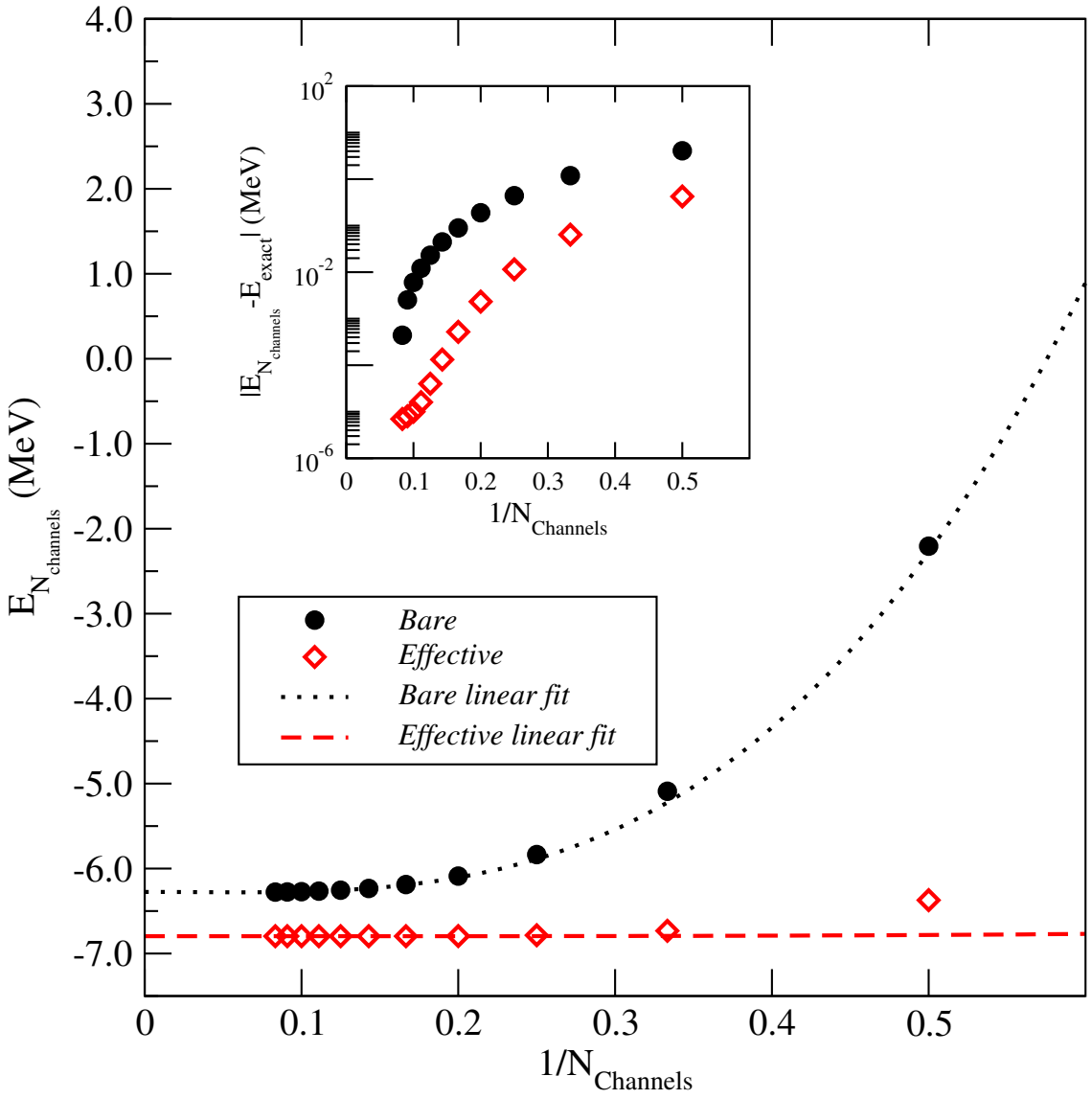

Figure 4.3. Hyper-spherical harmonics calculations of ground state energies for the three-body system in one dimension, obtained with a bare (circle) and an effective (diamond) interaction. The inset shows the corresponding rates of convergence. The linear fits for $N_{basis} \rightarrow \infty$ converge to the values $E_{\rm exact} = -6.278$ MeV for the bare potential and $E_{\rm exact} = -6.796$ MeV for the effective potential.

CHAPTER 5

SPIN CHAINS

5.1 Introduction

The zig-zag spin chain (Figure 1.1) can be mapped onto a linear spin chain with competing nearest neighbor (nn) and next-to-nearest neighbor (nnn) interactions described by the Hamiltonian:

$$\mathcal{H} = \sum_i \vec{S}_i \cdot \vec{S}_{i+1} + \alpha \vec{S}_i \cdot \vec{S}_{i+2} \tag{5.1}$$

where the parameter α is defined as the ratio of the nnn to nn interaction strengths and is a measure of the frustration in the system. Morningstar and Weinberg (M&W) have in past publications [35, 36] applied CORE to the Heisenberg anti-ferromagnetic spin-$\frac{1}{2}$ chain without frustration and developed a renormalization group equation that predicts its ground-state energy density in excellent agreement with Bethe's exact solution [40] and does significantly better than Anderson's spin wave approximation [50]. This formalism also predicts the correct massless spectrum. Their method relies on identifying a basic building block in the chain and performing a truncation of the selected basis, such that only the states that contribute the most to the low-energy spectrum of the block are included. Successively the Hamiltonian is renormalized in the form of a cluster expansion including effective interactions of (up to) n-connected blocks. In their work, the basis is truncated to retain a single state and the cluster expansion carried up to range-2. This scheme proves sufficient to extract the energy density and spin gap of the simple Heisenberg chain, but it does not allow to include frustration in the chain. The goals of this Chapter are multiple. First, we will expand M&W calculations to include chains with arbitrary spin. As we will show, this can be accomplished fairly easily in the framework of CORE's formalism. In order to treat frustrated chains, we will carry the cluster expansion to include range-3 terms.

Furthermore, we will show that as α is increased, the truncation scheme needs to be modified to include more states, since frustration reshapes the structure of the low-energy spectrum of the building block.

5.2 Formalism

The basic idea of any effective theory is that we should be able to simplify the problem at hand by somehow reducing the number of degrees of freedom of the exact theory. This is usually accomplished through a truncation procedure that excludes those states that do not contribute significantly to the low-energy properties of the system. The (hopefully) small contributions of these high-energy degrees of freedom are reintroduced by renormalizing the exact Hamiltonian, which as a result is transformed into a simpler, easier structure acting upon a significantly thinner Hilbert space. The first step in CORE's approach consists in identifying a basic building block upon which constructing the cluster expansion. The second step is to select a truncation scheme by retaining only the lowest energy states in the building block's energy spectrum. The retained states will therefore constitute the low energy degrees of freedom of the renormalized theory. It is extremely important, in view of the truncation procedure, to find a proper basis in order to simplify the task of identifying the high-energy degrees of freedom to be cut off. In other words, the basis must be chosen to suit the building block, in the sense that only a few of its states should contribute to the low-energy spectrum. This section will therefore be dedicated to the definition of our basic building block and the study of some of its relevant physical properties: this will allow us to define the truncation procedure and ultimately justify our choice of basis.

We identify out basic building structure as the "trimer" composed of three neighboring spins. This choice appears somehow obvious upon inspection of the zig-zag chain structure, which can be imagined as a series of spin triangles each interacting with its nearest neighbor. Also, the trimer structure is the largest block that is diagonalizable exactly by means of simple analytical manipulations. To this end, we will make extensive use of techniques, such as Racah algebra, routinely employed in the field of nuclear physics. Construction of range-n contributions to the cluster expansion requires exact solution of the corresponding structures. Therefore, in order to compute range-1 (range-2) terms in the CORE expansion,

the one-(two-)triangle spin structure must be solved exactly. In this paper, calculation will be carried up to range-3, hence in the following we will introduce our basis and construct the relevant matrix elements for chains of 3, 6 and 9 spins. We start with the basic three spins block. The Hamiltonian is given by:

$$\mathcal{H}_0 = \vec{S}_1 \cdot \vec{S}_2 + \vec{S}_2 \cdot \vec{S}_3 + \alpha \vec{S}_1 \cdot \vec{S}_3 \tag{5.2}$$

which can be written in the following form:

$$\begin{aligned} \mathcal{H}_0 &= (\vec{S}_1 + \vec{S}_3) \cdot \vec{S}_2 + \frac{1}{2}\alpha[(\vec{S}_1 + \vec{S}_3)^2 - \vec{S}_1^2 - \vec{S}_3^2] \\ &= \frac{1}{2}\left[\vec{J}^2 + (\alpha - 1)\vec{L}^2 - \alpha(\vec{S}_1^2 + \vec{S}_3^2) - \vec{S}_2^2\right] \\ &= \frac{1}{2}\left[\vec{J}^2 + (\alpha - 1)\vec{L}^2 - (2\alpha + 1)\vec{S}^2\right] \end{aligned} \tag{5.3}$$

where the angular momentum operators $\vec{J}$, $\vec{L}$ and $\vec{S}$ are defined as:

$$\vec{J} = \vec{S}_1 + \vec{S}_2 + \vec{S}_3\,, \quad \vec{L} = \vec{S}_1 + \vec{S}_3 \quad \text{and} \quad \vec{S}^2 = \vec{S}_1^2 = \vec{S}_2^2 = \vec{S}_3^2 \tag{5.4}$$

We now define a total angular momentum basis in which spins $\vec{S}_1$ and $\vec{S}_3$ are coupled to a "link" momentum $\vec{L}$ with quantum number l, which in turn is coupled to $\vec{S}_2$ to give the total triangle angular momentum j with projection m. The basis states will thus be defined as $|\phi\rangle = |(s_1 s_3)l, s_2\rangle_{jm}$; in the following we will simplify the notation to $|\phi\rangle = |lsj\rangle$, since due to the rotational symmetry of the Hamiltonian, the projection quantum number is irrelevant, and the quantum number s is just a parameter. The choice of this basis has numerous advantages compared to the more obvious choice of the S_z basis. To begin with, it is easy to realize that $\mathcal{H}_0$ is diagonalized by this basis, that is:

$$\mathcal{H}_0 \,|lsj\rangle = \frac{1}{2}\left[j(j+1) + (\alpha - 1)l(l+1) - (2\alpha + 1)s(s+1)\right]|lsj\rangle \tag{5.5}$$

For low ($\alpha \leq 1$) values of the frustration parameter the ground state is always obtained by selecting the lowest value of j compatible with the highest value of s, that is $|\phi_0\rangle = |l = 2s, j = s\rangle$ while the first excited state is given by $|\phi_1\rangle = |l = (2s-1), j = s\rangle$. The spectrum is completed by the stretched state $|\phi_2\rangle = |l = 2s, j = 3s\rangle$. Figure 5.1 illustrates the evolution of the three spin structure of the spectrum as a function of frustration. As α increases the two $J = S$ states converge to the same energy, until they become degenerate for $\alpha = 1$. This fact implies important consequences for the truncation procedure, as we will see later.

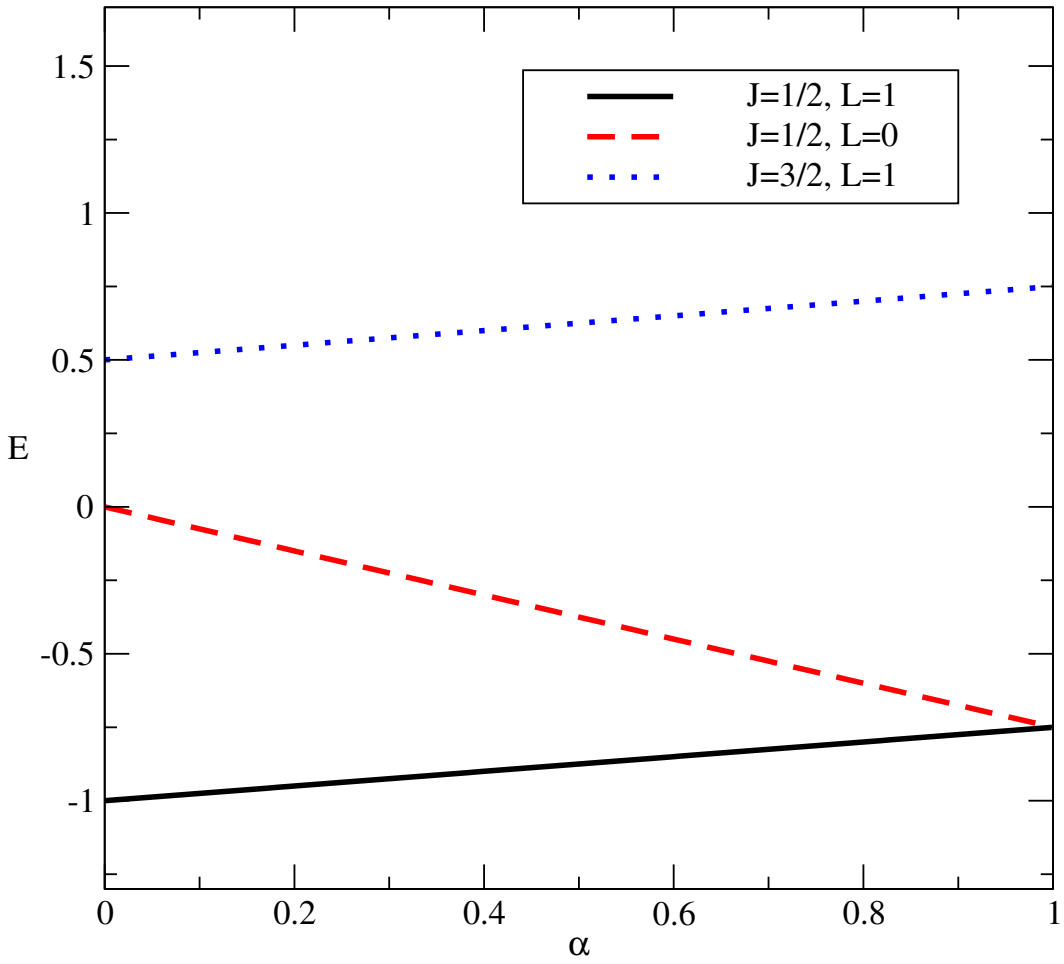

Figure 5.1. Energy spectrum evolution with frustration of the 3-spins chain. The relative weight of the $J = 1/2, L = 0$ state (dashed line) grows steadily as α increases.

On to the six spins. The explicit form of the Hamiltonian is the following:

$$\begin{aligned}\mathcal{H}_1 =& \vec{S}_1 \cdot \vec{S}_2 + \vec{S}_2 \cdot \vec{S}_3 + \alpha \vec{S}_1 \cdot \vec{S}_3 + \vec{S}_4 \cdot \vec{S}_5 + \vec{S}_5 \cdot \vec{S}_6 + \alpha \vec{S}_4 \cdot \vec{S}_6 + \vec{S}_3 \cdot \vec{S}_4 + \alpha \vec{S}_2 \cdot \vec{S}_4 + \alpha \vec{S}_3 \cdot \vec{S}_5 \\ =& \mathcal{H}_0(1) + \mathcal{H}_0(2) + \mathcal{V}(1,2) \end{aligned} \tag{5.6}$$

where $\mathcal{H}_0$ is single triangle Hamiltonian and $\mathcal{V}(1,2)$ is an "interaction" Hamiltonian involving spin belonging to different triangles. The basis states are constructed by coupling the angular momenta of the two triangles to a total value J: $|\psi\rangle = |l_1 j_1, l_2 j_2\rangle_J$. Computation of matrix elements in the coupled angular momentum basis can be quite tedious, but they are routinely

used in nuclear physics calculations, where one can take advantage of a sophisticated set of tools known as Racah algebra. The basic two triangles interaction matrix for a generic spin is given by:

$$
\begin{aligned}
&{}_J\langle l_1 j_1, l_2 j_2 \,|\mathcal{V}(1,2)|\, l_1' j_1', l_2' j_2'\rangle_J = \\
&\hat{s}^2 s(s+1)(-1)^{j_1'+j_2+J} \hat{j}_1 \hat{j}_2 \hat{j}_1' \hat{j}_2' \begin{Bmatrix} j_1 & j_1' & 1 \\ j_2' & j_2 & J \end{Bmatrix} \times \\
&\qquad \Bigg[\delta(l_1, l_1')(-1)^{l_1+l_2+l_2'+j_1+j_2'+1} \hat{l}_2 \hat{l}_2' \begin{Bmatrix} j_2 & j_2' & 1 \\ l_2' & l_2 & s \end{Bmatrix} \begin{Bmatrix} j_1 & j_1' & 1 \\ s & s & l_1 \end{Bmatrix} \begin{Bmatrix} l_2 & l_2' & 1 \\ s & s & s \end{Bmatrix} + \\
&\qquad (-1)^{l_2+l_2'+j_1'+j_2'+1} \hat{l}_1 \hat{l}_1' \hat{l}_2 \hat{l}_2' \begin{Bmatrix} j_1 & j_1' & 1 \\ l_1' & l_1 & \frac{1}{2} \end{Bmatrix} \begin{Bmatrix} j_2 & j_2' & 1 \\ l_2' & l_2 & s \end{Bmatrix} \begin{Bmatrix} l_1 & l_1' & 1 \\ s & s & s \end{Bmatrix} \begin{Bmatrix} l_2 & l_2' & 1 \\ s & s & s \end{Bmatrix} + \\
&\qquad\qquad \delta(l_2, l_2')(-1)^{l_2+j_1'+j_2+1} \hat{l}_1 \hat{l}_1' \begin{Bmatrix} j_1 & j_1' & 1 \\ l_1' & l_1 & s \end{Bmatrix} \begin{Bmatrix} j_2 & j_2' & 1 \\ s & s & l_2 \end{Bmatrix} \begin{Bmatrix} l_1 & l_1' & 1 \\ s & s & s \end{Bmatrix} \Bigg] \qquad (5.7)
\end{aligned}
$$

where the $\begin{pmatrix} a & b & c \\ d & e & f \end{pmatrix}$ are 6–j coefficients for the coupling of three angular momenta. Closed formulas are easily available for their computation [74]. We also employed the shorthand notation $\hat{x} = \sqrt{2x+1}$. With the evaluation of the inter-blocks matrix elements of Equation (5.7), we possess all the tools for the exact diagonalization of the 6-spins structure. It is instructive at this point to compare the probability distribution strengths of the ground-state E_{gs} ($|\langle E_{\text{gs}}|\psi_i\rangle|^2$, that is) in both the S_z and total J schemes, which will allow us to justify our previous choice in favor of the latter. For pedagogical purposes, we will restrict ourselves to the $S = \frac{1}{2}$, $\alpha = 0$ case. As illustrated in Figure 5.2, it is apparent that the 6-spins ground-state (a spin singlet) is noticeably more fragmented among the S_z basis states as compared to the J basis. In the first case, the ground-state is represented by a total of 64 states and no single state carries more than 20% of the total probability. On the other hand, in the coupled basis a single state $|\psi_0\rangle = \left|l_1 = 1 j_1 = \frac{1}{2}, l_2 = 1 j_2 = \frac{1}{2}\right\rangle_{J=0}$ approximates the ground-state by about 90%. From these simple facts we conclude that the coupled spin basis is more adequate to describe the physics of the ground-state of the chain, which represents one of the focal points of this paper. In fact, the coupled basis lends itself more readily to a truncation scheme, since it becomes immediately apparent which states have to be truncated and which have to be retained. In other words, in this scheme it is easier to identify the low-energy degrees of freedom of the effective theory.

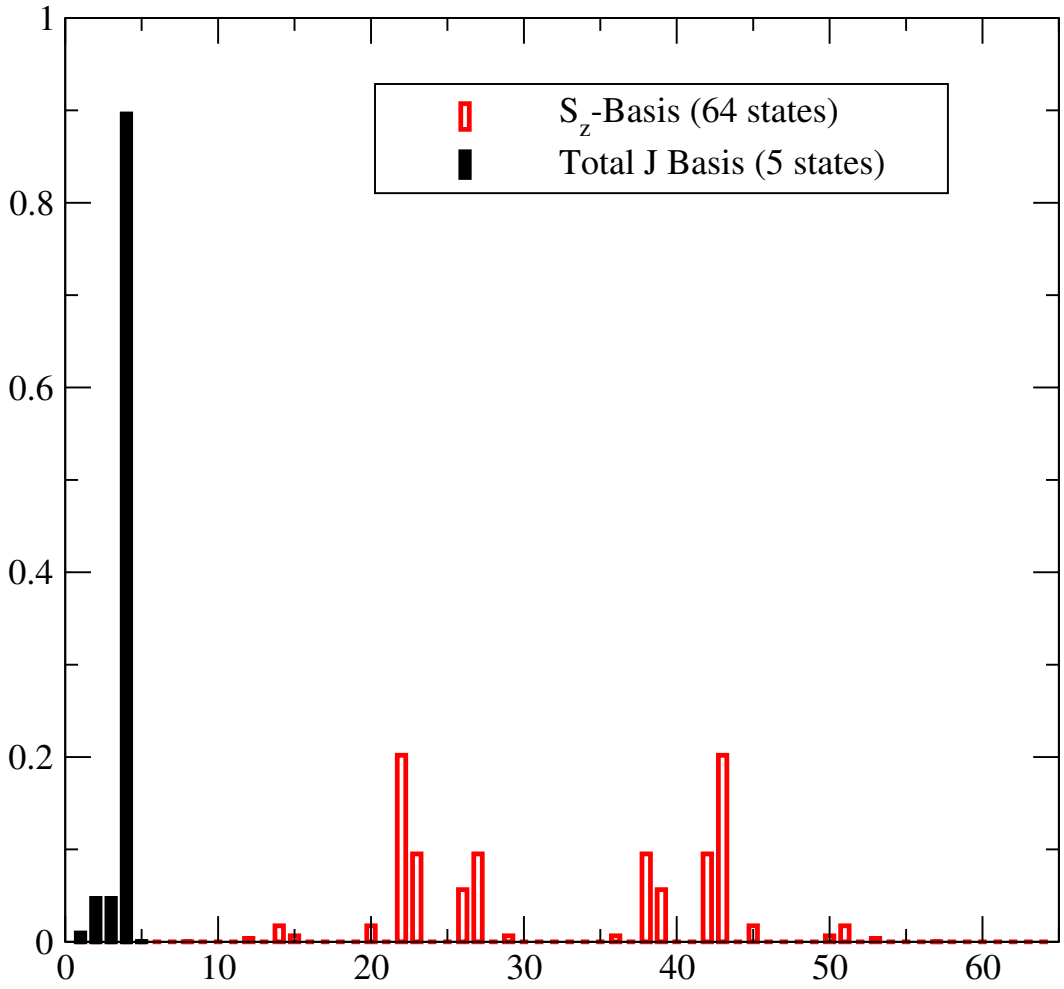

Figure 5.2. 6-spins chain ground-state distribution of strengths in the S_z and total J basis.

This ideal situation, however, deteriorates rapidly as frustration is turned on. Indeed, as is the case in the single three-spin block, more states contribute significantly to the low-energy spectrum and, as a consequence, we no longer have an extremely definite state that approximates the ground-state properties. In the case of the 6-spins chain, the contribution of $|\psi_0\rangle$ is no longer dominant and, for the extreme case of $\alpha = 1$, it is smaller compared to the two $|\psi_1\rangle = \left|l_1 = 0 j = \frac{1}{2}, l_2 = 1 j_2 = \frac{1}{2}\right\rangle_{J=0}$ and $|\psi_2\rangle = \left|l_1 = 1 j_1 = \frac{1}{2}, l_2 = 0 j_2 = \frac{1}{2}\right\rangle_{J=0}$ symmetric states (Figure 5.3)

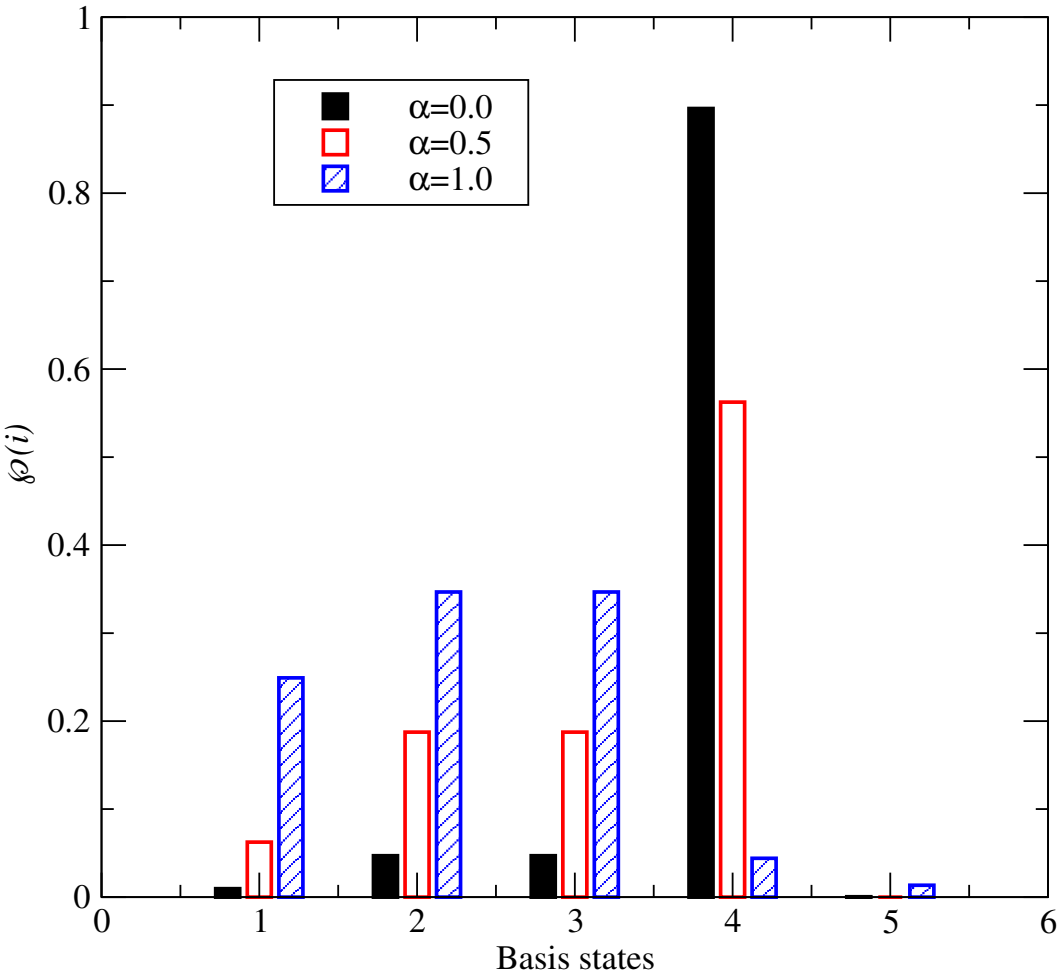

Figure 5.3. 6-spins chain ground-state distribution of strengths for different values of the frustration parameter.

The computation of the matrix elements for the 9-spin chain proceeds in a similar fashion. The only additional step is the re-coupling of the spins in the $\mathcal{V}(2,3)$ matrix element.

$$
\begin{aligned}
&{}_J\langle (l_1 j_1, l_2 j_2) j_{12}, l_3 j_3 \,|\mathcal{V}(2,3)|\, (l'_1 j'_1, l'_2 j'_2) j'_{12}, l'_3 j'_3 \rangle_J = \\
&\delta_{l_1 l'_1} \delta_{j_1 j'_1} \sum_{\{j_{23}\}} \hat{j_{12}} \hat{j'_{12}} \hat{j_{23}}^{\,2} \left\{ \begin{array}{ccc} j_1 & j_2 & j_{12} \\ j_3 & J & j_{23} \end{array} \right\} \left\{ \begin{array}{ccc} j'_1 & j'_2 & j'_{12} \\ j'_3 & J & j_{23} \end{array} \right\} {}_{j_{23}}\langle l_2 j_2, l_3, j_3 \,|\mathcal{V}(2,3)|\, l'_2 j'_2, l'_3 j'_3 \rangle_{j_{23}}
\end{aligned}
\tag{5.8}
$$

5.3 Application

At this point we proceed to construct the range-3 CORE renormalized Hamiltonian for spin-$\frac{1}{2}$ finite chains of arbitrary length. The ultimate goal is to develop a renormalized Hamiltonian that mimics the exact one in the low-energy regime. We will start with a discussion of the 1-state and 2-state truncation procedures and their physical implications. We will successively illustrate in detail the procedure to construct the effective Hamiltonian, and we will conclude with a few concrete examples and predictions of our model.

5.3.1 The truncated basis

As we mentioned previously, the purpose of the truncation is to single out the relevant states in the basis that contribute the most to low-energy properties and which will become our low-energy degrees of freedom. In the preceding section, we showed how frustration affects the spectrum of the basic spin block, which has important consequences on the choice of the states to be retained. For low values of α, only one state contributes significantly to the ground-state energy and the choice to only retain this state therefore appears obvious. In this scheme, both the L and J quantum numbers become "frozen". The net effect of this procedure is that the original three-spins triangle is mapped into a single "quasi-spin" with $J = S$: this new entity represents our low energy degree of freedom. A spin-S chain with N elements can now be reduced to a spin-S chain with $\frac{N}{3}$ elements having the same low-energy properties. As frustration is turned on, the contribution of the $L = 0$ state becomes significant, and can no longer be discarded: two states (out of a total of three) must then be retained. This truncation scheme is susceptible to the same physical interpretation as before, with the additional element that the "quasi-spin" assumes an internal degree of freedom in the form of the link angular momentum L, which can assume the values $L = 0$ or $L = 1$. Alternatively one could identify two different particles, a heavy and a light one, with a different projection of an "isospin" quantum number.

5.3.2 The cluster expansion

The procedures to construct the effective Hamiltonian starting from a single or two states truncation renormalization are technically the same; we will point out any differences along

the way. Eventually we will compare results obtained with both procedures with exact results for small finite chains. It is straightforward to construct the effective Hamiltonian for the single triangle, the range-1 contribution to the expansion:

$$\langle l'j' \left|\mathcal{H}_{\text{eff}}(B_1)\right| lj\rangle = \delta_{ll'}\delta_{jj'}\frac{1}{2}\left[j(j+1)+(\alpha-1)l(l+1)-(2\alpha+1)s(s+1)\right]\mathbf{1}_{d\times d} \equiv h_1 \quad (5.9)$$

where $\mathbf{1}_{d\times d}$ is the range d unity matrix with $d = (2s+1)$ for one-state truncations and $d = 2(2s{+}1)$ for 2-states truncations. One then proceeds to calculate the range-2 contribution by computing the effective Hamiltonian of a system that contains two connected blocks. This is the six spins Hamiltonian of Equation (5.6). In constructing the contribution to the cluster expansion, it is necessary to pay attention to the overlaps between the exact eigenstates of the Hamiltonian and the truncated basis states. Since it is easier to study them in a Hilbert space that reflects the symmetries of the Hamiltonian, we will diagonalize and renormalize the Hamiltonian separately in each J sector. Recall that since $[\mathcal{H}, J] = 0$, the Hamiltonian matrix in the total J basis is an irreducible representation. Also, keep in mind that the J sectors considered are only those allowed by coupling of the *truncated* basis. Now, it is a fundamental CORE theorem that any truncated basis state will contract onto the lowest exact eigenstate with which it has a nonzero overlap. Therefore, if $\langle\phi_1|E_0^{(j)}\rangle \neq 0$ and $\langle\phi_2|E_0^{(j)}\rangle \neq 0$, where $|E_0^{(j)}\rangle$ is the ground eigenstate in the j sector, it will follow that:

$$\lim_{t\to\infty} e^{-t\mathcal{H}}\left|\phi_1\right\rangle \propto \left|E_0^{(j)}\right\rangle \quad \text{and} \quad \lim_{t\to\infty} e^{-t\mathcal{H}}\left|\phi_2\right\rangle \propto \left|E_0^{(j)}\right\rangle \quad (5.10)$$

However CORE demands that each basis state contracts onto a *different* exact eigenstate. We must then be able to construct a new truncated basis $|\xi_i\rangle$ by performing a similarity transformation $\mathbf{S}$ on the original one such that:

$$\lim_{t\to\infty} e^{-t\mathcal{H}}\left|\xi_i\right\rangle \propto \left|E_i^{(j)}\right\rangle \quad \text{for } i = 1\ldots n; \quad j = 1\ldots m \quad (5.11)$$

where n is the size of the truncated space and m is the total number of allowed J sectors. The problem is thus equivalent to orthogonalizing the basis states, for each J sector, in the truncated subspace of energy eigenstates $E_i^{(j)}$, $i \leq n$. Eventually we obtain:

$$\langle\phi_i\|\,\mathcal{H}_{\text{eff}}(B_1,B_2)\,\|\phi_j\rangle = \langle\phi_i|\xi_l\rangle\,\langle\xi_l\|\,\mathcal{H}_{eff}(B_1,B_2)\,\|\xi_m\rangle\,\langle\xi_m|\phi_j\rangle = \mathbf{S}^\dagger\mathbf{H}\mathbf{S} \quad (5.12)$$

where $\langle\phi_i\|\,\mathcal{H}_{\text{eff}}(B_1,B_2)\,\|\phi_j\rangle$ are reduced matrix elements of the 6-spins chain and $\mathbf{H}$ is the diagonal matrix of eigenvalues of the exact Hamiltonian. Since the space of eigenvectors

is larger than the space of the truncated basis, finding the matrix elements $\langle\phi_j|\xi_k\rangle$ of the similarity transformation can be accomplished computationally through Singular Value Decomposition (SVD). Once the renormalized Hamiltonian has been computed in each sector it is straightforward, using standar Clebsh-Gordan coefficients, to compute the renormalized Hamiltonian in a direct product basis, defined as $|\chi_i\rangle = \bigotimes_i |l_i j_i m_i\rangle$:

$$\begin{aligned}\langle l_1 j_1 m_1, l_2 j_2 m_2|\, \mathcal{H}_{\text{eff}}(B_1, B_2)\, |l_1 j_1 m_1, l_2 j_2 m_2\rangle = \\ \delta_{m_1+m_2, m_1'+m_2'} \sum_J \langle l_1 j_1, l_2 j_2, J\|\, \mathcal{H}_{\text{eff}}(B_1, B_2)\, \|l_1 j_1, l_2 j_2, J\rangle \times \\ \langle j_1 m_1, j_2 m_2|Jm_1 + m_2\rangle \langle j_1 m_1, j_2 m_2|Jm_1 + m_2\rangle \quad (5.13)\end{aligned}$$

The range-2 contribution to the cluster expansion is the remainder of this 2-block Hamiltonian after subtraction of the 1-block terms already calculated from Equation (5.9), i.e.:

$$h_2(B_1, B_2) = \mathcal{H}_{\text{eff}}(B_1, B_2) - h_1(B_1) - h_2(B_2) \quad (5.14)$$

Computation of range-3 contribution proceeds in an identical fashion. The first step is to solve exactly the 9-spins structure in each separate sector. After SVD is performed and $\mathcal{H}_{\text{eff}}(B_1, B_2, B_3)$ computed in the direct product basis, one must remove range-1 and range-2 terms:

$$h_3(B_1, B_2, B_3) = \mathcal{H}_{\text{eff}}(B_1, B_2, B_3) - h_1(B_1) - h_2(B_2) - h(B_3) - h_2(B_1, B_2) - h_2(B_2, B_3) \quad (5.15)$$

Larger and larger renormalized connected blocks can be evaluated, but hopefully the expansion will converge fast enough so that only few leading order terms are necessary. Here, we will stop at range-3 contributions. Finally we can put all the pieces together and construct our approximate, up to range-3, normalized Hamiltonian:

$$\mathcal{H}_{\text{eff}} = \sum_{j=1}^{\infty} [h_1(B_j) + h_2(B_j, B_{j+1}) + h_3(B_j, B_{j+1}, B_{j+2})] \quad (5.16)$$

which now allows us to make *predictions* on low-energy properties of larger systems.

5.3.3 Results

Using the expression in Equation (5.16), we are able to construct an approximate Hamiltonian for finite chains of arbitrary size. The only limitations rest with computer

memory and CPU speed availability. The exact Hamiltonian for a N spin-$\frac{1}{2}$ chain contains 2^Ndegrees of freedom. After a 2-states truncation, these are reduced to $2^{\frac{2N}{3}}$ and after a 1-state truncation they are further cut down to $2^{\frac{N}{3}}$. It is then possible to solve renormalized chains containing $\frac{3}{2}N$ sites (2-states) or $3N$ (1-states) in the same amount of CPU time it takes to diagonalize exact chains containing N sites. In this work, we diagonalized exactly chains up to 18 spins as well as renormalized chains up to 54 spins (1-state truncation) and 27 spins (2-states truncation). We employed Lanczos method techniques [72, 73, 69] for the diagonalization of the larger matrices, so that exact diagonalization of the 18-spins chains only takes a few seconds on a 2.8 GHz PC. In fact, by far the more time consuming part of the computation is the evaluation of matrix elements. These were evaluated in the direct product space of the basis states $|l_i j_i m_i\rangle$ according to Equation (5.13). We exploited the conservation of the projection of the z-component of the total spin $m_{\rm t} = \sum_i m_i$ to reduce the number of matrix elements to be computed. The ground-state, for example, will be obtained by retaining only matrix elements for which $m_{\rm t} = \frac{1}{2}$. In Figure 5.4 we show values of the lowest $m_{\rm t} = \frac{1}{2}$ doublet (the ground state) of a 15-spins chain, computed for $0 \leq \alpha \leq 1$. Exact calculations are compared with CORE approximate calculations carried to increasingly higher order. As expected, a 1-state truncation collapses as frustration is turned on. Perhaps more surprising is the noticeable improvement obtained by introducing range-3 corrections. On the other hand, 2-states truncation calculations carried only to range-2 perform even better, remaining constantly within a fractional percent of the exact answer. Range-3 calculations do not present a noticeable improvement over their range-2 counterpart.

The accuracy of these results stimulates us to attempt a finite size scaling approach to extract properties of infinite chains. Energy densities for even numbered chains ($N_{\rm even} = 6, 12, 18, 24$) and odd numbered chains ($N_{\rm odd} = 9, 15, 21, 27$) were computed separately. This was necessary since the energies of even and odd numbered chains are staggered. Calculations were carried using a 2-states range-3 truncation scheme, and the energy densities in the $N \to \infty$ limit were extrapolated using a polynomial fit of the form:

$$\epsilon = a_0 + \frac{a_1}{N} + \frac{a_2}{N^2} + \cdots \tag{5.17}$$

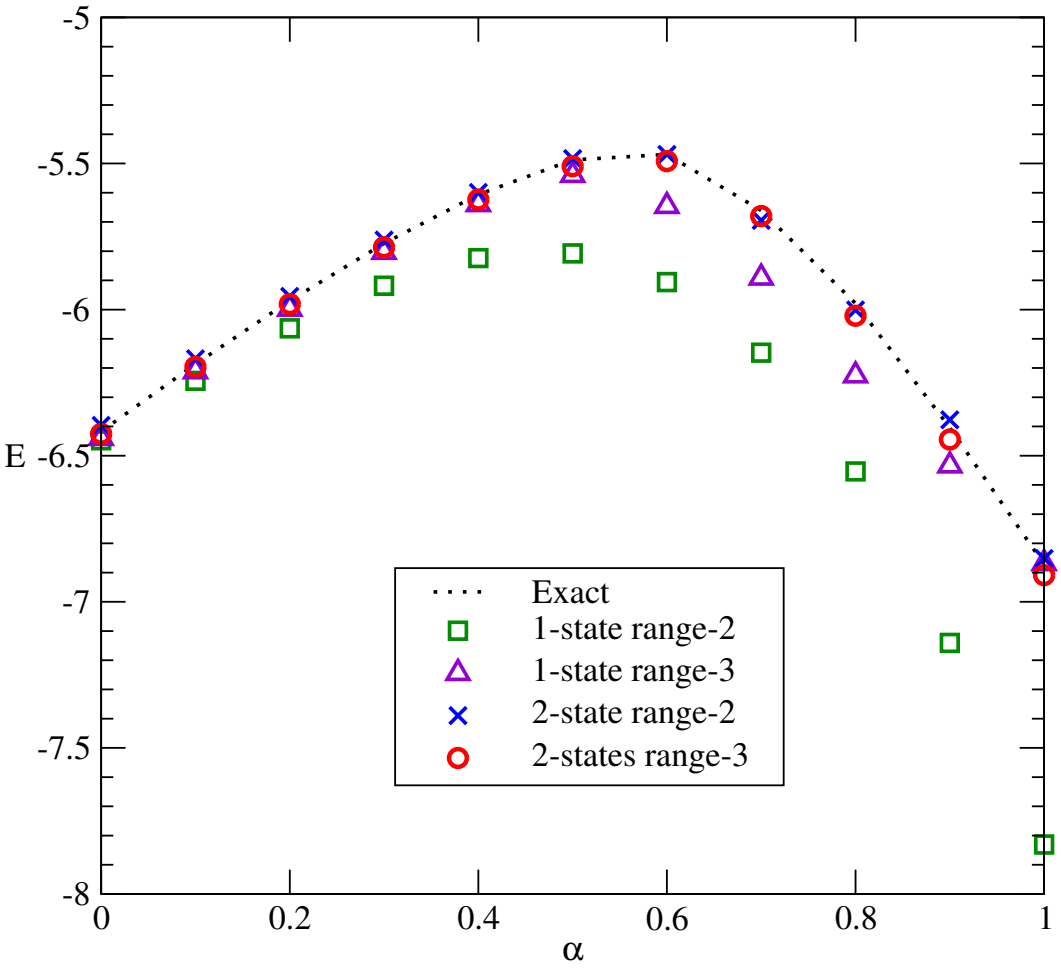

Figure 5.4. 15-spins chains ground-state energies evaluated with different approximations. Computations in the 2-states truncation schemes (X's & circles) mark a significant improvement over their 1-state truncation counterparts (squares & triangles), especially as α is increased.

where N is the number of spins in the chain. Results for the $\alpha = 0$ case are shown in Figure 5.5. The staggered energy densities of odd and even spin numbered chains converge to the value $\epsilon = -0.444$, which replicates within one part in four hundred Bethe's exact answer $\epsilon = -0.443147$.

Ground-state energies were extracted in a similar fashion for a variety of values of α, as shown in Table 5.1. Results are compared to computations by Tonegawa and Harada (T&H) [45] (first column) and Chitra *et al.* [49] (second column). The first authors

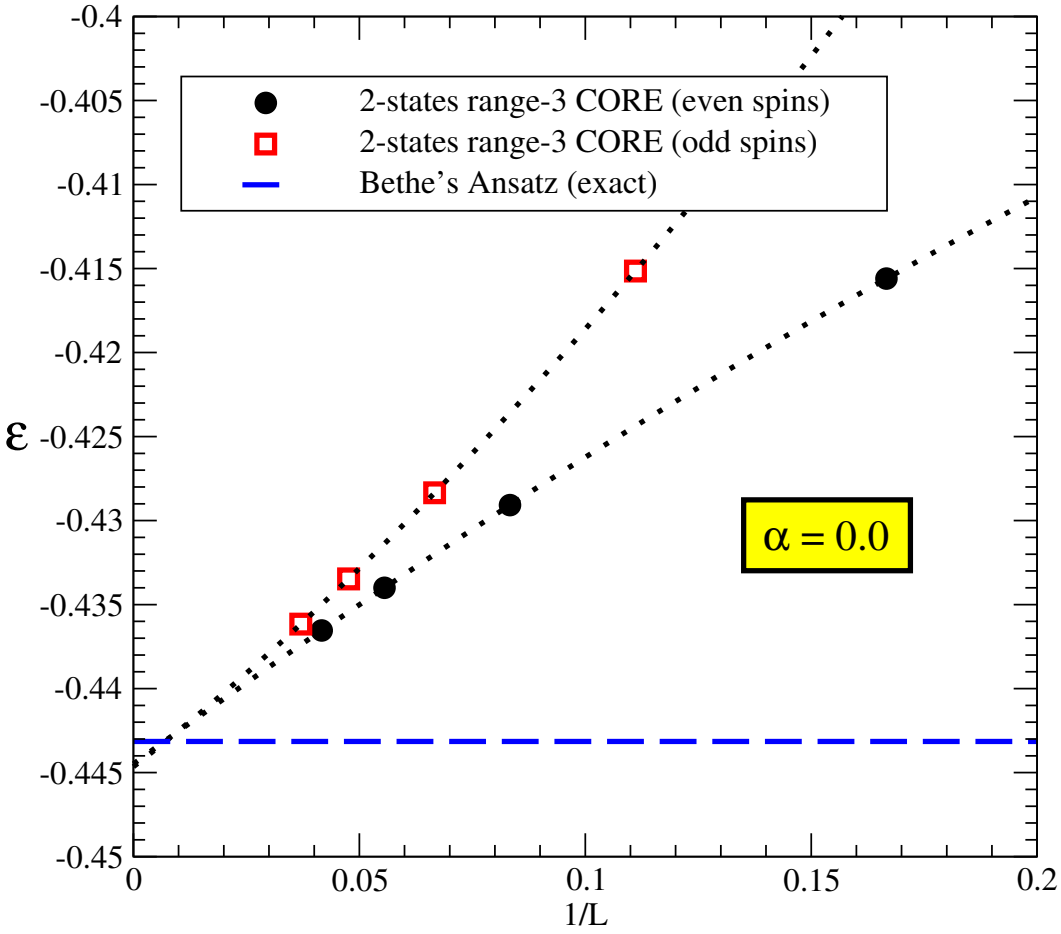

Figure 5.5. Extrapolation of ground-state energy density of the anti-ferromagnetic Heisenberg chain. L is the number of spins in the chain. The energies of odd and even spin number chains are staggered, but they converge to the same value $\epsilon = -0.444$. Bethe's Ansatz exact solution gives $\epsilon = -0.443147$.

used exact diagonaliztion techniques to compute ground-state energies for chains containing up to 20 spins, then extracted the energy in the thermodynamic limit using a so-called ε-alternating algorithm. The second performed a Density Matrix Renormalization Group (DMRG) calcuation.

The extrapolation of the spin gap proceeds along the same lines, but presents a few more challenges. The gap for even number of spins is defined as the difference between the lowest energies E_0 in the $m_t = 0$ and $m_t = 1$ sectors and has been computed for $N = 6, 12, 18, 24$.

Table 5.1. Compared DMRG and CORE ground-state energy densities for various values of α. The quantities in parenthesis represent the result's ratio to the exact value.

α	T & H	DMRG	CORE
0.0	-0.443145	–	-0.44448 (1.002)
0.1	-0.425345	-0.42517	-0.42690 (1.004)
0.2	-0.408505	-0.40885	-0.41035 (1.004)
0.3	-0.393070	-0.39284	-0.39509 (1.006)
0.4	-0.380350	-0.38028	-0.38314 (1.007)

Keep in mind, however, that it is extremely difficult to maintain the same level of accuracy as in energy density calculations, on account of error propagation derived from subtracting $E_0(m_t = 0)$ and $E_0(m_t = 1)$. Compare, for instance, the relative errors of approximated energies and gap in an 18-spins chain (Table 5.2).

Table 5.2. Values and relative errors of the lowest singlet ($m_\mathrm{t} = 0$) and triplet ($m_\mathrm{t} = 1$) energies and corresponding spin gaps of an 18-spins chain.

	Exact	CORE
$E_0(m_t = 0)$	-6.82728	-6.85781 (1.004)
$E_0(m_t = 1)$	-6.61047	-6.62141 (1.002)
ΔE	0.21681	0.23640 (1.09)

Even though CORE's calculation predicts $E_0(m_\mathrm{t} = 0)$ and $E_0(m_\mathrm{t} = 1)$ with an accuracy better than 0.4%, the spin gap relative error levitates up to 9%. Figure 5.6 shows the gap extrapolation procedure for a range of frustration values. Spin gap behaviour versus α is illustrated in Figure 5.7, where it is compared to two separate DMRG calculations by White [48] and Chitra [49]. Even though relative errors remain in the order of several percent, our approximation describes in a qualitatively satisfactory fashion the transition to the gapped phase in the neighborhood of $\alpha = 0.3$. It should also be noted that the determination of spin gaps presents a serious challenge even for the most sophisticated DMRG techniques. This is confirmed by the fact that the two DMRG caluculations cited here disagree noticeably in the $\alpha > 0.5$ region.

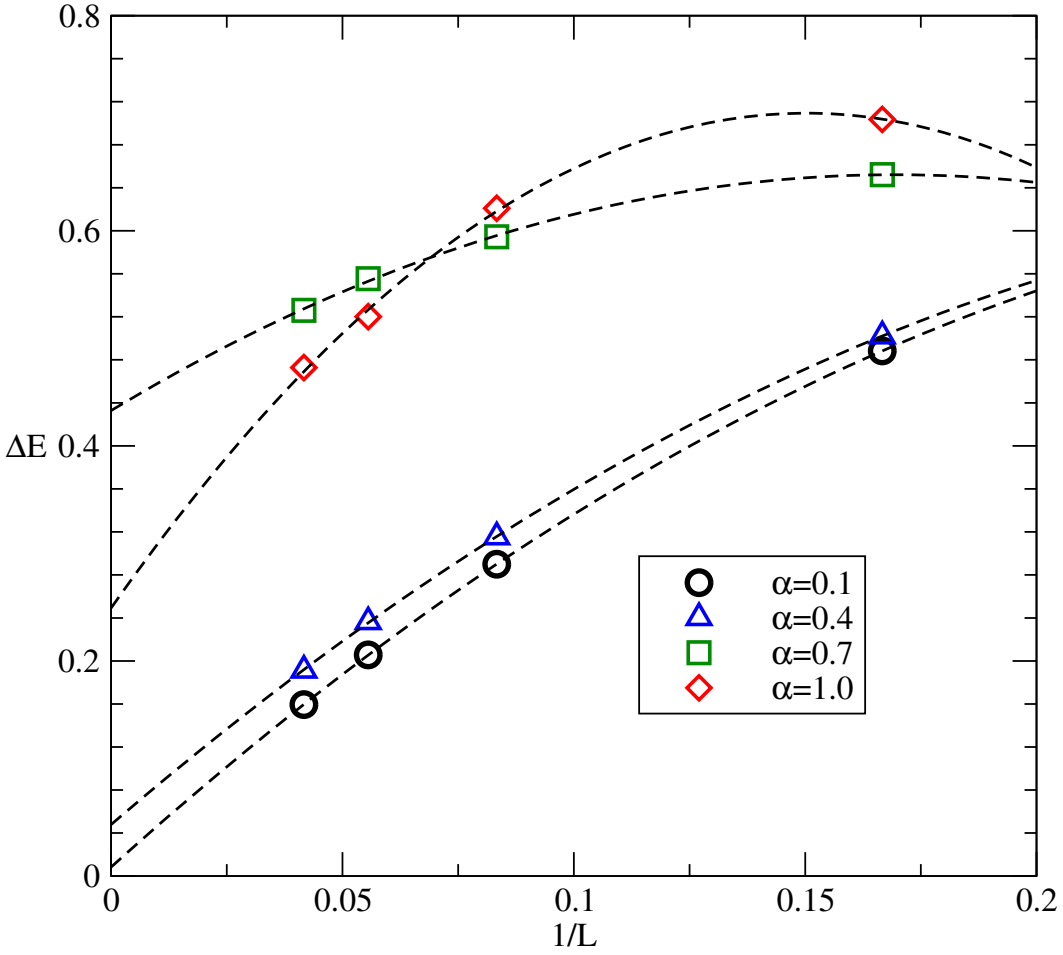

Figure 5.6. Extrapolation of singlet-triplet gaps. L is the number of spins in the chain.

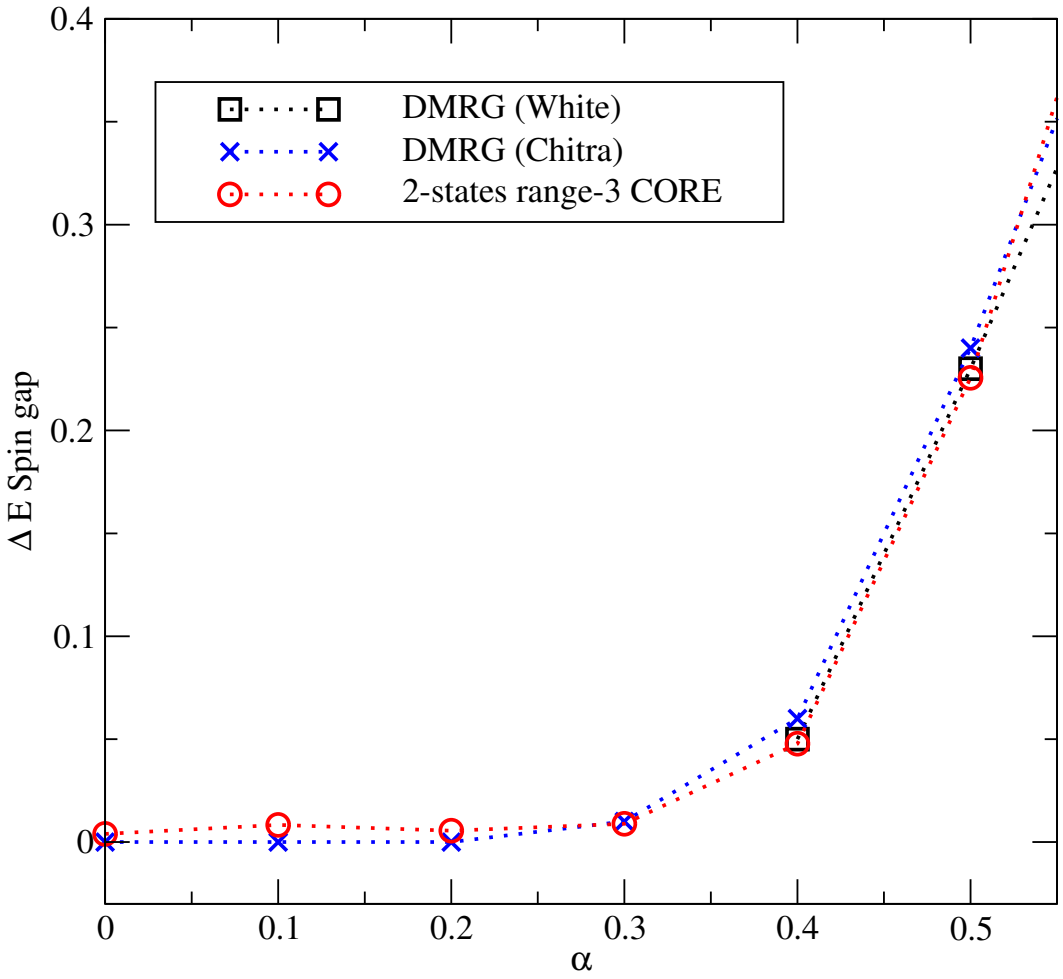

Figure 5.7. Comparison of extrapolated singlet-triplet gaps using CORE and DMRG calculations.

CHAPTER 6

RENORMALIZATION GROUP EQUATIONS

6.1 Introduction

In this Chapter we will develop a renormalization group equation for arbitrary spin frustrated chains by iterating the effective Hamiltonian derivation procedure described in Chapter 5. The basic idea is the following: each step of the renormalization maps the elementary three-spins triangle onto a "quasi-spin" entity with the same spin quantum number as the original site. In doing this, we find ourselves with a chain described by an Hamiltonian with the same structure as the original one *but with only one third of the number of degrees of freedom*. The iteration can be repeated indefinitely and the degrees of freedom continuously thinned. We will also consider two different cases. In the first one, we will simply extend Morningstar and Weinberg's results to arbitrary spin and compare our results to DMRG solutions and Anderson's spin wave approximation. In the second one, we will include frustrated systems, which requires including range-3 terms.

6.2 Range-2 expansion

The system we will consider here is the unfrustrated anti-ferromagnetic Heisenberg chain, which we will parametrize in the form of a "step zero" renormalized Hamiltonian:

$$\mathcal{H} = \sum_{n=1}^{N} \vec{S}_n \cdot \vec{S}_{n+1} = \sum_{n=1}^{N} \left\{ J_0^{(0)} + J_1^{(0)} \vec{S}_n \cdot \vec{S}_{n+1} \right\} \equiv \mathcal{H}_{\text{ren}}^{(0)} \tag{6.1}$$

with $J_0^{(0)} = 0$ and $J_1^{(0)} = 1$. We start once more with the treatment of range-1 terms. Using the energy spectrum of Equation (5.5) with $\alpha = 0$, we deduce that the ground state of the spin triangle is $|\phi_0\rangle = |l = 2s, j = s\rangle$ with energy $\epsilon_0^{(0)} = -s(2s+1)$. Note once more that

the ground state energy of the triangle always has the same spin quantum number as the original spin. In this way the range-1 Hamiltonian is given by:

$$h_1^{(1)}(n) = \alpha_0^{(0)}\mathbf{1}(n) = -s(2s+1)\mathbf{1}(n) \tag{6.2}$$

where $\mathbf{1}(n)$ is the $(2s+1)\times(2s+1)$ unit matrix. Symmetry suggests that the renormalized two-triangles Hamiltonian must have the parametrized form:

$$\mathcal{H}_{\rm ren}^{(1)}(1,2) = \beta_0^{(0)} + \beta_1^{(0)}\vec{S}_1\cdot\vec{S}_2 \tag{6.3}$$

which is identical to the exact Hamiltonian up to an additive factor. The constants $\beta_0^{(0)}$ and $\beta_1^{(0)}$ can easily be extracted from the lowest singlet $\epsilon_0^{(0)}$ and triplet $\epsilon_1^{(0)}$ energies:

$$\epsilon_0^{(0)} = \beta_0^{(0)} - \beta_1^{(0)}s(s+1); \qquad \epsilon_1^{(0)} = (\beta_0^{(0)} + \beta_1^{(0)}) - \beta_1^{(0)}s(s+1) \tag{6.4}$$

which upon inversion give:

$$\beta_0^{(0)} = \epsilon_0^{(0)} + (\epsilon_1^{(0)} - \epsilon_0^{(0)})s(s+1) = \epsilon_0^{(0)} + \Delta^{(0)}s(s+1) \tag{6.5}$$

$$\beta_1^{(0)} = (\epsilon_1^{(0)} - \epsilon_0^{(0)}) = \Delta^{(0)} \tag{6.6}$$

The range-2 connected Hamiltonian is obtained by subtracting the range-1 contributions:

$$h_2^{(1)}(1,2) \equiv \mathcal{H}_{\rm ren}^{(1)}(1,2) - h_1^{(1)}(1) - h_1^{(1)}(2) \tag{6.7}$$

$$= (\beta_0^{(0)} - 2\alpha_0^{(0)}) + \beta_1^{(0)}\vec{S}_1\cdot\vec{S}_2 \tag{6.8}$$

The renormalized Hamiltonian for an N-spins chain now becomes:

$$\begin{aligned}
\mathcal{H}_{\rm ren}^{(1)} &= \sum_{n=1}^{N/3}\Big\{h_1^{(1)}(n) + h_2^{(1)}(n,n+1)\Big\} \\
&= \sum_{n=1}^{N/3}\Big\{\alpha_0^{(0)} + (\beta_0^{(0)} - 2\alpha_0^{(0)}) + \beta_1^{(0)}\vec{S}_n\cdot\vec{S}_{n+1}\Big\} \\
&= \sum_{n=1}^{N/3}\Big\{(\beta_0^{(0)} - \alpha_0^{(0)}) + \beta_1^{(0)}\vec{S}_n\cdot\vec{S}_{n+1}\Big\} \\
&= \sum_{n}^{N/3}\Big\{J_0^{(1)} + J_1^{(1)}\vec{S}_n\cdot\vec{S}_{n+1}\Big\}
\end{aligned} \tag{6.9}$$

where:

$$J_0^{(1)} = \beta_0^{(0)} - \alpha_0^{(0)}; \qquad J_1^{(1)} = \beta_1^{(0)} \tag{6.10}$$

Since the effective Hamiltonian is identical in structure to the original one as displayed in Equation (6.1), we can carry an additional step in the renormalization procedure, by computing singlet and triplet energies of the new six spin structure and extracting the parameters $J_0^{(2)}$ and $J_1^{(2)}$ through Equations (6.10) to obtain :

$$\mathcal{H}_{\text{ren}}^{(2)} = \sum_{n=1}^{N/9} \left\{ J_0^{(2)} + J_1^{(2)} \vec{S}_n \cdot \vec{S}_{n+1} \right\} \tag{6.11}$$

In general it is found that after k iterations of the process the Hamiltonian will retain the form:

$$\mathcal{H}_{\text{ren}}^{(k)} = \sum_{n=1}^{N/3^k} \left\{ J_0^{(k)} + J_1^{(k)} \vec{S}_n \cdot \vec{S}_{n+1} \right\} \tag{6.12}$$

with the evolution of the parameters given by:

$$J_0^{(k)} = 3^k J_0^{(0)} + b \frac{\left[3^k - \left(\Delta^{(0)} \right)^k \right]}{3 - \Delta^{(0)}} J_1^{(0)}; \qquad J_1^{(k)} = \left(\Delta^{(0)} \right)^k J_1^{(0)} \tag{6.13}$$

where $b \equiv \epsilon_0^{(0)} + s(2s+1) + \Delta^{(0)} s(s+1)$. The evolution of the J_1 parameter is of relevance for the determination of the spin gap. It is easy to realize that the theory will exhibit a spin gap in the thermodynamic limit only if $\lim_{k\to\infty} J_1^{(k)} \neq 0$. In the case under consideration $J_1^{(0)} = 1$, hence $J_1^{(k)} = \left(\Delta^{(0)} \right)^k$. Therefore, the theory will have a gap-less spectrum if $\Delta^{(0)} < 1$, which is the case for all half-integer spins, as shown in Table (6.1).

Table 6.1. Six-spins chain singlet-triplet gaps for various half-integer spins.

Spin	$\frac{1}{2}$	$\frac{3}{2}$	$\frac{5}{2}$	$\frac{7}{2}$	$\frac{9}{2}$
$\Delta^{(0)}$	0.4915	0.2994	0.3058	0.3128	0.3170

Hence we obtain from Equation (6.13):

$$\lim_{k \longrightarrow \infty} J_0^{(k)} = b \frac{3^k}{3 - \Delta^{(0)}} \quad \text{and} \quad \lim_{k \longrightarrow \infty} J_1^{(k)} = 0 \tag{6.14}$$

The renormalized Hamiltonian density becomes:

$$\frac{\mathcal{H}_{\text{ren}}^{(k)}}{N} = \sum_{n=1}^{N/3^k} J_0^{(k)} = \left(\frac{b}{3 - \Delta^{(0)}} \right) \tag{6.15}$$

which allows us to predict the ground state energy density of chains with arbitrary spin (see Figure 6.1).

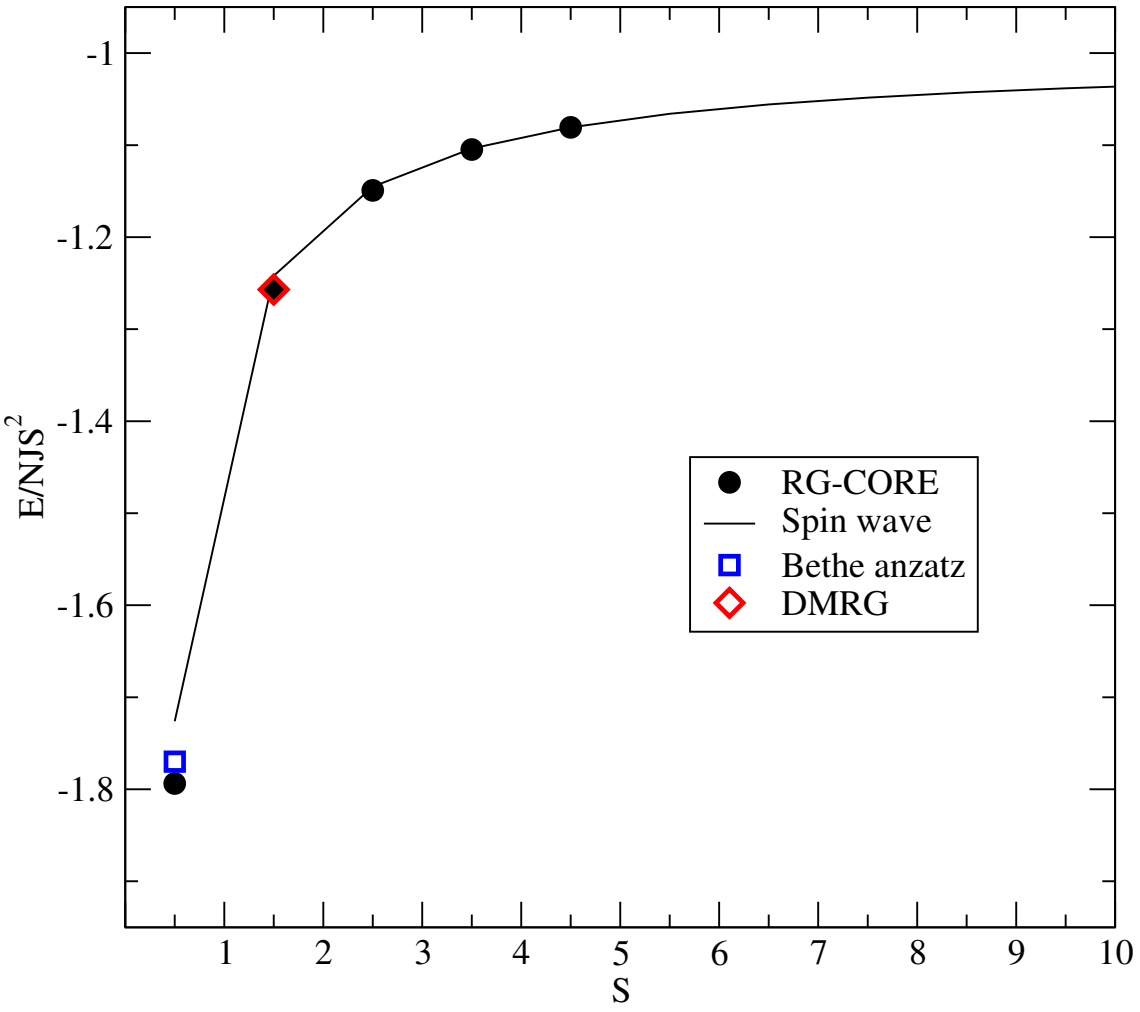

Figure 6.1. Ground state energy density for various half-integer spins calculated with a range-2 CORE renormalization group equation.

6.3 Range-3 expansion

Our starting point is once again Equation (5.1). Computation of range-1 and range-2 terms proceeds in a similar fashion as described in the previous section. We now parametrize the renormalized range-3 Hamiltonian as follows:

$$H_{\rm ren}(1,2,3) = \gamma_0 + \gamma_1 \left[\vec{S}_1 \cdot \vec{S}_2 + \vec{S}_2 \cdot \vec{S}_3\right] + \gamma_2 \vec{S}_1 \cdot \vec{S}_3 \tag{6.16}$$

This Hamiltonian can be solved either numerically or analytically and we obtain the spectrum:

$$E = \gamma_0 + \frac{\gamma_1}{2}\left[S_{123}(S_{123}+1) - \left(1 - \frac{\gamma_2}{\gamma_1}\right) S_{13}(S_{13}+1) - \left(1 + 2\frac{\gamma_2}{\gamma_1}\right) S(S+1)\right] \tag{6.17}$$

The coefficients of the parametrization are extracted from the two lowest $S = \frac{1}{2}$ and the lowest $S = \frac{3}{2}$ eigenstates of the 9-spin Hamiltonian. That is:

$$\begin{aligned}
\epsilon_a &= E(S_{13}=1; S_{123}=\frac{1}{2}) = \gamma_0 - \gamma_1 + \gamma_2/4 \\
\epsilon_b &= E(S_{13}=0; S_{123}=\frac{1}{2}) = \gamma_0 - 3\gamma_2/4 \\
\epsilon_c &= E(S_{13}=1; S_{123}=\frac{3}{2}) = \gamma_0 + \gamma_1/2 + \gamma_2/4
\end{aligned}$$

which may be easily inverted to give:

$$\begin{aligned}
\gamma_0 &= (\epsilon_a + \epsilon_b + 2\epsilon_c)/4 \\
\gamma_1 &= (-2\epsilon_a + 2\epsilon_c)/3 \\
\gamma_2 &= (\epsilon_a - 3\epsilon_b + 2\epsilon_c)/3
\end{aligned}$$

In this manner the connected range-3 contribution becomes equal to:

$$\begin{aligned}
h_3(1,2,3) &= H_{\rm ren}(1,2,3) - h_2(1,2) - h_2(2,3) - h_1(1) - h_1(2) - h_1(3) \\
&= \left[\gamma_0 + \gamma_1(\vec{S}_1 \cdot \vec{S}_2 + \vec{S}_2 \cdot \vec{S}_3) + \gamma_2 \vec{S}_1 \cdot \vec{S}_3\right] - \\
&\left[2(\beta_0 - 2\alpha_0) + \beta_1(\vec{S}_1 \cdot \vec{S}_2 + \vec{S}_2 \cdot \vec{S}_3)\right] - 3\alpha_0
\end{aligned}$$

or:

$$h_3(n,n+1,n+2) = (\gamma_0 - 2\beta_0 + \alpha_0) + (\gamma_1 - \beta_1)(\vec{S}_n \cdot \vec{S}_{n+1} + \vec{S}_{n+1} \cdot \vec{S}_{n+2}) + \gamma_2 \vec{S}_n \cdot \vec{S}_{n+2}$$

$$\gamma_0 = (\epsilon_a + \epsilon_b + 2\epsilon_c)/4; \quad \gamma_1 = (-2\epsilon_a + 2\epsilon_c)/3; \quad \gamma_3 = (\epsilon_a - 3\epsilon_b + 2\epsilon_c)/3$$

Finally, the renormalized Hamiltonian corrected to include up to range-3 contribution is given by the following expression:

$$\begin{aligned} H_{\text{ren}} &= \sum_{n=1}^{N/3} [h_1(n) + h_2(n, n+1) + h_3(n, n+1, n+2)] \\ &= \sum_{n=1}^{N/3} \left[\alpha_0 + \left[(\beta - 2\alpha_0) + \beta_1 \vec{S}_n \cdot \vec{S}_{n+1}\right]\right] + \\ &\quad \left[(\gamma_0 - 2\beta_0 + \alpha_0) + (\gamma_1 - \beta_1)\left(\vec{S}_n \cdot \vec{S}_{n+1} + \vec{S}_{n+1} \cdot \vec{S}_{n+2}\right) + \gamma_2 \vec{S}_n \cdot \vec{S}_{n+2}\right] \\ &= \sum_{n=1}^{N/3} \left[(\gamma_0 - \beta_0) + (2\gamma_1 - \beta_1)\, \vec{S}_n \cdot \vec{S}_{n+1} + \gamma_2 \vec{S}_n \cdot \vec{S}_{n+2}\right] \end{aligned}$$

or:

$$H_{\text{ren}} = \sum_{n=1}^{N/3} \left\{J_0 + J_1 \vec{S}_n \cdot \vec{S}_{n+1} + J_2 \vec{S}_n \cdot \vec{S}_{n+2}\right\} \tag{6.18}$$

where

$$J_0 = \gamma_0 - \beta_0; \quad J_1 = 2\gamma_1 - \beta_1; \quad J_2 = \gamma_2 \tag{6.19}$$

Although the renormalized Hamiltonian retains the form of the exact one with nnn coupling and frustration, Equation (5.1), and it could be possible to develop a simple analytic equation for the evolution of the parameters, it is much simpler to compute numerically the relevant energies at each step and extract from the latter the required parameters. For instance, the energies of the 9-spins of Equation (5.1) are given by:

$$\begin{aligned} \epsilon_a^{(1)} &= 9J_0^{(1)} + J_1^{(1)} \epsilon_a^{(0)}(\alpha^{(1)}) \\ \epsilon_b^{(1)} &= 9J_0^{(1)} + J_1^{(1)} \epsilon_b^{(0)}(\alpha^{(1)}) \\ \epsilon_c^{(1)} &= 9J_0^{(1)} + J_1^{(1)} \epsilon_c^{(0)}(\alpha^{(1)}) \end{aligned}$$

where $\epsilon_a^{(0)}(\alpha^{(1)})$ is the lowest $j = \frac{1}{2}$ of a 9-spin chain with frustration $\alpha^{(1)} = \frac{J_2^{(1)}}{J_1^{(1)}}$. Numerical convergences of $J_0/3^k$, J_1 and J_2 for various values of α are shown in Figure 6.2. For every frustration parameters we tested, J_1 and J_2 appear to converge to zero, which would indicate a gap-less theory. It seems quite obvious that this situation is identical for all α: this is however not the correct answer. On the other hand, the disappearance of J_1 and J_2 implies that the value of $J_0/3^k$ is now a prediction of the ground state energy density. We computed energy densities for a variety of values of α in the case $S = \frac{1}{2}$ (Table 6.2).

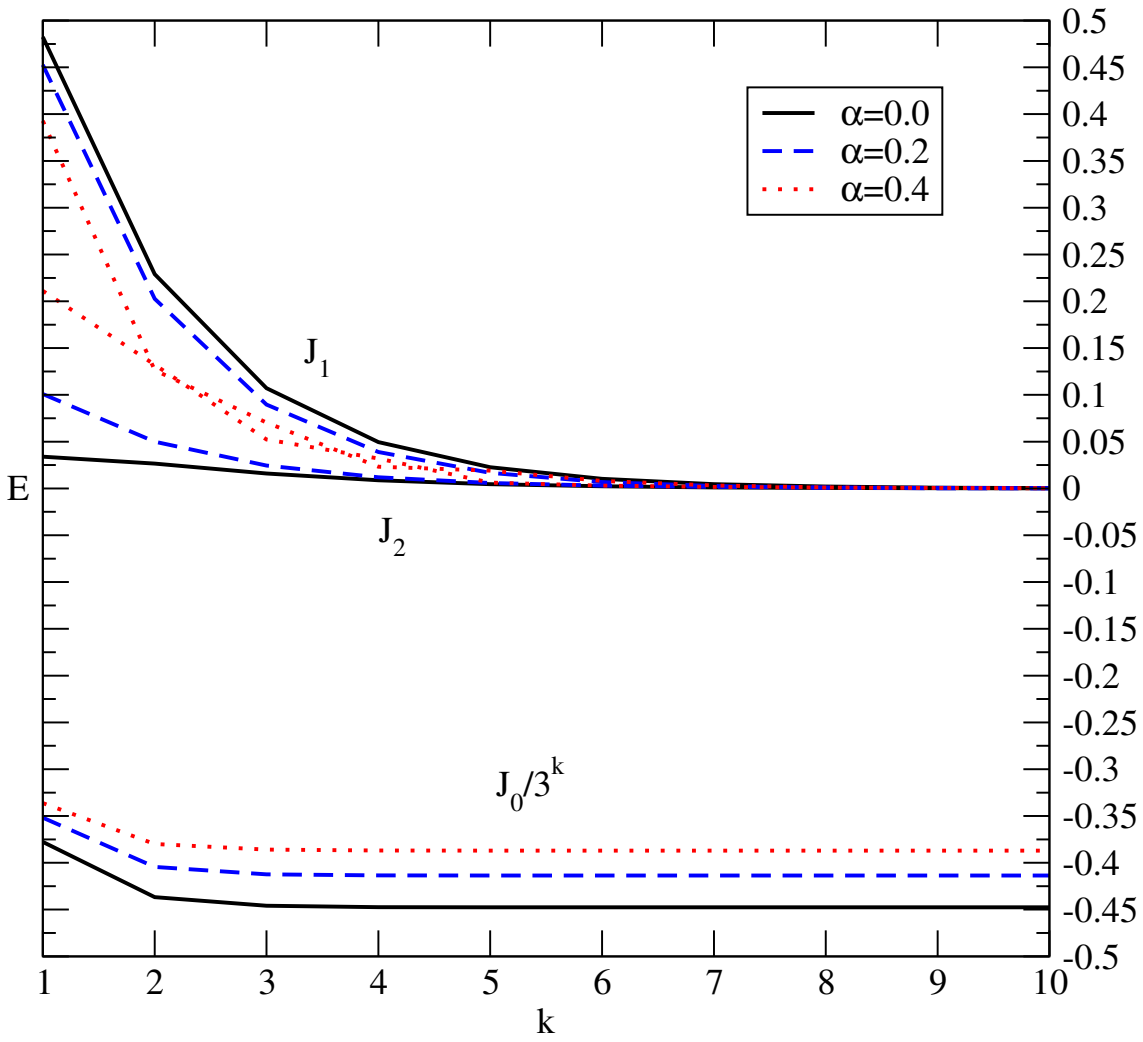

Figure 6.2. Evolution of the renormalization parameters for various values of frustration.

Table 6.2. Energy densities for a range of frustration parameters obtained from DMRG calculations and CORE renormalization group equations. Quantities within parentheses represent ratios to DMRG values.

α	DMRG	CORE
0.1	-0.42517	-0.430197 (1.012)
0.2	-0.40885	-0.413619 (1.012)
0.3	-0.39284	-0.398240 (1.014)
0.4	-0.38028	-0.387067 (1.018)

CHAPTER 7

CONCLUSIONS

While the field of nuclear structure has benefited from recent advances in numerical algorithms and sheer computational power, the shell-model problem, in its purest form, remains intractable. As a result, an important part of the nuclear-structure program for many years has focused on the construction of effective interactions for use in shell-model calculations. Two of the most promising approaches are based on the so-called similarity transformation methods (in its many varieties) and on effective-field-theory techniques. The main tenet underlying both approaches is that the short-distance structure of a theory (which is complicated and possibly unknown) is hidden to a long-wavelength probe. It should then be possible to modify the corresponding short-range portion of the potential while leaving all low-energy properties of the theory intact.

The first part of this dissertation work consisted of the determination of single-particle operators which can be employed consistently in conjunction with wave-functions obtained using effective interactions. As observed by many authors, such consistency is essential to the correct implementation of effective theories. For computational simplicity we adopted a one-dimensional NN interaction, which nevertheless incorporates the well-known pathologies of a realistic NN potential. The central result of this work is the proposal and implementation of a single underlying approach for the construction of both effective interactions and effective operators. The construction of the effective interaction follows a well-known approach that is based on a textbook derivation of the scattering effective-range expansion.

Results from such an implementation are very gratifying, as evinced from a variety of calculations of ground-state observables. For those observables insensitive to the short-range structure of the potential, such as the root-mean-square radius of the deuteron, the renormalization of the bare operator, while required by consistency, has little phenomenological impact. Yet failing to properly renormalize operators sensitive to short-range physics, such as

the elastic form factor of the deuteron at high-momentum transfers, can yield discrepancies as large as 200%. The consistent renormalization procedure advocated here yields in all cases errors of less than 1%.

The effective nucleon-nucleon potential derived here was also applied to the solution of a one-dimensional three-nucleon system. We employed various methods to solve Schrödinger's equation for the three-body problem including only pairwise potentials, both bare and effective. Three-body forces, both real and induced, were here neglected for simplicity. The solutions proposed here were based on 1) the standard No-Core Shell Model (NCSM) approach, 2) a Jacobi coordinates transformation leading to a translationally invariant Hamiltonian and 3) a Hyper-spherical Harmonic technique. In many cases we heavily relied on the development of a Lanczos algorithm for the diagonalization of large symmetric matrices. Our results show that Schrödinger's equation for the three-body system can be handled quite well by each of the methods, which ultimately show very good agreement in ground-state binding energies. However, the discrepancy between the ground state energy in the bare and effective scheme confirms the need, already established in shell model calculations with realistic nucleon-nucleon potentials, for many-body effective correction terms. On the other hand, these calculations were able to confirm the usefulness of effective potential when dealing with pathologically intractable interactions such as the nuclear one. In fact, we were able to prove that the size of the model space necessary to achieve convergence of the results is considerably smaller when a renormalized potential is employed. This is due to the fact that high-energy modes are excluded from the softened potential, all relevant high-energy physics having been incorporated in the parameters of the expansion. This is true for both the calculations in the No-Core Shell Model and Jacobi transformation schemes. By the same token, a significantly smaller number of coupled differential equations is necessary in the Hyper-spherical Harmonic calculation.

We conclude this section with a short comment on future work. The results presented here are encouraging and lend validity to the proposed approach, which is currently being extended to the three-body system. The results obtained here also constitute a promising first step toward our ultimate goal of combining similarity-transformation methods with effective interactions. The effective interactions and operators obtained here—with their sharp short-range features no longer present—could provide a more suitable

starting point for the numerically-intensive approaches based on similarity transformations. Finally, the method proposed here will have to be extended to three-spatial dimensions. Other than numerical complexity, we do not foresee other serious challenges. Indeed, the approach presented here for the construction of effective interactions (whose three-dimensional derivation may be found in several textbooks) had to be adapted to one spatial dimension. In summary, a novel approach for the renormalization of operators in a manner consistent with the construction of the effective potential has been proposed and implemented with considerable success. The results obtained here are gratifying and suggest how in the future effective theories may be profitably combined with more traditional methods to tackle the nuclear many-body problem.

In a second part of this work we applied the CORE renormalization technique to the study of low-energy properties of frustrated spin chains. To a large degree, we were motivated in the choice of this specific application by the desire to prove the great flexibility and wide range of applicability of the method itself. Moreover, the subject of quantum spin compounds has in recent years enjoyed a surge in interest due mainly to the great variety of interesting and often surprising properties that the presence of frustration induces. More specifically, we dedicated our attention to the low-energy properties of half-integer zig-zag chains, with nearest-neighbor (nn) and next-to-nearest neighbor (nnn) coupling. Frustration in such systems arises when the strengths of the nn and nnn couplings are allowed to take different values. We successfully managed to show that a simple CORE renormalization can reproduce, often with great accuracy, many of the characteristic properties of the system. According to CORE's procedure a basic building block was identified in the triangle composed of three neighboring spins. We exploited Racah's algebra techniques to define a basis in which the spins are coupled to a definite value of the total angular momentum. Two different truncation schemes were defined: in the first one only the lowest state of the basic block is retained, mapping three spins in the chain to a single "quasi-particle" which can be shown to possess the same total angular momentum quantum number of the original chain. In the second scheme, two lowest states are retained. These new entities can be interpreted to be the the low-energy degrees of freedom of our effective theory, much like nucleons are low-energy representations of their underlying quark structure. Our analysis proceeded along two lines. In the first approach, the Hamiltonian for two and three basis

building blocks was renormalized according to CORE's prescription and a cluster expansion was developed to predict low-energy observables of larger structures. Ground state energy densities were computed for chains up to 54 spins, when only one state is retained in the truncation procedure, and up to 27 spin, when two states are retained. Our results concluded that the one-state truncation procedure is no longer accurate when frustration in turned on due to mixing of lowest energy states. The need for a two-states truncation scheme for frustration values $\alpha > 0.3$ represents one of the major findings of our research. Furthermore, our results compare quite well against precise Density Matrix Renormalization Group calculations, with deviations that constantly remain under 1% in the $\alpha < 0.5$ range. These results are especially encouraging if one considers that our calculations are much lighter and computationally less demanding. A further advantage of CORE's approach over DMRG's is the possibility of computing dynamical properties such as transition amplitudes. Spin gaps for a variety of frustration parameters were also computed, albeit with a lesser degree of accuracy due to the simple fact that this quantity has to be extracted by subtraction of two others (the $J = 0$ and $J = 1$ ground state energies) of the same order of magnitude, with consequent propagation of relative error. When compared to DMRG calculations, the deviation of our results levitates up to 9%. However, at least for frustration $\alpha < 0.4$, we are still able to qualitatively describe the behavior of the spin gap as a function of frustration, including the predicted disappearing of the gap-less phase around $\alpha = 0.3$ and the asymptotic fallout as the zigzag chain converges to two coupled linear chains with simple nn couplings. In a second approach, we exploited the fact that the renormalized Hamiltonian can be cast in a form that is identical to the bare one to construct a renormalization group equation that, through iteration of the renormalization procedure, is able to predict energy densities for infinite chains. The renormalization group equation for zero frustration was first developed by Morningstar & Weinstein for spin-$\frac{1}{2}$ chains. In this case the authors were able to truncate the cluster expansion at range-2 contributions, since only nearest neighbor interactions need to be included. In our contribution we extended the formalism to treat arbitrary integer and half-integer spin chains, which can be accomplished rather easily in the framework of CORE's formalism. One of the most remarkable features of this method is that a simple two-parameter equation is able to reproduce with great accuracy ($< 1\%$) Bethe's exact answer (for $S = \frac{1}{2}$), DMRG calculations (for $S = \frac{3}{2}$, that we are aware

of) and Anderson's approximate spin wave calculations (for arbitrary half-integer spins). In addition, we developed a similar renormalization group equation to include frustrated chains, which required the inclusion of range-3 effective interaction, as well as of two more additional parameters. Results for energy densities agree with DMRG calculations within a few percent, therefore proving to be slightly less accurate than our previous results. This is almost certainly due to the fact that the RG equation as we constructed it employs throughout a one (rather than two) states truncation. This finding goes to further enhance our previous claim that a two-state truncation is necessary to achieve accuracy in our frustrated chains renormalization scheme. It should finally be added that the RG formalism is, as of yet, unable to predict spin gaps. So far, it is not clear to us how this extremely important feature can be implemented in the RG approach.

APPENDIX A

DERIVATION OF MOSHINSKY BRACKETS FOR A GENERAL ORTHOGONAL TRANSFORMATION

The recursion relation for the Hermite polynomials is given by:

$$\exp(-s^2+2st)=\sum_{n=0}^{\infty}\frac{s^n}{n!}H_n(t) \tag{A.1}$$

from which the the following recursion relations are derived:

$$\begin{cases} H_{n+1}(t) & = 2tH_n(t)-snH_{n-1}(t) \\ H_n'(t) & = 2nH_{n-1}(t) \end{cases} \tag{A.2}$$

Now define:

$$\begin{aligned} R &\equiv \frac{1}{\sqrt{2}}(ax_1+bx_2) & \sigma &\equiv \frac{1}{\sqrt{2}}(as+bt) \\ & \text{and} & & \\ X &\equiv \frac{1}{\sqrt{2}}(bx_1-ax_2) & \tau &\equiv \frac{1}{\sqrt{2}}(bs-at) \end{aligned} \tag{A.3}$$

with $a^2+b^2=1$. This transformation is clearly orthogonal. Then we have:

$$s^2+t^2-2sx_1-2tx_2=\sigma^2+\tau^2-2\sigma R-2\tau x \tag{A.4}$$

or

$$(e^{-s^2+2sx_1})(e^{-t^2+2stx_2})=(e^{-\sigma^2+2\sigma R})(e^{-\tau^2+2\tau X})$$

from which, using Equation (A.1) one obtains:

$$\sum_{n=0}^{\infty}\sum_{m=0}^{\infty}\frac{s^m}{m!}\frac{t^n}{n!}H_n(x_1)H_m(x_2)=\sum_{k=0}^{\infty}\sum_{l=0}^{\infty}\frac{\sigma^k}{k!}\frac{\tau^l}{l!}H_k(R)H_l(X) \tag{A.5}$$

This equation can be expanded using the binomial relations:

$$\begin{cases} \sigma^k = \left[\frac{(as+bt)}{\sqrt{2}}\right]^k & = \frac{1}{2^{k/2}} \sum_{i=0}^{k} \begin{pmatrix} k \\ i \end{pmatrix} s^i t^{k-i} a^i b^{k-i} \\ \tau^l = \left[\frac{(bs-at)}{\sqrt{2}}\right]^l & = \frac{1}{2^{l/2}} \sum_{j=0}^{l} \begin{pmatrix} l \\ j \end{pmatrix} s^j (-t)^{l-j} b^j a^{l-j} \end{cases} \tag{A.6}$$

Equations (A.6) can be plugged into Equation (A.5):

$$\begin{aligned} &\sum_{n=0}^{\infty}\sum_{m=0}^{\infty} \frac{s^m}{m!}\frac{t^n}{n!} H_n(x_1)H_m(x_2) = \\ &\quad \sum_{k=0}^{\infty}\sum_{l=0}^{\infty}\sum_{i=0}^{k}\sum_{j=0}^{l} \frac{\begin{pmatrix} k \\ i \end{pmatrix} a^i b^{k-i}}{2^{k/2}k!} \frac{\begin{pmatrix} l \\ j \end{pmatrix} b^j a^{l-j}}{2^{l/2}l!} (-1)^{l-j} s^{i+j} t^{k+l-i-j} H_k(R)H_l(X) = \\ &\quad \sum_{k=0}^{\infty}\sum_{l=0}^{\infty}\sum_{i=0}^{k}\sum_{j=0}^{l} A_1(k,i)A_2(l,j)(-1)^{l-j} s^{i+j} t^{k+l-i-j} H_k(R)H_l(X) = \\ &\quad \sum_{i=0}^{\infty}\sum_{j=0}^{\infty}\sum_{k=i}^{\infty}\sum_{l=j}^{\infty} A_1(k,i)A_2(l,j)(-1)^{l-j} s^{i+j} t^{k+l-i-j} H_k(R)H_l(X) = \\ &\quad \sum_{i=0}^{\infty}\sum_{j=0}^{\infty}\sum_{k=0}^{\infty}\sum_{l=0}^{\infty} A_1(k+i,i)A_2(l+j,j)(-1)^{l} s^{i+j} t^{k+l} H_k(R)H_l(X) = \\ &\quad \sum_{m=0}^{\infty}\sum_{n=0}^{\infty}\sum_{u=-m}^{m}\sum_{v=-n}^{n} A_1[(m+n+v+u)/2,(m+u)/2]A_2[(m+n-v-u)/2,(m-u)/2]\times \\ &\qquad\qquad (-1)^{(n-v)/2} H_{(m+n+v+u)/2}(R)H_{(m+n-v-u)/2}(X) s^m t^n \end{aligned} \tag{A.7}$$

which, by equating the coefficients term by term, gives

$$\frac{H_{n_1}(x_1)}{n_1!}\frac{H_{n_2}(x_2)}{n_2!} = \sum_{i=-n_1}^{n_1}\sum_{j=-n_2}^{n_2} (-1)^l A_1(N,N-k)A_2(n,n-l)H_N(R)H_n(X) \tag{A.8}$$

where we have defined:

$$\begin{aligned} N &= (n_1+n_2+i+j)/2 \quad ; \qquad k = (n_2+j)/2 \\ n &= (n_1+n_2-i-j)/2 \quad ; \qquad l = (n_2-j)/2 \end{aligned}$$

and

$$A_1(N,N-k) = \frac{a^{N-k}b^k}{2^{N/2}k!(N-k)!}; \qquad A_2(n,n-l) = \frac{b^{n-l}a^l}{2^{n/2}l!(n-l)!} \tag{A.9}$$

This suggests that we can re-write Equation (A.8) in the following form:

$$\left(\frac{H_{n_1}(x_1)}{n_1!\sqrt{n_1!}}\right)\left(\frac{H_{n_2}(x_2)}{n_2!\sqrt{n_2!}}\right) = \sum_{i=-n_1}^{n_1}\sum_{j=-n_2}^{n_2}(-1)^l\left(\frac{\sqrt{n_1!}}{2^{n_1/2}}\right)\left(\frac{\sqrt{n_2!}}{2^{n_2/2}}\right)\frac{a^{N-k}b^k}{2^{N/2}k!(N-k)!}\frac{b^{n-l}a^l}{2^{n/2}l!(n-l)!}H_N(R)H_n(X) \quad \text{(A.10)}$$

or

$$\phi_{n_1}(x_1)\phi_{n_2}(x_2) = \sum_{i=-n_1}^{n_1}\sum_{j=-n_2}^{n_2}(-1)^l\frac{\sqrt{n_1!n_2!N!n!}a^{N-k+l}b^{n+k-l}}{2^{(n_1+n_2)/2}k!l!(N-k)!(n-l)!}\phi_N(R)\phi_n(X) \quad \text{(A.11)}$$

where $\phi_n(x)$ is the n^{th} order simple harmonic oscillator wave-function defined as:

$$\phi_n(x) = \sqrt{\frac{1}{\sqrt{\pi}2^n n!}}H_n(x)e^{-x^2/2}$$

We now change variables to

$$N \equiv (n_1+n_2+i+j)/2 \qquad \text{and} \qquad k = (n_2+j)/2 \qquad \text{or} \qquad N = (n_1+i)/2+k$$

With these changes we obtain:

$$\begin{aligned} n &= [(n_1+n_2)-(i+j)]/2 = n_1+n_2-N \\ l &= (n_2-j)/2 = n_2-k \quad \text{or} \quad n-l = n_1-N+k \end{aligned}$$

Clearly $N_{min}=0$, $N_{max}=(n_1+n_2)$, $k_{min}=0$ and $k_{max}=n_2$. The values of k are correlated to the values of N. If we let N take on the whole range of its allowed values, k is constrained by $k = N-(n_1+i)/2$ which implies $k_{min} = N-n_1$ and $k_{max}=N$. Considering the constraints for k above, we get $k_{min}=\max(0,N-n_1)$ and $k_{max}=\min(N,n_2)$. With these changes we get:

$$n = [(n_1+n_2)-(i+j)]/2 = n_1-n_2-N, \quad l=(n_2-j)/2 = n_2-k \quad \text{or} \quad n-l = n_1-N+k$$

Thus, finally:

$$\phi_{n_1}(x_1)\phi_{n_2}(x_2) = \sum_{N=0}^{n_1+n_2}\sum_{k=k_{min}}^{k_{max}}(-1)^{n_2-k}\frac{\sqrt{n_1!n_2!N!(n_1+n_2-N)!}a^{N-k+l}b^{n+k-l}}{2^{(n_1+n_2)/2}k!(n_2-k)!(N-k)!(n_1+k-N)!}\phi_N(R)\phi_{n_1+n_2-N}(X) \quad \text{(A.12)}$$

or

$$\phi_{n_1}(x_1)\phi_{n_2}(x_2) = \sum_{N=0}^{n_1+n_2} M_{n_1 n_2 N}(a,b)\phi_N(R)\phi_{n_1+n_2-N}(X) \tag{A.13}$$

with

$$M_{n_1 n_2 N}(a,b) = \sum_{k=k_{min}}^{k_{max}} (-1)^{n_2-k} \frac{\sqrt{n_1!n_2!N!(n_1+n_2-N)!}a^{N-k+l}b^{n+k-l}}{2^{(n_1+n_2)/2}k!(n_2-k)!(N-k)!(n_1+k-N)!}$$

$$k_{min} = \max(0, N-n_1) \qquad \text{and} \qquad k_{max} = \min(N, n_2)$$

which are our general transformation (Moshinsky) brackets. Let us now consider the kind of two-dimesional integrals we met in Chapter 3, i.e.:

$$\mathcal{I}_1 \equiv \langle n_1' n_2' | \mathcal{V}\left(\sqrt{2}\left|\frac{1}{2}\xi_1 - \frac{\sqrt{3}}{2}\xi_2\right|\right) |n_1 n_2\rangle = \int_{-\infty}^{\infty}\int_{-\infty}^{\infty} \phi_{n_1'}(\xi_1)\phi_{n_2'}(\xi_2)\mathcal{V}\left(\sqrt{2}\left|\frac{1}{2}\xi_1 - \frac{\sqrt{3}}{2}\xi_2\right|\right)\phi_{n_1}(\xi_1)\phi_{n_2}(\xi_2)\,\mathrm{d}\xi_1\,\mathrm{d}\xi_2$$

Now apply the cooridinates rotation:

$$\xi_1' = \frac{1}{\sqrt{2}}\left(\sqrt{\frac{3}{2}}\xi_1 + \sqrt{\frac{1}{2}}\xi_2\right) \qquad \text{and} \qquad \xi_2' = \frac{1}{\sqrt{2}}\left(\sqrt{\frac{1}{2}}\xi_1 - \sqrt{\frac{3}{2}}\xi_2\right)$$

which is of the form of Equation A.3, with $R = \xi_1'$, $X = \xi_2'$, $a = \sqrt{\frac{3}{2}}$ and $b = \sqrt{\frac{1}{2}}$. Using Equation A.13 to substitute for the products $\phi_{n_1}(\xi_1)\phi_{n_2}(\xi_2)$ we obtain:

$$\begin{aligned}
\mathcal{I}_1 = \langle n_1' n_2' | \mathcal{V}\left(\sqrt{2}\left|\frac{1}{2}\xi_1 - \frac{\sqrt{3}}{2}\xi_2\right|\right) |n_1 n_2\rangle &= \langle n_1' n_2' | \mathcal{V}\left(\sqrt{2}\,|\xi_2'|\right) |n_1 n_2\rangle = \\
&\sum_{N=0}^{n_1+n_2}\sum_{N'=0}^{n_1'+n_2'} M_{n_1 n_2 N}\left(\sqrt{\frac{3}{2}}, \sqrt{\frac{1}{2}}\right) M_{n_1' n_2' N'}\left(\sqrt{\frac{3}{2}}, \sqrt{\frac{1}{2}}\right) \times \\
&\int_{-\infty}^{\infty} \phi_N(\xi_1')\phi_{N'}(\xi_1')\,\mathrm{d}\xi_1' \int_{-\infty}^{\infty} \phi_{n_1'+n_2'-N'}(\xi_2')V(\sqrt{2}\,|\xi_2'|)\phi_{n_1+n_2-N}(\xi_2')\,\mathrm{d}\xi_2' = \\
&\sum_{N=0}^{n_1+n_2}\sum_{N'=0}^{n_1'+n_2'} M_{n_1 n_2 N}\left(\sqrt{\frac{3}{2}}, \sqrt{\frac{1}{2}}\right) M_{n_1' n_2' N'}\left(\sqrt{\frac{3}{2}}, \sqrt{\frac{1}{2}}\right) \delta_{N,N'} \times \\
&\int_{-\infty}^{\infty} \phi_{n_1'+n_2'-N'}(\xi_2')V(\sqrt{2}\,|\xi_2'|)\phi_{n_1+n_2-N}(\xi_2')\,\mathrm{d}\xi_2'
\end{aligned} \tag{A.14}$$

by virtue of the orthonormality of the ϕ_n's. A similar result can be obtained for the integral

$$\mathcal{I}_2 \equiv \langle n_1' n_2' | \mathcal{V} \left(\sqrt{2} \left| \frac{1}{2}\xi_1 + \frac{\sqrt{3}}{2}\xi_2 \right| \right) | n_1 n_2 \rangle = \int_{-\infty}^{\infty} \int_{-\infty}^{\infty} \phi_{n_1'}(\xi_1) \phi_{n_2'}(\xi_2) \mathcal{V} \left(\sqrt{2} \left| \frac{1}{2}\xi_1 + \frac{\sqrt{3}}{2}\xi_2 \right| \right) \phi_{n_1}(\xi_1) \phi_{n_2}(\xi_2) \, \mathrm{d}\xi_1 \, \mathrm{d}\xi_2$$

by using the transformation $a = \sqrt{\frac{1}{2}}$ and $b = \sqrt{\frac{3}{2}}$ to obtain:

$$\mathcal{I}_2 = \langle n_1' n_2' | \mathcal{V} \left(\sqrt{2} \, |\xi_1'| \right) | n_1 n_2 \rangle = \sum_{N=0}^{n_1+n_2} \sum_{N'=0}^{n_1'+n_2'} M_{n_1 n_2 N} \left(\sqrt{\frac{1}{2}}, \sqrt{\frac{3}{2}} \right) M_{n_1' n_2' N'} \left(\sqrt{\frac{1}{2}}, \sqrt{\frac{3}{2}} \right) \delta_{n_1+n_2-N, n_1'+n_2'-N'} \times \int_{-\infty}^{\infty} \phi_N(\xi_1') V(\sqrt{2} \, |\xi_1'|) \phi_{N'}(\xi_1') \, \mathrm{d}\xi_1'$$

APPENDIX B

HYPER-SPHERICAL HARMONICS DIFFERENTIAL EQUATIONS FOR THE THREE-BODY SYSTEM

Start with Schrödinger's equation in hyper-spherical harmonics coordinates:

$$\left\{\frac{\partial^2}{\partial r^2}+\frac{1}{r^2}\frac{\partial^2}{\partial\theta^2}+\frac{1}{4r^2}-k^2-U(r,\theta)\right\}\psi(r,\theta)=0 \tag{B.1}$$

where $U(r,\theta)$ is defined as:

$$U(r,\theta)\equiv\frac{1}{2m}\times \left\{V\left(\sqrt{2}\,|r\cos\theta|\right)+V\left(\frac{r}{\sqrt{2}}\left|\cos\theta-\sqrt{3}\sin\theta\right|\right)+V\left(\frac{r}{\sqrt{2}}\left|\cos\theta+\sqrt{3}\sin\theta\right|\right)\right\}$$

with $k^2\equiv -2mE$ and $\psi(r,\theta)\equiv\frac{1}{\sqrt{r}}\phi(r,\theta)$. A solution to this differential equation can be attempted in the form of a Fourier expansion, in which the r and θ dependence is explicitly separated:

$$\phi=\sum_{m=0}^{\infty}\{g_m(r)\cos(\theta)+f_m(r)\sin(\theta)\} \tag{B.2}$$

One can verify that the potential possesses the following symmetries:

$$\begin{cases}V(r,\theta) &= V\left(r,\theta\pm\frac{\pi}{3}\right)\\ V(r,\theta) &= V(r,-\theta)\end{cases} \tag{B.3}$$

Equation B.3 allows us to eliminate the antisymmetric (sine) moments of the solution, since:

$$V_m^{(-)}(r)=\frac{1}{2\pi}\int_0^{2\pi}V(r,\theta)\sin m\theta\,\mathrm{d}\theta=0$$

We now proceed to compute the cosine moments of the potential, defined as:

$$\begin{aligned} V_m^{(+)}(r) &= \frac{1}{2\pi}\int_0^{2\pi} V(r,\theta)\cos m\theta\,\mathrm{d}\theta \\ &= \frac{1}{2\pi}\int_0^{\pi} V(r,\theta)\cos m\theta\,\mathrm{d}\theta + \frac{1}{2\pi}\int_\pi^{2\pi} V(r,\theta)\cos m\theta\,\mathrm{d}\theta \\ &= \frac{1}{2\pi}\int_0^{\pi} V(r,\theta)\cos m\theta\,\mathrm{d}\theta + \frac{1}{2\pi}\int_0^{\pi} V(r,\theta+\pi)\cos m(\theta+\pi)\,\mathrm{d}\theta \\ &= \frac{1}{2\pi}\int_0^{\pi} V(r,\theta)\cos m\theta\,[1+(-1)^m]\;\mathrm{d}\theta \end{aligned}$$

or

$$V_m(r) = \begin{cases} \frac{1}{\pi}\int_0^{2\pi} V(r,\theta)\cos m\theta\,\mathrm{d}\theta & \text{if } m \text{ is even} \\ 0 & \text{if } m \text{ is odd} \end{cases} \tag{B.4}$$

Furthermore, using B.3

$$U_k(r) = \frac{1}{\pi/3}\int_0^{\pi/3} V(r,\theta)\cos(6k\theta)\,\mathrm{d}\theta \tag{B.5}$$

where we have redefined the nonzero moments of the potential to include a factor 6 in the cosine. Our generalized solution now can be simplified to:

$$\phi(r,\theta) = \sum_{m=0}^{\infty} g_m(r)\cos(6m\theta) \tag{B.6}$$

which plugged into Equation B.1 yields:

$$\begin{aligned} &\left\{\frac{\partial^2}{\partial r^2} + \frac{1}{r^2}\frac{\partial^2}{\partial\theta^2} + \frac{1}{4r^2} - k^2 - U(r,\theta)\right\}\sum_{m=0}^{\infty} g_m(r)\cos(6m\theta) = \\ &\qquad \sum_{m=0}^{\infty}\left\{\frac{\mathrm{d}^2}{\mathrm{d}r^2} - \frac{(6m)^2-1/4}{r^2} - k^2 - U(r,\theta)\right\} g_m(r)\cos(6m\theta) = \\ &\qquad\qquad \sum_{m=0}^{\infty}\left\{\hat{D}_{km}(r) - U(r,\theta)\right\} g_m(r)\cos(6m\theta) = 0 \end{aligned} \tag{B.7}$$

where we have defined the differential operator:

$$\hat{D}_{km}(r) \equiv \frac{\mathrm{d}^2}{\mathrm{d}r^2} - \frac{(6m)^2-1/4}{r^2} - k^2 \tag{B.8}$$

Integrating both sides with $\frac{1}{2\pi}\int_0^{2\pi}\cos(6n\theta)\,\mathrm{d}\theta$ one obtains:

$$\begin{aligned} &\sum_{m=0}^{\infty}\hat{D}_{km}(r)g_m(r)\left[\frac{1}{2\pi}\int_0^{2\pi}\cos(6m\theta)\cos(6n\theta)\,\mathrm{d}\theta\right] \\ &\qquad - \sum_{m=0}^{\infty} g_m(r)\left[\frac{1}{2\pi}\int_0^{2\pi} U(r,\theta)\cos(6m\theta)\cos(6n\theta)\,\mathrm{d}\theta\right] = 0 \end{aligned} \tag{B.9}$$

Now use (for $n \neq 0$) $\frac{1}{2\pi}\int_0^{2\pi}\cos(6n\theta)\cos(6m\theta)\,\mathrm{d}\theta = \frac{1}{2}\delta_{n,m}$ and:

$$\frac{1}{2\pi}\int_0^{2\pi}\cos(6n\theta)U(r,\theta)\cos(6m\theta)\,\mathrm{d}\theta = \frac{1}{2}\left\{\frac{1}{2\pi}\int_0^{2\pi}\cos[6(n+m)\theta]U(r,\theta)\,\mathrm{d}\theta + \frac{1}{2\pi}\int_0^{2\pi}\cos[6(n-m)\theta]U(r,\theta)\right\} = \frac{1}{2}\left[U_{n+m}(r) + U_{|n-m|}(r)\right]$$

so that Equation B.9 becomes:

$$\hat{D}_{kn}(r)g_n(r) - \sum_{m=0}^{\infty}\left\{U_{|n+m|}(r) + U_{|n-m|}(r)\right\}g_m(r) = 0, \qquad n \neq 0 \tag{B.10}$$

In the case $n = 0$, using $\frac{1}{2\pi}\int_0^{2\pi}\cos(6m\theta)\,\mathrm{d}\theta = \delta_{0,m}$we obtain simply:

$$\hat{D}_{kn}(r)g_n(r) - \sum_{m=0}^{\infty}U_m(r)g_m(r) = 0, \qquad n = 0$$

The last two equations can be grouped into a single one:

$$\hat{D}_{kn}(r)g_n(r) - \sum_{m=0}^{\infty}U_{mn}(r)g_m(r) = 0$$

where:

$$U_{mn}(r) \equiv \begin{cases} U_m(r) & n = 0 \\ U_{|n+m|}(r) + U_{|n-m|}(r) & n \neq 0 \end{cases}$$

REFERENCES

[1] R.V. Reid, Ann. Phys. **50**, 411 (1968).

[2] M. Lacombe *et al.*, Phys. Rev. C **21**, 861 (1980).

[3] R.B. Wiringa, V.G. Stokes and S. Schiavilla, Phys. Rev. C **51**, 38 (1995).

[4] R. Machleidt, F. Sammarruca and Y. Song, Phys. Rev. C **53**, R1483 (1996).

[5] V.G. Stokes *et al.*, Phys. Rev. C **49**, 2950 (1994).

[6] S.A. Coon *et al.*, Nucl. Phys. A **317**, 242 (1979).

[7] M.F. Jang, R. Machleidt, D.B. Stout and T.T.S. Kuo, Phys. Rev. C **46**, 910 (1992).

[8] A. Nogga, H. Kamada and W. Glöckle, Phys. Rev. Lett. **85**, 944 (2000).

[9] J. Carlson, V.R. Pandharipande and R.B. Wiringa Nucl. Phys. A **401**, 59 (1983).

[10] S.C. Pieper *et al.* Phys. Rev. C **64**, 014001 (2001).

[11] S .C. Pieper, K. Varga and R.B. Wiringa, `nucl-th/0206061`.

[12] S.C. Pieper and R.B. Wiringa, Ann. Rev. Nucl. Part. Sci. **51**, 53 (2001), `nucl-th/0103005`.

[13] A. Covello, L. Coraggio, A. Gargano and N. Itaco, `nucl-th/0111056`.

[14] B.R. Barrett and M.W. Kirson, Nucl. Phys. A **148**, 145 (1970).

[15] W.C. Haxton and C.L. Song, Phys. Rev. Lett. **84**, 5484 (2000); `nucl-th/9906082`.

[16] W.C. Haxton and T. Luu, Nucl. Phys. A **690**, 15 (2001).

[17] W.C. Haxton and T. Luu, `nucl-th/0204072`.

[18] G.P. Lepage, "How to Renormalize the Schrödinger Equation", `nucl-th/9706029`.

[19] S.R. Beane, P.F. Bedaque, W.C. Haxton, D.R. Phillips and M.J. Savage, `nucl-th/0008064`.

[20] D.B. Kaplan, `nucl-th/9506035`.

[21] J. Richert, `quant-ph/0209119`.

[22] R.J. Furnstahl, nucl-th/0307099.

[23] T. Barford and M. Birse, hep-ph/0206146.

[24] P. Bedaque and U. van Kolck, Ann. Rev. Nucl. Part. Sci **52**, 339 (2002).

[25] M. Birse, J. McGovern and K. Richardson, Phys. Lett. B **454**, 167 (1999).

[26] S.K. Bogner and T.T.S. Kuo, Phys. Lett. B **500**, 279 (2001).

[27] S.K. Bogner, A. Schwenk, T.T.S. Kuo and G.E. Brown, nucl-th/0111042.

[28] E.M. Krenciglowa and T.T.S. Kuo, Nuclear Physics A **235**, 171 (1974).

[29] K. Suzuki and S.Y. Lee, Prog. Theor. Phys. **64**, 2091 (1980).

[30] K. Suzuki, Prog. Theor. Phys. **68**, 246 (1982).

[31] K. Suzuki and R. Okamoto, Prog. Theor. Phys. **70**, 439 (1983).

[32] P. Navrátil, G.P. Kamuntavičius and B.B. Barrett, Phys. Rev. C **61**, 044001 (2000).

[33] P. Navrátil, J.P. Vary and B.B. Barrett, Phys. Rev. C **62**, 054311 (2000); Phys. Rev. Lett. **84**, 5728 (2000).

[34] M.S. Fayache, J.P. Vary, B.R. Barrett, P. Navratil and S. Aroua, nucl-th/0112066.

[35] C.J. Morningstar and M. Weinstein, Phys. Rev. Lett. **73**, 1873 (1994).

[36] C.J. Morningstar and M. Weinstein, Phys. Rev. D **54**, 4131 (1996).

[37] H. Mueller, J. Piekarewicz and J.R. Shepard, Phys. Rev. C **66**, 024324 (2002).

[38] C. Felline, N.P. Mehta, J. Piekarewicz and J.R. Shepard, Phys. Rev. C **68**, 034003 (2003).

[39] D.L. Stein, *"Spin Glasses"*, Scientific American, July 1989.

[40] H. Bethe, Z. Phys. **71**, 205.

[41] R. Botet and J. Jullien, Phys. Rev. B **27**, 613 (1983).

[42] F.D.M. Haldane, Phys. Rev. B **25**, 4925 (1982).

[43] F.D.M. Haldane, Phys. Rev. B **26**, 5257 (1982).

[44] X.F. Jiang, H. Chen, D.Y. Xing and J.M. Dong, J. Phys. Cond. Matt. **13**, 6519 (2001).

[45] T. Tonegawa and I. Harada, J. Phys. Soc. Jpn. **56**, 2153 (1987).

[46] G. Bouzerar, A.P. Kampf and G.L. Japaridze, Phys. Rev. B **58**, 58 (1998).

[47] D. Augier and D. Poilblanc, cond-mat/9705032.

[48] S.R. White and I. Affleck, Phys. Rev. B **54**, 9862 (1996).

[49] R. Chitra, S. Pati, H.R. Krishnamurty, D. Sen, S. Ramasesha Phys. Rev. B **52**, 6581 (1995).

[50] P.W. Anderson, Phys. Rev. **86**, 694 (1952).

[51] K. Okamoto and K. Nomura, Phys. Lett A **169**, 433 (1992).

[52] K. Okamoto and Y. Ueno, J. Phys. Soc. Jpn. **64**, 86 (1994).

[53] H. Kikuchi, H. Nagasawa, V. Ajiro, T. Asano and T. Goto, Physica B **284-288**, 1631 (2000).

[54] M. Hagiwara *et al.*, Physica B **294-295**, 83 (2001).

[55] J. Piekarewicz and J.R. Shepard, Phys. Rev. B **56**, 5366 (1997).

[56] J. Piekarewicz and J.R. Shepard, Rev. Mex. Fis. **44**, 113 (1998).

[57] J. Piekarewicz and J.R. Shepard, Phys. Rev. B **57**, 10260 (1998).

[58] J. Piekarewicz and J.R. Shepard, Phys. Rev. B **58**, 9326 (1998).

[59] J. Piekarewicz and J.R. Shepard, Phys. Rev. B **60**, 9456 (1999).

[60] E. Dagotto and T.M. Rice, Science **271**, 618 (1996).

[61] L.I. Schiff, *Quantum Mechanics* (McGraw-Hill, New York, 1968).

[62] J.R. Taylor, *Scattering Theory* (John Wiley and Sons, 1972).

[63] James V. Steele and R.J. Furnstahl, Nucl. Phys. A **637**, 46 (1998).

[64] James V. Steele and R.J. Furnstahl, Nucl. Phys. A **645**, 439 (1999).

[65] H. Kamada, A. Nogga, W. Glöcle *et al.*, Phys. Rev. Lett. **64**, 04400 (2001).

[66] M. Moshinsky "The Harmonic Oscillator in Modern Physics: From Atoms to Quarks", Gordon and Breach, New York, 1969.

[67] T.A. Brody and M. Moshinsky "Tables of Transformation brakets for Nuclear Shell-Model Calculations", 1967.

[68] G.P. Kamuntavičius *et al.*, `nucl-th/0105009` (2001).

[69] E. Dagotto, "Correlated electrons in high-temperature superconductors", Rev. Mod. Phys. Vol. 66 No. 3 (July 1994).

[70] H. Goldstein *"Classical mechanics"*, 2nd Edition, Addison Wesley, 1980.

[71] G.B. Arfken *et al.*, *"Mathematical methods for physicists"*, 5th Edition, Academic Press, 2000.

[72] C. Lanczos, J. Res. Natl. Bur. Stand. **45**, 255 (1950).

[73] J.K. Cullum and R.A. Willoughby, *"Lanczos algorithm for large symmetric eigenvalue computations"* (Birchäuser, Boston, 1985).

[74] D.M. Brink and G.R. Satchler *"Angular Momentum"* (Oxford Science Publications, Oxford, 1993).

BIOGRAPHICAL SKETCH

Cosimo Felline

Education

1999-2004 Ph.D., Theoretical Nuclear Physics, Department of Physics,
Florida State University.

1991-1998 Laurea (BS with thesis) in Physics (cum laude), High Energy Physics,
University of Cagliari, Italy.

Experience

1999-2004 Research assistant, Nuclear Theory,
Florida State University.

1999-2000 Teaching Assistant, Physics Department,
Florida State Univerisy.

Publications

1 C.Felline, N.P.Mehta, J.Piekarewicz and J.R.Shepard,
Low energy operators in effective theories,
Phys. Rev. C **68**, 034003 (2003).